Stony Brook University

Advances in Theory of Coherent Electron Cooling

A Dissertation presented

by

Andrey Elizarov

to

The Graduate School

in Partial Fulfillment of the

Requirements

for the Degree of

Doctor of Philosophy

in

Physics

Stony Brook University

May 2015

Stony Brook University

The Graduate School

Andrey Elizarov

We, the dissertation committee for the above candidate for the

Doctor of Philosophy degree, hereby recommend

acceptance of this dissertation

Dr. Vladimir Litvinenko - Dissertation Advisor
Professor, Department of Physics and Astronomy

Dr. Thomas Hemmick - Chairperson of Defense
Distinguished Teaching Professor, Department of Physics and Astronomy

Dr. Dmitri Kharzeev
Professor of Physics, Department of Physics and Astronomy

Dr. Elke-Caroline Aschenauer
Senior Scientist, Physics Department, Brookhaven National Laboratory

This dissertation is accepted by the Graduate School

Charles Taber
Dean of the Graduate School

Abstract of the Dissertation

Advances in Theory of Coherent Electron Cooling

by

Andrey Elizarov

Doctor of Philosophy

in

Physics

Stony Brook University

2015

The coherent electron cooling is a novel hadron beam cooling technique that is being developed at Brookhaven National Laboratory. It is a realization of the stochastic cooling, in which an electron beam is used in the modulator, amplifier and kicker. In the modulator, hadrons create electron density perturbations. Then these perturbations are amplified in the free electron laser, while hadrons pass through dispersion section, where they are placed such that, in the kicker, amplified perturbations' electric fields accelerate or decelerate hadrons, depending on their velocities, cooling the beam. In the present dissertation, we describe ways to model the modulator section of the coherent electron cooling. The electron beam can be modeled as an infinite plasma and in this model even analytical solutions can be obtained for the density perturbations. Obviously, infinite electron plasma is unrealistic model of an electron beam in accelerator. The main result of the dissertation is a method to compute dynamics of shielding of a moving charged particle (hadron) in a confined plasma, which represents a realistic model of an electron beam. This is a longstanding problem in plasma physics with applications ranging from cosmology to advanced particle accelerator techniques. However, only solutions for an infinite unrealistic plasma

are available. We developed a novel method to solve this problem, which consists of transformation of the Vlasov-Poisson differential equations to an integral equation for the Laplace image of the electron density perturbation created by an external charge. The integral equation is then solved numerically via the piecewise polynomial collocation method and the fast Fourier transform. We present thorough analysis of the results obtained and their physical interpretation. We also consider infinite plasma model and derive some formulas for the free electron laser section within this approximation.

Contents

List of Figures

List of Tables

List of Abbreviations

BNL – Brookhaven National Laboratory
CeC – Coherent electron Cooling
DFT – Discrete Fourier Transform
FEL – free electron laser
FFT – Fast Fourier Transform
GK – Gauss-Kronrod (method)
GNU – GNU is Not Unix
GSL – GNU Scientific Library
IPAC – International Particle Accelerator Conference
KV – Kapchinskij-Vladimirskij (distribution)
LHS – Left-Hand Side
LU – Lower Upper (decomposition)
MPI – Message Passing Interface
NERSC – National Energy Research Scientific Computing Center
ODE – Ordinary Differential Equation
PIC – Particle-In-Cell
PoP – Proof-of-Principle
PPCM – Piecewise Polynomial Collocation Method
RHIC – Relativistic Heavy Ion Collider
SASE – Self-Amplified Spontaneous Emission
WB – Water-Bag (distribution)

Acknowledgements

I would like to thank my scientific advisor Prof. Vladimir Litvinenko for introducing me to coherent electron cooling, for giving me an interesting problem, which is both challenging and has many applications. Also, I would like to thank Dr. Gang Wang for many useful discussions. I would also like to thank Dr. Alexey Fedotov for useful comments on my work and attracting my attention to some related research.

I also would like to thank members of my dissertation committee, Prof. Hemmick, Prof. Kharzeev, and Dr. Elke-Caroline Aschenauer for a great attention to my work.

I would also like to thank Prof. K.-J. Kim, Prof. Z. Huang, and Dr. R. Lindberg for a very interesting course on theory of free electron lasers, which I attended on the US Particle Accelerator School.

Also, I am very grateful to all colleagues to whom I talked during FEL and IPAC conferences.

I am very grateful to Dr. Vahid Ranjbar and Dr. Ilya Pogorelov for sharing with me their supercomputing recourses, and to National Energy Research Scientific Computing Center (NERSC) for awarding me my own. Without this supercomputing resources the work simply couldn't be done.

I'm very grateful to our Graduate Program Director Prof. Jacobus Verbaarschot and all other Stony Brook University professors for a very interesting graduate program and lectures.

I am also very grateful to all Stony Brook University and Brookhaven National Laboratory staff, especially, to Sara Lutterbie and Pamela Manning, for a great help during my graduate studies. I am thankful to Avril Woodhead for proofreading my research papers.

1 Introduction

Particle accelerators [1, 2], which are devices that propel charged particles to high energies and contain them in beams, are very important tools in modern science and technology. Their primary purpose is to provide particle beams for research in particle and nuclear physics, however, they are also very useful in solid state physics, biology, medicine etc. It is impossible to list all the applications of particle accelerators. It is very important to provide beams of high quality.

Typically, particles in a beam are grouped into "bunches". One of the most important parameters of a particle accelerator is its luminosity:

$$L = \frac{N^2 f}{4\pi\sigma^2}, \tag{1}$$

where N is a number of electrons in a bunch, f is its repetition frequency, σ^2 is a variance of the transverse spatial density distribution of the bunch. The transverse emittance $\epsilon_\perp$ is defined as an area of the cross section of the phase space volume occupied by the bunch:

$$\epsilon_\perp = \int\limits_{B_\perp} d\vec{x} d\vec{p}, \tag{2}$$

where $B_\perp$ stands for the cross section of the region in phase space occupied by the bunch (we omit longitudinal coordinates for simplicity, typically, emittance is constant along the bunch) and $\vec{x}$ and $\vec{p}$ are the coordinate and momentum vectors, respectively. Defining beta function β via

$$\beta = \frac{\sigma^2}{\epsilon_\perp}, \tag{3}$$

we can rewrite luminosity in a form:

$$L = \frac{N^2 f}{4\pi\epsilon\beta}. \tag{4}$$

Obviously, one of the ways to increase luminosity is to reduce emittance. Reduction of the emittance of the beam is called "beam cooling".

There are few well-known cooling techniques, i.e., ionization cooling, electron cooling, and stochastic cooling. In the ionization cooling, particles pass

through some material and their momentum is reduced as they ionize atoms of the material; this technique is mostly used to cool muon beams. In the electron cooling, which was invented by G. Budker in 1966, an accelerated electron beam merged with a particle beam being cooled and the heat of the particle beam is transferred to the electron beam through collisions and, as a result, emittance of the particle beam is reduced. In the stochastic cooling, individual particles in a beam create some electrical signals, then these signals are amplified and then they "kick" particles, reducing emittance of the beam. The first section of the stochastic cooling is called "modulator" or "pickup" and the last – "kicker". This cooling technique can be used for transverse and longitudinal cooling.

Currently, electron cooling and stochastic cooling are used to cool hadron beams. However, these methods are unable to cool beams with energies of TeV order. Recently, the coherent electron cooling (CeC), which is a new realization of stochastic longitudinal cooling, was proposed as a new cooler for Relativistic Heavy Ion Collider (RHIC) [3] at Brookhaven National Laboratory (BNL). It was estimated [4], that CeC is able to cool 250 Gev proton beam (at RHIC) in under 10 minutes and 7 TeV proton beam (at LHC) in under an hour. Currently, a corresponding facility is under construction at Brookhaven National Laboratory, for the present status of the developments of the machine, we refer to [5]. In the next subsection, we discuss CeC in more detail.

1.1 Coherent electron cooling

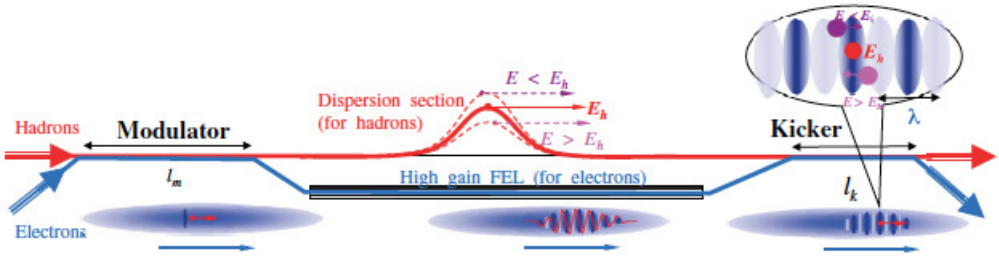

Figure 1: The scheme of the coherent electron cooler [4].

The CeC is a modern realization of the stochastic electron cooling, where the electron beam is used in the modulator, amplifier and kicker. In the

modulator, the information about a hadron beam is recorded as electron density perturbations resulting from shielding of the hadrons. Then these perturbations are amplified in the free electron laser (FEL) section [6, 7, 8], and then, in the kicker, every hadron experience an electric field produced by its own amplified perturbation receiving kicks. Before the kicker, in the dispersion section, each hadron is placed such that these kicks accelerate or decelerate it depending on its velocity toward the desired one reducing the velocity spread of the hadron beam. The scheme of the CeC device is depicted in Fig. 1. To analyze the performance of the CeC, all sections of the device has to be studied in detail.

1.1.1 CeC modulator and test charge problem

In the modulator, electron and hadron beams are merged and hadrons create electron density perturbations in the electron beam. Precise computation of the dynamics of shielding of a hadron in an electron beam is required to provide a theoretical description of CeC device and obtain the correct parameters' values for the facility, which is currently under construction at Brookhaven National Laboratory [5].

The simplest formulation of the test charge problem is an evaluation of screening of a stationary particle in an infinite plasma (by *plasma* we mean a collisionless single-species electron plasma), this is the well-known Debye screening. For a particle moving in an infinite plasma, it is possible to solve the corresponding equations, i.e., the Vlasov-Poisson system, via the Laplace and Fourier transforms [9, 10, 11]. For the 1D infinite plasma with the Cauchy equilibrium velocity distribution, the exact solution can be obtained [10]. For the 3D infinite plasma with the Lorentz equilibrium velocity distribution, the solution can be expressed as a one-dimensional integral [9], we will discuss these results in more detail in subsection 1.1.2. For other cases, the integral transforms must be inverted numerically [10]. In section 2, we will describe our exhaustive considerations of the dynamical shielding of a charged particle in the infinite plasma following [10].

An infinite plasma is an unrealistic model of an electron beam. Many effects are very different in finite and infinite plasmas and so the shielding, as we shall see in section 4. For the first time, the Vlasov-Poisson equations for a finite plasma with the microcanonical equilibrium distribution was considered by Gluckstern [12]; then these ideas were further developed by him and Venturini in [13]. In these papers, they studied a plasma's response

to an external magnetic field of a special form. However, plasma with the microcanonical equilibrium distribution doesn't represent a realistic model of a physical system and they didn't study shielding of an external charge. There also have been some considerations of a test charge problem for a semi-infinite bounded plasma [14].

Main result of the present thesis is a development of a novel method for computation of shielding of a charged particle in a confined plasma. Confined plasma is defined as plasma with an integrable equilibrium distribution, at least over some spatial coordinates; velocity distribution is integrable even for the infinite plasma. An example of such plasma is an electron beam with the finite emittance along these coordinates. There are two cases of practical interest: a fully confined plasma (its spatial distribution is integrable over all coordinates), e.g., a ball in 3D space with the normal (Maxwell) spatial distribution, which is a realistic model of an electron bunch in a bunched beam, and a partially confined plasma (its spatial distribution is integrable over some coordinates), e.g., a longitudinally infinite electron beam with the finite transverse emittance. Although, with some modifications, the method can be applied to infinite and partially confined plasmas, we will focus on a fully confined case, since this model is more realistic.

Potential applicability of the methods developed extends far beyond particle beams with finite sizes. For example, they can be used to describe interstellar phenomena, such as propagation of a planet or star through a dust cloud or low density interstellar plasma, and screening effects in solar and stellar interiors. Also, the methods can be applied to plasmas with charged dust particles, since the method can be easily modified to deal with finite size charged particles.

Section 4 is devoted to the test charge problem in the confined plasma. We will start with the formulation of the problem. Then we describe two different methods, which are similar, but one is less general and more effective numerically than the other. They both lead to the Fredholm integral equation of the second type for the Laplace image of the perturbation's density. We call such equations the Laplace-Fredholm equations for the density perturbation. Then, we review the piecewise polynomial collocation method (PPCM) for the Fredholm integral equation, and describe our numerical method for the Laplace-Fredholm equation that utilizes the PPCM and the discrete Fourier transform. Thereafter, we present numerical results for shielding of a charged particle in the 1D, 2D and 3D plasmas with the normal (Maxwell) spatial and velocity distributions. We compare the results to those obtained previously

for the infinite plasma [10] and provide physical interpretation of the results. We will then discuss application of these results to the CeC device now being constructed at Brookhaven National Laboratory.

All the methods discussed solve this problem via solving the Vlasov-Poisson system of equations either analytically or numerically. Alternatively, the shielding problem can be solved via simulations [15]. So called "particle-in-cell" (PIC) method is used for that. For the infinite plasma, after verification with the results of [9], the PIC method is working fine. However, there are some difficulties with applying PIC for the realistic case of the confined plasma, which make the results of the present thesis very important for future tests of the PIC simulations for the confined plasma.

1.1.2 Recent considerations of the test charge problem

Dynamical test charge problem for the infinite plasma was recently considered by Gang Wang and Michael Blaskiewicz [9], our colleagues from BNL. Here we briefly present and discuss their results.

They started with the Vlasov-Poisson system of equations:

$$\frac{\partial}{\partial t} f_1(\vec{x},\vec{v},t) + \vec{v}\cdot\frac{\partial}{\partial \vec{x}} f_1(\vec{x},\vec{v},t) - \frac{e\vec{E}}{m_e}\cdot\frac{\partial}{\partial \vec{v}} f_0(\vec{v}) = 0, \tag{5}$$

$$\frac{\partial}{\partial \vec{x}}\cdot\vec{E}(\vec{x},t) = \frac{\rho(\vec{x},t)}{\epsilon_0}, \tag{6}$$

where $f_1(\vec{x},\vec{v},t)$ is an unknown perturbation's density, $f_0(\vec{v})$ is an equilibrium density, m_e is an electron mass, ϵ_0 is a vacuum permittivity, $\vec{E}(\vec{x},t)$ is an electric field, and $\rho(\vec{x},t)$ is given by

$$\rho(\vec{x},t) = Ze\delta(\vec{x}) - en_1(\vec{x},t), \tag{7}$$

where

$$n_1(\vec{x},t) = \int f_1(\vec{x},\vec{v},t)d\vec{v}. \tag{8}$$

Doing Fourier transform and integrating over time, we can obtain an integral equation for the Fourier image of $n_1(\vec{x},t)$:

$$\tilde{n}_1(\vec{k},t) = \omega_p^2 \int_0^t \left(\tilde{n}_1(\vec{k},t) - Z\right)(t_1 - t)g(\vec{k}(t-t_1))dt_1, \tag{9}$$

where

$$g(\vec{u}) \equiv \frac{1}{n_0}\int f_0(\vec{v})\mathrm{e}^{-i\vec{u}\cdot\vec{v}}d\vec{v},\ \omega_p^2 = \frac{n_0 e^2}{m_e\epsilon_0},\ \text{and}\ n_0 = \int f_0(\vec{v})d\vec{v}. \tag{10}$$

The main result of their work was an analytical expression for $\tilde{n}_1(\vec{k},t)$, for some special distribution $f_0(\vec{v})$, namely, for the Lorentzian distribution[1]:

$$f_0(\vec{v}) = \frac{n_0}{\pi^2\beta_x\beta_y\beta_z}\left(1+\frac{(v_x+v_{0x})^2}{\beta_x^2}+\frac{(v_y+v_{0y})^2}{\beta_y^2}+\frac{(v_z+v_{0z})^2}{\beta_z^2}\right)^{-2}, \tag{11}$$

where β_x, β_y, β_z, and $\vec{v}_0$ are some parameters. With this distribution, the integral equation (9) can be transformed to the inhomogeneous ordinary differential equation (ODE) for $\tilde{H}_1(\vec{k},t)$ defined via:

$$\tilde{H}_1(\vec{k},t) = \tilde{n}_1(\vec{k},t)\mathrm{e}^{-\lambda(\vec{k})t}, \tag{12}$$

where

$$\lambda(\vec{k}) = i\vec{k}\cdot\vec{v}_0 - \sqrt{(k_x\beta_x)^2+(k_y\beta_y)^2+(k_z\beta_z)^2}. \tag{13}$$

The ODE looks as follows:

$$\frac{d^2}{dt^2}\tilde{H}_1(\vec{k},t) + \omega_p^2\tilde{H}_1(\vec{k},t) = \omega_p^2 Z\mathrm{e}^{-\lambda(\vec{k})t}, \tag{14}$$

This equation can be solved and the following expression for $\tilde{n}_1(\vec{k},t)$ can be obtained:

$$\tilde{n}_1(\vec{k},t) = \frac{\omega_p^2}{\omega_p^2+\lambda(\vec{k})^2}\left(1-\mathrm{e}^{-\lambda(\vec{k})t}\left(\cos(\omega_p t)-\frac{\lambda(\vec{k})}{\omega_p}\sin(\omega_p t)\right)\right). \tag{15}$$

Inverting the Fourier transform, it is possible to obtain the following expression for $n_1(\vec{x},t)$:

$$n_1(\vec{\bar{x}},t) = \frac{Z}{\pi^2 a_x a_y a_z}\int_0^{\psi}\psi_1\sin\psi_1\left(\psi_1^2+(\bar{x}+u_{0x}\psi_1)^2+(\bar{y}+u_{0y}\psi_1)^2+\right.$$
$$\left.+(\bar{z}+u_{0z}\psi_1)^2\right)^{-2}d\psi_1, \tag{16}$$

[1]In mathematics this distribution is known as the Cauchy distribution.

wherein normalized variables are defined as $\psi = \omega_p t$, $a_i = \beta_i/\omega_p$, $\bar{x}_i = x_i/a_i$, $u_{0i} = v_{0i}/\beta_i$, and $i = x,\, y,\, z$.

This result was a very important step forward in this theory. Before it, there were only numerical solutions of the equation (9), which are not very convenient. This result allowed to verify the PIC code for this problem, which is widely used for simulations of this process. This cannot be considered as a final result in this theory for the following reasons. This is done for the unrealistic infinite plasma. The unrealistic Lorentzian distribution is used. Although, its profile looks similar to the profile of realistic normal distribution, this distribution doesn't have mean and variance, while empirical velocity distribution, obviously, does. And, finally, this is still a 1D integral, which must be evaluated numerically. In the present thesis, we will address all this issues, in sections 2 and 4, we will present and discuss our results.

Another important result of the paper [9] is an expression for the density perturbation for $t \to \infty$. It was shown that for the equilibrium distributions satisfying $f_0(\vec{v}) = f_0(v)$,

$$\lim_{t\to\infty} n_1(\vec{\bar{x}}, t) = \frac{Z}{4\pi c_x c_y c_z} \frac{\mathrm{e}^{-\bar{r}}}{\bar{r}}, \tag{17}$$

where $c_i \equiv \sqrt{\eta_0}\beta_i/\omega_p$ for $i = x,\, y\, z$, $\bar{r} = \sqrt{x^2/a_x^2 + y^2/a_y^2 + z^2/a_z^2}$, and

$$\eta_0 = \left(4\pi\beta_x\beta_y\beta_z \int_0^\infty f_0(u)du \right)^{-1}. \tag{18}$$

In particular, this means that plasma oscillations are damped completely at infinity. We will elaborate on this a bit more in section 4.

Recently, Gang Wang, Michael Blaskiewicz, and Vladimir Litvinenko extended this theory and took into account longitudinal space charge fields [16].

1.1.3 Free electron lasers

Free electron laser (FEL) is a laser, in which radiation is produced by electrons moving through a magnetic structure called undulator. In the FEL, the beam of electrons moving with a speed close to the speed of light passes through a periodic magnetic field created by the undulator. Because of the

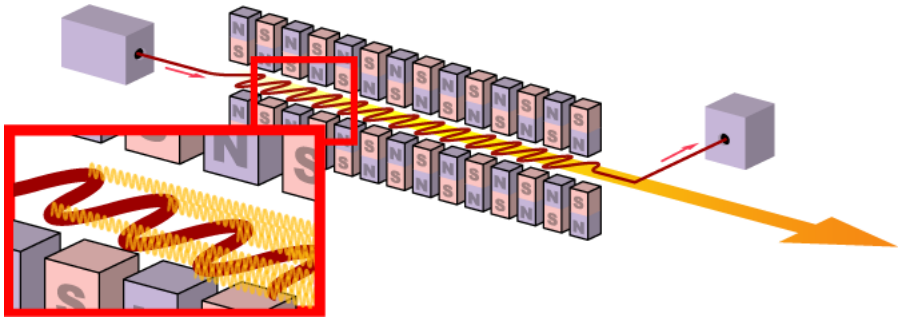

Figure 2: The scheme of a free electron laser. The set of alternating magnets is an undulator, an electron beam is shown as red line, and radiation is shown as a yellow arrow. The picture is taken from [17]

undulator magnetic field, electrons move along sinusoidal trajectories, i.e., they have alternating transverse accelerations and thus emit photons.

Suppose, N_u is a number of sections in the undulator and each section has length λ_u. We define the wavevector of the undulator k_u:

$$k_u = \frac{2\pi}{\lambda_u}. \tag{19}$$

We also introduce the radiation length seen by observer λ_1:

$$\lambda_1 = \frac{\lambda_u}{2\gamma^2}, \tag{20}$$

and corresponding wave vector k_1:

$$k_1 = \frac{2\pi}{\lambda_1}. \tag{21}$$

γ is a ratio of the electron's kinetic energy and its rest mass energy:

$$\gamma = \frac{E_e}{mc^2}, \tag{22}$$

typically, for free electron lasers, $\gamma \sim 10^3 - 10^4$. These notations will be used later. The FEL principle is illustrated in Fig. 2.

The free electron lasers are sources of an almost monochromatic radiation and radiation frequency ω_r is defined by a certain resonance condition [18].

We further develop the FEL theory in subsection 1.1.5, in section 3, and in appendix D.

In the CeC, the FEL is used in a non-standard way, i.e., the radiation is not used, instead, we are interested in amplification of the density perturbations in the electron beam. This effect will be discussed in subsection 1.1.5 and in section 3.

1.1.4 FEL section and kicker

In the FEL section, the perturbations generated in the modulator are amplified via the high gain FEL. The 1D FEL theory [18, 19, 20, 21, 22] can be used to derive expressions for the amplified perturbation density and for the density corresponding to the self-amplified spontaneous emission (SASE), which can be used to estimate the saturation length, providing the limitations on the density perturbations amplification, and, as a result, on performance of the whole CeC machine. In section 3, we derive these expressions, they contains many inverse integral transforms and can be evaluated numerically using the fast Forurier transform (FFT) algorithm.

In the kicker, the hadrons interact with the electric field produced by their own amplified density perturbations [23]. Mathematically, the problem is very similar to the one solved for the modulator, but, in the kicker, as initial density perturbation we have the hadron's charge and the amplified electron density from the FEL section. Solving for the Fourier image of the density perturbation, we can easily obtain the potential of the field in the Fourier domain. And then, doing the inverse Fourier transform we can compute the potential in the space domain.

1.1.5 Recent considerations of the FEL section

Theoretical model of the FEL section was recently developed by Stephen Webb, Gang Wang, and Vladimir Litvinenko [6]. The model was developed in the framework of the FEL theory described in the book by E. Saldin, E.V. Schneidmiller, M.V. Yurkov [18].

Dynamics of individual particles in the undulator is described by the

Hamilton's equations:

$$\frac{dH}{dz} = \frac{1}{c}\left[-\frac{1}{p_0}\left(\frac{e}{c}\right)^2 \vec{A}_u \cdot \vec{A}_\perp + \frac{e}{c}\frac{\partial A_z}{\partial t}\right], \tag{23}$$

$$\frac{dt}{dz} = \frac{1}{c}\left[1 + \frac{1}{2}\frac{1}{p_0^2}\left[\left(\frac{e}{c}\right)^2\left(A_u^2 + 2\vec{A}_u \cdot \vec{A}_\perp\right) + m^2c^2\right]\right], \tag{24}$$

where $p_0 = \frac{H}{c}$, $\vec{A}_u = \frac{B_u}{k_u}(\cos k_u z \vec{e}_y - \sin k_u z \vec{e}_x)$ is the undulator potential for the helical undulator and k_u is the wavevector of the undulator, $\vec{e}_x$, $\vec{e}_y$ are unit vectors, B_u is some constant, $\vec{A}_\perp$ is the laser field, and A_z is the longitudinal space charge.

Dynamics of the phase space density of the electron beam is described by the Vlasov equation:

$$\frac{\partial f}{\partial z} + \frac{dH}{dz}\frac{\partial f}{\partial H} + \frac{dt}{dz}\frac{\partial f}{\partial t} = 0. \tag{25}$$

Representing the density f as $f = f_0 + f_1$, where f_0 is a thermal background and f_1 is an instabilty, the Vlasov equation can be linearized:

$$\frac{\partial f_1}{\partial z} + \frac{1}{c}\left[1 + \frac{1}{2}\frac{1}{\gamma_0^2}\left(1 + K^2\right)\left(1 - 2\frac{E}{E_0}\right)\right]\frac{\partial f_1}{\partial t} + \\ + \left[\frac{1}{E_0}\left(\frac{e}{c}\right)^2 \vec{A}_u \cdot \frac{\vec{A}}{\partial t} + eE_z\right]\frac{\partial f_0}{\partial E} = 0, \tag{26}$$

where $K = \frac{eA_u}{m_e c^2}$ is the undulator parameter.

We define the longitudinal current density j_z via

$$j_z = -ec\int dH f_1, \tag{27}$$

and its Fourier transform $\tilde{j}_z$ via

$$j_z = \frac{1}{\sqrt{2\pi}3}\int d\nu d^2k_\perp \mathrm{e}^{i\vec{k}_\perp \vec{r}_\perp}\mathrm{e}^{i\nu\omega_r(z/c-t)}\mathrm{e}^{ik_u z}\mathrm{e}^{-ik_\perp^2 cz/(2\nu\omega_r)}\tilde{j}_z, \tag{28}$$

where ω_r is a radiation frequency. It is possible to solve the FEL equations

and obtain the following expression for $\tilde{j}_z$:

$$\tilde{j}_z\left(\hat{z},\hat{C},\vec{k}_\perp\right) = -\,ec\frac{\rho E_0}{2\nu}\int d\hat{E}\mathrm{e}^{i(\hat{C}+\hat{E}-k_\perp^2)\hat{z}}\tilde{f}_1\Big|_{\hat{z}=0} + \\ + \int d\hat{E}\int\limits_0^{\hat{z}} d\hat{z}'\,\mathrm{e}^{i(\hat{C}+\hat{E}-\hat{k}_\perp^2)(\hat{z}'-\hat{z})}\int d^2\hat{q}\mathrm{e}^{i(\hat{q}^2-\hat{k}_\perp^2)\hat{z}'}\times \\ \times\left[\int\limits_0^{\hat{z}'} d\hat{z}''\tilde{j}_z(\vec{q}) + i\hat{\Lambda}_p^2\tilde{j}_z(\vec{q})\right]\frac{d\hat{F}}{d\hat{E}}\hat{R}(\vec{q}-\vec{k}_\perp), \tag{29}$$

where dimensionless units were used and

$$\hat{C} = \frac{1-\nu}{\rho}, \tag{30}$$

$$\hat{\Lambda}_p^2 = \frac{8\pi e^2 n_0\Gamma^{-1}(1+K^2)}{\gamma_0^3 mc^3}, \tag{31}$$

$$\hat{E} = \frac{2\nu E}{\rho E_0}, \tag{32}$$

$$\hat{k}^2 = \frac{k^2 c\Gamma^{-1}}{2\nu\omega_r}, \tag{33}$$

n_0 is a normalization factor of f_0, i.e.,

$$f_0 = n_0 F(E)R(\vec{r}_\perp), \tag{34}$$

$$\Gamma = \left(\frac{E_0^2 c^2\gamma}{2\pi\nu e^3 K k_u n_0}\right)^{-\frac{1}{3}}, \tag{35}$$

and Pierce parameter is given by

$$\rho = \Gamma k_u^{-1}. \tag{36}$$

In the infinite beam approximation, $R(\vec{q}-\vec{r}_\perp) = \delta(\vec{q}-\vec{r}_\perp)$ and expression (29) can be significantly simplified and the following expression for the Laplace image (over z) of the electron density perturbation can be obtained:

$$\tilde{f}_1(s,\hat{C}_{3\mathrm{D}},\hat{k}_\perp,\hat{E}) = \int d\hat{E}' G_{\mathrm{FEL}}(s,\hat{C}_{3\mathrm{D}},\hat{k}_\perp,\hat{E}|\hat{E}')\;\tilde{f}_1(\hat{C}_{3\mathrm{D}},\hat{k}_\perp,\hat{E})\Big|_0, \tag{37}$$

where $G_{\mathrm{FEL}}(s, \hat{C}_{3\mathrm{D}}, \hat{k}_\perp, \hat{E}|\hat{E}')$ is the FEL Green's function:

$$G_{\mathrm{FEL}}(s, \hat{C}_{3\mathrm{D}}, \hat{k}_\perp, \hat{E}|\hat{E}') = \frac{\delta(\hat{E}-\hat{E}')}{s+i(\hat{C}_{3\mathrm{D}}+\hat{E})} + \cdots + \frac{1}{s+i(\hat{C}_{3\mathrm{D}}+\hat{E})} \times$$
$$\times \left[\frac{1}{s-\hat{D}(1-is\hat{\Lambda}_p^2)} + i\hat{\Lambda}_p^2 s \frac{1}{s-\hat{D}(1-is\hat{\Lambda}_p^2)} \right] \frac{d\hat{F}}{d\hat{E}} \frac{1}{s+i(\hat{C}_{3\mathrm{D}}+\hat{E})}, \quad (38)$$

$\hat{C}_{3\mathrm{D}} = \hat{C} - \hat{k}_\perp^2$, and $\tilde{f}_1(\hat{C}_{3\mathrm{D}}, \hat{k}_\perp, \hat{E})\Big|_0$ represents initial density perturbation.

The FEL Green's function has two components. The first one represents Landau damping and single-particle non-cooperative motion in the undulator, this process doesn't lead to gain and this component can be neglected, and the second one contains the growing roots of the dispersion relation and represents gain process of the FEL.

The expression (38) for the FEL Green's function is for arbitrary initial perturbation. For further details and application of the formula for some particular initial perturbation, we refer to [6], where finite beam case is also considered via eigenmode expansion.

1.2 Organization of the manuscript

In section 2, the test charge problem for the infinite plasma will be considered. We will introduce convenient dimensionless units, which also will be used in later sections with some modifications. General solution for the problem will be derived in terms of the inverse Laplace and Fourier transforms. For the 1D Cauchy equilibrium distributions, we will derive exact analytical solution, which will serve as a testing ground for the numerical solutions. For other 1D, 2D, and 3D distributions, we will present numerical solutions obtained using the fast Fourier transform algorithm. Some technical details regarding inversion of integral transforms and evaluation of the special functions used will be presented in the appendix.

In section 3, we will present our considerations for the FEL sections in the formalism of the 1D FEL theory [20, 22]. We will derive expressions for the amplified density in terms of the inverse integral transforms, they are closely related to the formulas for the modulator for the infinite plasma model.

In section 4, we will describe the test charge problem for the confined plasma. We will transform the Vlasov-Poisson system into the Fredholm

integral equation. We will derive two different equations, one is more general, but the other can be solved faster. We will describe in detail numerical methods for these equations and software that was developed for this problem. We will discuss parallelization of the algorithms for the systems with distributed memory; some algorithms will be discussed in the appendix. We will perform numerical tests of the software and show numerical results for some particular cases. We will conclude this section with discussion of the physics of the solutions.

We will summarize our results in section 5.

Many technical details of the work are discussed in appendixes.

2 Shielding of a charge in the infinite plasma

In this section, we will consider shielding of a charged particle in the infinite electron plasma [10, 24]. We will start with the Vlasov-Poisson system of equations, solve it via the Fourier and Laplace transforms. Then, we will derive an exact solution for the 1D Cauchy equilibrium distribution and show numerical results for other distributions.

2.1 The Vlasov-Poisson system

Generally, shielding of a charged particle in a plasma is described by the Vlasov-Poisson system of equations [25], i.e., the dynamics of the electron density is governed by the Vlasov equation and the electric field by the Poisson equation. We first describe the system in a co-moving frame of reference, then derive a formal solution via the integral transforms, then introduce convenient dimensionless variables, and finally write a solution for a particle moving along a straight line.

2.1.1 General formulation for an infinite plasma

We consider the Vlasov-Poisson system for the 1D, 2D and 3D plasmas simultaneously, which means that $\vec{x}$ is a one-, two- or three-dimensional vector depending on the dimensionality of the plasma we are considering and by x we denote its absolute value, even for the 1D case; the same conventions are applied for the dimensionless vectors that we will introduce in subsection 2.1.3. For the electron phase-space density $f(\vec{x}, \vec{p}, t)$, the Hamiltonian H, and the electric potential $U(\vec{x}, t)$, we have the Vlasov equation, the Hamilton's equations and the Poisson equation:

$$\frac{\partial f}{\partial t} + \vec{v} \cdot \frac{\partial f}{\partial \vec{x}} + \frac{d\vec{p}}{dt}\frac{\partial f}{\partial \vec{p}} = 0, \qquad f \equiv f(\vec{x}, \vec{p}, t), \tag{39}$$

$$\vec{v} = \frac{\partial H}{\partial \vec{p}}, \qquad \frac{d\vec{p}}{dt} = -\frac{\partial H}{\partial \vec{x}}, \qquad H = \frac{p^2}{2m_0} + eU(\vec{x}, t), \tag{40}$$

$$\frac{\partial^2}{\partial \vec{x}^2} U(\vec{x}, t) = -\frac{e}{\epsilon_0} n(\vec{x}, t), \quad n(\vec{x}, t) = \int f(\vec{x}, \vec{p}, t) d\vec{p}, \tag{41}$$

and the charge density is $en(\vec{x})$. For this system, we consider the test charge problem with an external time-dependent density $d(\vec{x}, t)$. We assume that $f = f_0 + f_1$, where $f_0 = f_0(\vec{v})$ is an equilibrium electron density, and $f_1 =$

$f_1(\vec{x}, \vec{p}, t)$ is an unknown perturbation resulting from the interaction with the test charge. The linearized Vlasov-Poisson system looks as follows:

$$\frac{\partial f_1}{\partial t} + \vec{v} \cdot \frac{\partial f_1}{\partial \vec{x}} - \frac{e}{m_0} \frac{\partial U}{\partial \vec{x}} \frac{\partial f_0}{\partial \vec{v}} = 0, \tag{42}$$

$$\frac{\partial^2}{\partial \vec{x}^2} U(\vec{x}, t) = -\frac{e}{\epsilon_0} \left(n_1(\vec{x}, t) + d(\vec{x}, t) \right). \tag{43}$$

2.1.2 Solving the Vlasov-Poisson system via the integral transforms

The Poisson equation (43) can be solved via the Fourier transform:

$$k^2 \tilde{U}(\vec{k}, t) = \frac{e}{\epsilon_0} \left(\tilde{n}_1(\vec{k}, t) + \tilde{d}(\vec{k}, t) \right), \tag{44}$$

where $\tilde{U}(\vec{k}, t)$, $\tilde{n}_1(\vec{k}, t)$, and $\tilde{d}(\vec{k}, t)$ are the Fourier images of the corresponding functions. Using this solution, we transform the equation (42) to [11]:

$$\tilde{N}_1(\vec{k}, s) = \frac{-e^2}{m_0 \epsilon_0} \mathcal{LF}_{\vec{k}t} \left(t f_0 \left(\vec{v} \right) \right) \left(\tilde{N}_1(\vec{k}, s) + \mathcal{LF} d(\vec{x}, t) \right), \tag{45}$$

where, $\tilde{N}_1(\vec{k}, s)$ and $\mathcal{LF} d(\vec{x}, t)$ are, respectively, the Laplace-Fourier images of $n_1(\vec{x}, t)$ and $d(\vec{x}, t)$:

$$\tilde{N}_1(\vec{k}, s) \equiv \mathcal{LF} n_1(\vec{x}, t) = \int_0^\infty \int n_1(\vec{x}, t) \mathrm{e}^{-i\vec{k} \cdot \vec{x} - ts} d\vec{x} dt, \tag{46}$$

$$\mathcal{LF} d(\vec{x}, t) = \int_0^\infty \int d(\vec{x}, t) \mathrm{e}^{-i\vec{k} \cdot \vec{x} - ts} d\vec{x} dt, \tag{47}$$

and

$$\mathcal{LF}_{\vec{k}t} \left(t f_0 \left(\vec{v} \right) \right) = \int_0^\infty \mathrm{e}^{-ts} t \int f_0 \left(\vec{v} \right) \mathrm{e}^{-i\vec{k} \cdot \vec{v} t} d\vec{v} dt. \tag{48}$$

Denoting the inverse Fourier and Laplace transforms, respectively, by $\mathcal{F}^{-1}$ and $\mathcal{L}^{-1}$, we obtain the following expression:

$$n_1(\vec{x},t) = -\frac{e^2}{m_0\epsilon_0}\mathcal{F}^{-1}\mathcal{L}^{-1}\frac{\mathcal{L}\mathcal{F}d(\vec{x},t)}{\left(\mathcal{L}\mathcal{F}_{\vec{k}t}\left(tf_0\left(\vec{v}\right)\right)\right)^{-1}+\frac{e^2}{m_0\epsilon_0}}, \tag{49}$$

for the details on definitions of the integral transforms and our notations, see appendix A. Generally, the expression (49) can be complex. Looking back to our initial equations and assuming complex f_1, we note that the equation with $\mathrm{Im}f_1$ corresponds to the equation without an external charge, while the equation with $\mathrm{Re}f_1$ is the one with it, consequently, $\mathrm{Im}f_1 = 0$ and it is confirmed by further computations. Hence, the expression (49) is real, as it should be.

Even though the Poisson equations and their Green's functions differ for the 1D, 2D, and 3D cases, their solutions in the Fourier domain (44) and the expression (49) for $n_1(\vec{x},t)$ have the same form.

In proceeding further, we need to specify the dimension of the problem, the external charge density $d(\vec{x},t)$, and the equilibrium distribution, but first we introduce dimensionless variables.

2.1.3 Introducing dimensionless variables

We define the dimensionless variables, denoting them using the sans-serif font, as follows:

$$\vec{\mathsf{x}} = \frac{\vec{x}}{r_\mathrm{D}},\ \vec{\mathsf{v}} = \frac{\vec{v}}{v_\mathrm{rms}},\ \mathsf{t} = \frac{t}{t_\mathrm{p}},\ \vec{\mathsf{k}} = \vec{k}r_\mathrm{D},\ \mathsf{s} = \frac{s}{\omega_\mathrm{p}}, \tag{50}$$

where

$$v_\mathrm{rms} = \sqrt{\frac{1}{\rho}\int v^2 f_0(\vec{v})d\vec{v}}, \quad \omega_\mathrm{p} \equiv \frac{1}{t_\mathrm{p}} = \sqrt{\frac{e^2\rho}{m_0\gamma\epsilon_0}}, \tag{51}$$

$$r_\mathrm{D} = \frac{v_\mathrm{rms}}{\omega_\mathrm{p}}, \tag{52}$$

are, respectively, the root-mean-square velocity, the plasma frequency, and the Debye radius. The equilibrium density is normalized via:

$$\int f_0(\vec{v})d\vec{v} = \rho. \tag{53}$$

We introduce the dimensionless equilibrium density $\mathsf{f}_0(\vec{\mathsf{v}})$ by the relation:

$$f_0(\vec{v}) = \rho f_d \mathsf{f}_0(\vec{\mathsf{v}}), \tag{54}$$

wherein all the dimensional constants are gathered into f_d and d stands for the dimensionality of the space, and can be 1, 2, or 3. We have the following dimensionalities for other quantities:

$$[\epsilon_0] = \frac{C^2T^2}{L^dM}, \quad [n(\vec{x},t)] = [\rho] = L^{-d}, \quad [f_d] = [v_{\text{rms}}]^{-d}. \tag{55}$$

We note that f_d and v_{rms} are not the same for the different equilibrium densities and must be computed via (51) and (54); for the non-integrable densities, the values have to be chosen voluntarily; among the densities we consider, only the Cauchy one is of that type. Using the dimensionless units, we rewrite formula (49) as follows:

$$\mathsf{n}_1(\vec{\mathsf{x}},\mathsf{t}) = -\mathsf{L}^{-1}\mathsf{F}^{-1}\left[\frac{\mathsf{LF}\big(\mathsf{d}(\vec{\mathsf{x}},\mathsf{t})\big)}{\big(\mathsf{LF}_{\vec{\mathsf{kt}}}(\mathsf{tf}_0(\vec{\mathsf{v}}))\big)^{-1}\frac{1}{f_d v_{\text{rms}}^d}+1}\right], \tag{56}$$

where $\mathsf{LF}\big(\mathsf{d}(\vec{\mathsf{x}},\mathsf{t})\big)$ and $\mathsf{LF}_{\vec{\mathsf{kt}}}(\mathsf{tf}_0(\vec{\mathsf{v}}))$ are the dimensionless analogs of (47) and (48), respectively, $\frac{1}{f_d v_{\text{rms}}^d}$ is a dimensionless factor, and L^{-1}, F^{-1} are the inverse Laplace and Fourier transforms for the dimensionless variables.

2.1.4 The external point charge

We assume that the charge's trajectory is unaffected by the space charge fields and consider the charge moving along a straight line $\vec{y}(t) = \vec{x}_0 + \vec{v}_0 t$, we have:

$$d(\vec{x},t) = -Z\delta\left(\vec{x} - \vec{y}(t)\right), \tag{57}$$

this assumption is reasonable for a hadron moving in an electron beam, as the hadron's mass is much larger than the electron's. For simplicity, we assume $Z = 1$ and the final density for the non-unitary charge can be recovered just by multiplying it by Z. Using the dimensionless units introduced, for any number of the spatial dimensions, we have:

$$\mathsf{LF}\big(\mathsf{d}(\vec{\mathsf{x}},\mathsf{t})\big) = -\int_0^\infty\int \delta\left(\vec{\mathsf{x}} - \vec{\mathsf{y}}(\mathsf{t})\right)\mathrm{e}^{-i\vec{\mathsf{k}}\cdot\vec{\mathsf{x}}-\mathsf{ts}}d\vec{\mathsf{x}}d\mathsf{t} = -\frac{\mathrm{e}^{-i\vec{\mathsf{k}}\cdot\vec{\mathsf{x}}_0}}{\mathsf{s}+i\vec{\mathsf{k}}\cdot\vec{\mathsf{v}}_0}, \tag{58}$$

$$\vec{\mathsf{y}}(\mathsf{t}) = \vec{\mathsf{x}}_0 + \vec{\mathsf{v}}_0\mathsf{t}. \tag{59}$$

Finally, we can write the expression for the electron density perturbation resulting from the interaction with the external charge moving along a straight line $\vec{\mathsf{y}}(\mathsf{t}) = \vec{\mathsf{x}}_0 + \vec{\mathsf{v}}_0\mathsf{t}$, valid in 1D, 2D, and 3D spaces:

$$\mathsf{n}_1(\vec{\mathsf{x}}, \mathsf{t}) = \mathsf{L}^{-1}\mathsf{F}^{-1}\left[\frac{\mathrm{e}^{-i\vec{\mathsf{k}}\cdot\vec{\mathsf{x}}_0}}{\left(\frac{f_d^{-1}v_{\mathrm{rms}}^{-d}}{\mathsf{LF}_{\vec{\mathsf{k}}\mathsf{t}}(\mathsf{tf}_0(\vec{\mathsf{v}}))}+1\right)\left(\mathsf{s}+i\vec{\mathsf{k}}\cdot\vec{\mathsf{v}}_0\right)}\right]. \tag{60}$$

In the next subsection, we consider this solution for some particular equilibrium densities $\mathsf{f}_0(\vec{\mathsf{v}})$; for each case, we just need to compute $\mathsf{LF}_{\vec{\mathsf{k}}\mathsf{t}}(\mathsf{tf}_0(\vec{\mathsf{v}}))$ and $f_d^{-1}v_{\mathrm{rms}}^{-d}$ and insert them into (60).

2.2 Application to the particular equilibrium distributions

Generally, the equilibrium distribution $\mathsf{f}_0(\vec{\mathsf{v}})$ has to be a solution of the unperturbed Vlasov equation, i.e., it has to be a function of the unperturbed Hamiltonian, in our dimensionless units it is v^2, thus we consider the following functions:

$$\delta(\mathsf{v}^2-1), \tag{61}$$

$$\Theta(-\mathsf{v}^2+1), \tag{62}$$

$$\mathrm{e}^{-\mathsf{v}^2}, \tag{63}$$

$$(1+\mathsf{v}^2)^{-\frac{1+d}{2}}. \tag{64}$$

They correspond to the Kapchinskij-Vladimirskij (KV) [1, 26], water-bag (WB), normal (or Maxwell), and Cauchy (or Lorentz) equilibrium distributions, $\Theta(v)$ stands for the Heaviside step function, d is the dimensionality of the space, and $\vec{\mathsf{v}}$ is a one-, two-, or three-dimensional vector. However, for the case of the infinite plasma that we are considering here, any function of velocity is a solution of the unperturbed Vlasov equation; thus, all our formulae can be easily generalized for the equilibrium distributions of the form:

$$\mathsf{f}_0\left(\sum_{i=1}^{d}(\mathsf{a}_i\mathsf{v}_i)^2\right), \tag{65}$$

corresponding to an anisotropic plasma, where a_i, $i = 1, ..., d$ are dimensionless constants characterizing the plasma's temperatures. The changes should

be applied only to the expression for $\mathsf{LF}_{\vec{\mathsf{kt}}}\left(\mathsf{tf}_0\left(\vec{\mathsf{v}}\right)\right)$, i.e., k_i should be substituted with $\mathsf{k}_i/\mathsf{a}_i$ for $i = 1, ..., d$, and the whole expression should be divided by $\prod_{i=1}^{d} \mathsf{a}_i$.

For the 1D Cauchy distribution, the inverse Laplace and Fourier transforms in (60) can be evaluated analytically, while for the other distributions, the numerical techniques should be applied. We describe the 1D Cauchy case in detail and just quote the results for the other distributions starting with the KV and WB, which have different expressions for $\mathsf{LF}_{\vec{\mathsf{kt}}}\left(\mathsf{tf}_0\left(\vec{\mathsf{v}}\right)\right)$ in spaces of different dimensionalities. We conclude this section with the Cauchy and normal distributions that have the same expressions for this quantity in all cases. Although, below we present v_{rms} computed via (51), we considered dimensionless equilibrium distributions, $\mathsf{f}_0\left(\vec{\mathsf{v}}\right)$, corresponding to

$$v_{\text{rms}} = \sqrt{\frac{H_c}{\beta}}, \tag{66}$$

with this v_{rms}, in all cases, $\frac{1}{f_d v_{\text{rms}}^d} = 1$ and $\mathsf{f}_0\left(\vec{\mathsf{v}}\right)$ has a simpler form.

2.2.1 1D Cauchy distribution

For the 1D Cauchy distribution, we have

$$f_0\left(\vec{v}\right) = \rho \frac{\beta}{H_c} \frac{1}{\pi\left(1 + \frac{\beta}{H_c} v^2\right)}, \tag{67}$$

where β and H_c are dimensional constants that can be used for fitting the experimental distributions. Computing $\mathcal{LF}_{\vec{kt}}\left(tf_0\left(\vec{v}\right)\right)$ via (48), we obtain the following expression:

$$\mathcal{LF}_{\vec{kt}}\left(tf_0\left(\vec{v}\right)\right) = \frac{\rho}{\left(s + k\sqrt{\frac{H_c}{\beta}}\right)^2}, \tag{68}$$

or, using the dimensionless variables:

$$\mathsf{f}_0(\vec{\mathsf{v}}) = \frac{1}{\pi\left(1 + \mathsf{v}^2\right)}, \quad \mathsf{LF}_{\vec{\mathsf{kt}}}\left(\mathsf{tf}_0\left(\vec{\mathsf{v}}\right)\right) = \frac{1}{(\mathsf{s} + \mathsf{k})^2}, \tag{69}$$

$$v_{\text{rms}} = \sqrt{\frac{H_c}{\beta}}, \quad f_d = \sqrt{\frac{\beta}{H_c}}, \quad \frac{1}{f_d v_{\text{rms}}^d} = 1. \tag{70}$$

Then, we insert the expression for $\mathsf{LF}_{\vec{\mathsf{kt}}}\left(\mathsf{tf}_0\left(\vec{\mathsf{v}}\right)\right)$ into the formula (60) and obtain:

$$\mathsf{n}_1\left(\vec{\mathsf{x}},\mathsf{t}\right)=\mathsf{L}^{-1}\mathsf{F}^{-1}\left[\frac{\mathrm{e}^{-i\vec{\mathsf{k}}\cdot\vec{\mathsf{x}}_0}}{\left(1+\left(\mathsf{s}+\mathsf{k}\right)^2\right)\left(\mathsf{s}+i\vec{\mathsf{k}}\cdot\vec{\mathsf{v}}_0\right)}\right]. \tag{71}$$

For all distributions we are considering, excepting the 1D Cauchy, the inverse integral transforms in the corresponding expressions for $\mathsf{n}_1\left(\vec{\mathsf{x}},\mathsf{t}\right)$ have to be inverted numerically, while, for the 1D Cauchy, they can be computed analytically giving the following expression:

$$\begin{aligned}\mathsf{n}_1\left(\vec{\mathsf{x}},\mathsf{t}\right)=&\frac{1}{4\pi}\frac{1}{\mathsf{v}_0-i}\left(\mathrm{e}^{-\mathcal{A}_+}\left(\mathrm{Ei}(\mathcal{A}_+)-\mathrm{Ei}(\mathcal{B}_+)\right)+\mathrm{e}^{\mathcal{A}_+}\left(\mathrm{E}_1(\mathcal{A}_+)-\mathrm{E}_1(\mathcal{B}_+)\right)\right)+\\&+\frac{1}{4\pi}\frac{1}{\mathsf{v}_0+i}\left(\mathrm{e}^{-\mathcal{A}_-}\left(\mathrm{Ei}(\mathcal{A}_-)-\mathrm{Ei}(\mathcal{B}_-)\right)+\mathrm{e}^{\mathcal{A}_-}\left(\mathrm{E}_1(\mathcal{A}_-)-\mathrm{E}_1(\mathcal{B}_-)\right)\right),\end{aligned} \tag{72}$$

where

$$\mathcal{A}_\pm=\frac{\mathsf{tv}_0-\mathsf{x}+\mathsf{x}_0}{1\pm i\mathsf{v}_0},\quad \mathcal{B}_\pm=\frac{\mathsf{x}_0-\mathsf{x}\pm i\mathsf{t}}{1\pm i\mathsf{v}_0}, \tag{73}$$

and $\mathrm{E}_1(z)$ and $\mathrm{Ei}(z)$ are the exponential integral functions [27] that can be computed via the series expansions, for details, see appendix B.1; for derivation of this formula, we refer to appendix C. The whole expression (72) is real even though it contains complex numbers.

In Figures 3 and 4, we show the densities obtained via the exact formula (72) and the ones obtained by the discussed in subsection 2.3 numerical inversion of the integral transforms for $\mathsf{x}_0=0$ and $\mathsf{v}_0=1.0$, 0.2, 10.0. We note perfect agreement of the exact solution and the numerical one. The solution has several interesting features, i.e., starting from some time, the left tail of the density has negative values, meaning that there is an accumulation of the charge of the same sign as that of the external perturbation, its maximum is oscillating, and the shape of the peak depends on the charge's velocity, being spiky for small velocities, widening as it increases, and, for large velocities, a discontinuity of the density's shape derivative appears in the right tail. All these features are equally well captured by the numerical computations and the analytical formula. We will comment further on the parameters' values in subsection 2.3.2.

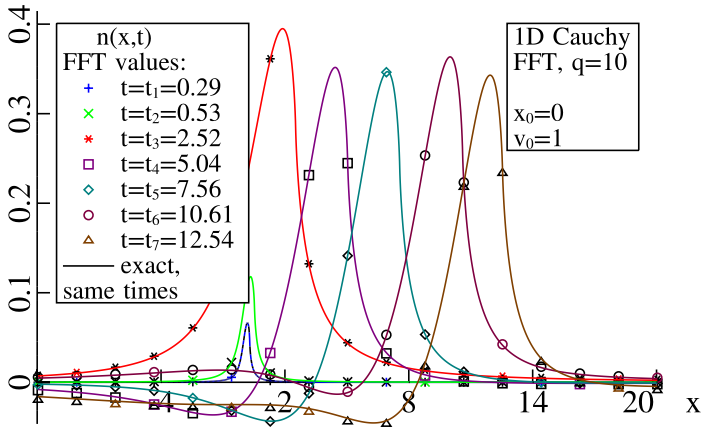

Figure 3: The density $\mathsf{n}_1(\vec{\mathsf{x}}, \mathsf{t})$ for the infinite plasma with the 1D Cauchy velocity distribution obtained via exact formula (72) and numerically via the FFT.

2.2.2 1D KV and WB distributions

For the 1D KV distribution, we have

$$f_0(\vec{v}) = \rho H_c \sqrt{\frac{\beta}{H_c}} \delta\left(\beta v^2 - H_c\right). \tag{74}$$

Using the dimensionless variables, we obtain:

$$\mathsf{f}_0(\vec{\mathsf{v}}) = \delta(\mathsf{v}^2 - 1), \quad \mathsf{LF}_{\vec{\mathsf{kt}}}\left(\mathsf{tf}_0\left(\vec{\mathsf{v}}\right)\right) = \frac{\mathsf{s}^2 - \mathsf{k}^2}{\left(\mathsf{s}^2 + \mathsf{k}^2\right)^2}, \tag{75}$$

$$v_{\text{rms}} = \sqrt{\frac{H_c}{\beta}}, \quad f_d = \sqrt{\frac{\beta}{H_c}}, \quad \frac{1}{f_d v_{\text{rms}}} = 1. \tag{76}$$

For the 1D WB, we have:

$$f_0\left(v\right) = \frac{1}{2}\rho\sqrt{\frac{\beta}{H_c}}\Theta\left(-\frac{\beta}{H_c}v^2 + 1\right), \tag{77}$$

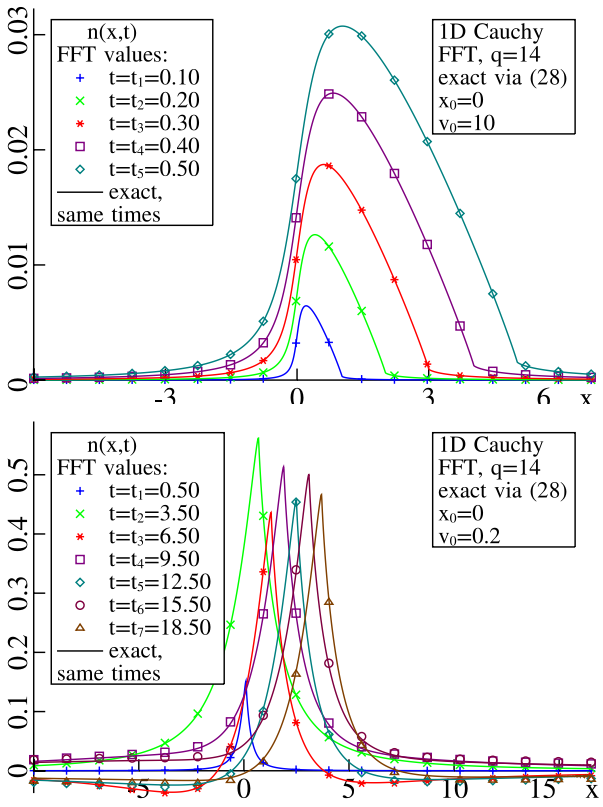

Figure 4: The exact values and the ones obtained numerically via the FFT for the 1D Cauchy distribution, for the various velocities of the external charge. Solid lines represent the exact values and the FFT values are shown by marks of different shapes regarding the times.

$$\mathsf{f}_0(\vec{\mathsf{v}}) = \frac{1}{2}\Theta(1-\mathsf{v}^2), \tag{78}$$

$$\mathsf{LF}_{\vec{\mathsf{kt}}}\left(\mathsf{tf}_0\left(\vec{\mathsf{v}}\right)\right) = \frac{1}{\mathsf{k}^2+\mathsf{s}^2}, \tag{79}$$

$$v_{\rm rms} = \frac{1}{\sqrt{3}}\sqrt{\frac{H_c}{\beta}}, \quad f_d = \sqrt{\frac{\beta}{H_c}}, \quad \frac{1}{f_d v_{\rm rms}} = \sqrt{3}. \tag{80}$$

2.2.3 2D KV and WB distributions

In the 2D case, we have for the KV distribution:

$$f_0\left(\vec{v}\right) = \rho H_c \frac{1}{\pi}\frac{\beta}{H_c}\delta\left(\beta v^2 - H_c\right), \tag{81}$$

$$\mathsf{f}_0(\vec{\mathsf{v}}) = \frac{1}{\pi}\delta\left(\mathsf{v}^2-1\right), \tag{82}$$

$$\mathsf{LF}_{\vec{\mathsf{kt}}}\left(\mathsf{tf}_0\left(\vec{\mathsf{v}}\right)\right) = \frac{\mathsf{s}}{\left(\mathsf{s}^2+\mathsf{k}^2\right)^{\frac{3}{2}}}, \tag{83}$$

$$v_{\rm rms} = \sqrt{\frac{H_c}{\beta}}, \quad f_d = \frac{\beta}{H_c}, \quad \frac{1}{f_d v_{\rm rms}^2} = 1, \tag{84}$$

and, for the 2D WB:

$$f_0\left(\vec{v}\right) = \rho\frac{\beta}{Hc}\frac{1}{\pi}\Theta\left(-\frac{\beta}{H_c}v^2+1\right), \tag{85}$$

$$\mathsf{f}_0(\vec{\mathsf{v}}) = \frac{1}{\pi}\Theta\left(1-\mathsf{v}^2\right), \quad \mathsf{LF}_{\vec{\mathsf{kt}}}\left(\mathsf{tf}_0\left(\vec{\mathsf{v}}\right)\right) = \frac{2}{\mathsf{k}^2}\frac{\sqrt{\mathsf{k}^2+\mathsf{s}^2}-s}{\sqrt{\mathsf{k}^2+\mathsf{s}^2}}, \tag{86}$$

$$v_{\rm rms} = \frac{1}{\sqrt{2}}\sqrt{\frac{H_c}{\beta}}, \quad f_d = \frac{\beta}{H_c}, \quad \frac{1}{f_d v_{\rm rms}^2} = 2. \tag{87}$$

2.2.4 3D KV and WB distributions

The expressions are slightly bulkier in the 3D case; we obtain for the 3D KV:

$$f_0\left(\vec{v}\right) = \rho\delta\left(\beta v^2 - H_c\right)\frac{1}{2\pi}H_c\left(\frac{\beta}{H_c}\right)^{3/2}, \tag{88}$$

$$\mathsf{f}_0(\vec{\mathsf{v}}) = \frac{1}{2\pi}\delta(\mathsf{v}^2 - 1), \tag{89}$$

$$\mathsf{LF}_{\vec{\mathsf{kt}}}\left(\mathsf{tf}_0\left(\vec{\mathsf{v}}\right)\right) = \frac{1}{2}\hat{I}(\mathsf{s}, \vec{\mathsf{k}}, 1), \tag{90}$$

$$v_{\mathrm{rms}} = \sqrt{\frac{H_c}{\beta}}, \quad f_d = \left(\frac{\beta}{H_c}\right)^{\frac{3}{2}}, \quad \frac{1}{f_d v_{\mathrm{rms}}^3} = 1, \tag{91}$$

where

$$\hat{I}(\mathsf{s}, \vec{\mathsf{k}}, \mathsf{v}) = \frac{i\mathsf{k}_3\mathsf{v}\left(\mathcal{S}_- - \mathcal{S}_+\right) + s\left(\mathcal{S}_- + \mathcal{S}_+\right)}{(\mathsf{s}^2 + \mathsf{k}^2\mathsf{v}^2)\mathcal{S}_-\mathcal{S}_+}, \tag{92}$$

$$\mathcal{S}_\pm = \sqrt{\left(\mathsf{s} \pm i\frac{\mathsf{k}_3^2\mathsf{v}}{\mathsf{k}}\right)^2}, \tag{93}$$

and k_3 is a third component of $\vec{\mathsf{k}}$; for the 3D WB, we obtain:

$$f_0\left(\vec{v}\right) = \rho\frac{3}{4\pi}\Theta\left(-\frac{\beta}{H_c}v^2 + 1\right)\left(\frac{\beta}{H_c}\right)^{3/2}, \tag{94}$$

$$\mathsf{f}_0(\vec{\mathsf{v}}) = \frac{3}{4\pi}\Theta(1 - \mathsf{v}^2), \tag{95}$$

$$\mathsf{LF}_{\vec{\mathsf{kt}}}\left(\mathsf{tf}_0\left(\vec{\mathsf{v}}\right)\right) = \frac{3}{2}\int_0^1 \mathsf{v}^2\hat{I}(\mathsf{s}, \vec{\mathsf{k}}, \mathsf{v})d\mathsf{v}, \tag{96}$$

$$v_{\mathrm{rms}} = \sqrt{\frac{3H_c}{5\beta}}, \quad f_d = \left(\frac{\beta}{H_c}\right)^{\frac{3}{2}}, \quad \frac{1}{f_d v_{\mathrm{rms}}^3} = \left(\frac{5}{3}\right)^{\frac{3}{2}}, \tag{97}$$

the integral in (96) has to be computed numerically.

2.2.5 Cauchy distribution

For the Cauchy distribution, we obtained the expressions valid in 1D, 2D, and 3D cases:

$$f_0\left(\vec{v}\right) = \rho\left(\frac{\beta}{H_c}\right)^{\frac{d}{2}} \frac{\Gamma(\frac{1+d}{2})}{\Gamma(\frac{1}{2})\pi^{\frac{d}{2}}}\left(1+\frac{\beta v^2}{H_c}\right)^{-\frac{1+d}{2}}, \tag{98}$$

$$\mathsf{f}_0(\vec{\mathsf{v}}) = \frac{\Gamma(\frac{1+d}{2})}{\Gamma(\frac{1}{2})\pi^{\frac{d}{2}}}\frac{1}{\left(1+\mathsf{v}^2\right)^{\frac{1+d}{2}}}, \tag{99}$$

$$\mathsf{LF}_{\vec{\mathsf{kt}}}\left(\mathsf{tf}_0\left(\vec{\mathsf{v}}\right)\right) = \frac{1}{\left(\mathsf{s}+\mathsf{k}\right)^2}, \tag{100}$$

$$v_{\mathrm{rms}} = \sqrt{\frac{H_c}{\beta}}, \quad f_d = \left(\frac{\beta}{H_c}\right)^{\frac{d}{2}}, \quad f_d^{-1} v_{\mathrm{rms}}^{-d} = 1. \tag{101}$$

2.2.6 Normal distribution

For the normal distribution, we also found universal formulas valid in 1D, 2D, and 3D cases:

$$f_0\left(\vec{v}\right) = \frac{\rho}{\pi^{d/2}}\left(\frac{H_c}{\beta}\right)^{-\frac{d}{2}} \exp^{-\frac{\beta v^2}{H_c}}, \tag{102}$$

$$\mathsf{f}_0(\vec{\mathsf{v}}) = \pi^{-\frac{d}{2}} \mathrm{e}^{-\mathsf{v}^2}, \tag{103}$$

$$\mathsf{LF}_{\vec{\mathsf{kt}}}\left(\mathsf{tf}_0\left(\vec{\mathsf{v}}\right)\right) = \frac{2}{\mathsf{k}^2}\left[1-\sqrt{\pi}\mathrm{e}^{\frac{\mathsf{s}^2}{\mathsf{k}^2}}\frac{s}{\mathsf{k}}\mathrm{Erfc}\frac{s}{\mathsf{k}}\right], \tag{104}$$

$$v_{\mathrm{rms}} = \sqrt{\frac{dH_c}{2\beta}},\ f_d = \left(\frac{\beta}{H_c}\right)^{\frac{d}{2}},\ f_d^{-1} v_{\mathrm{rms}}^{-d} = (2/d)^{\frac{d}{2}}, \tag{105}$$

where $\mathrm{Erfc}(z)$ is the complementary error function [27], for its definition and some computational details, see Appendix B.2.

2.3 Numerical methods and results

In this subsection, we briefly discuss numerical methods we employed and present our results.

2.3.1 A few remarks on integral transforms inversion

To evaluate expression (60) for a particular distribution, we first need to compute $\mathsf{LF}_{\vec{\mathsf{kt}}}\left(\mathsf{tf}_0\left(\vec{\mathsf{v}}\right)\right)$ via the formulas presented in the previous section; the

expressions are either elementary functions or include special functions or a one-dimensional integral, all these things can be computed straightforwardly. Next step is an evaluation of the inverse Fourier and Laplace transforms. It is well-known that the inverse Fourier transform can be approximated by the discreet Fourier transform and then computed using the FFT algorithm, for details, see appendix A. In this algorithm, the domain of interest of the resulting function is divided into $N = 2^q$ segments. The inverse Laplace transform can be expressed via the inverse Fourier transform:

$$\mathcal{L}^{-1}\tilde{f}\,(s) = \frac{\mathrm{e}^{\sigma t}}{2\pi}\int\limits_{-\infty}^{\infty}\tilde{f}\,(\sigma+ik)\,\mathrm{e}^{ikt}dk = \mathrm{e}^{\sigma t}\mathcal{F}_k^{-1}\tilde{f}\,(\sigma+ik)\,, \qquad (106)$$

which can be evaluated in a way that we described above, σ is a real constant greater than the real parts of all singularities of $\tilde{f}$. For more details on integral transforms, we refer to appendix A. In the upcoming subsection, we graphically present our results using the dimensionless units. We note that the dimensionless values for the different distributions are not always comparable to each other, since the values for v_{rms} can be different; the corresponding conversion factors should be applied.

2.3.2 Numeircal results

In this subsection, we discuss the results obtained numerically and shown in Figures 5, 6, 7, and 8; the velocity of the external charge, v_0, is measured in units of v_{rms} corresponding to the electron's density equilibrium distribution and the initial position of the charge, x_0, is measured in units of r_{D}. The possible space-time ranges differ for different distributions and are limited by the required precision and the number of points $N = 2^q$ in the FFT algorithm. For each plot, we increased q until the values stabilized; the values used are shown in the legends in each plot. The most well-behaving case corresponds to the Cauchy distribution, the KV and normal distributions require greater values of q. For the 1D Cauchy distribution, the numerical results were already shown in Fig. 4.

In Fig. 5, we show the densities computed numerically for all 1D distributions for $\mathsf{v}_0 = 1$. For the 1D KV distribution, we see that beam's response is a delta function-like peak, for the WB, the density is very spiked and asymmetric. For all distributions, excepting the KV, an accumulation of the

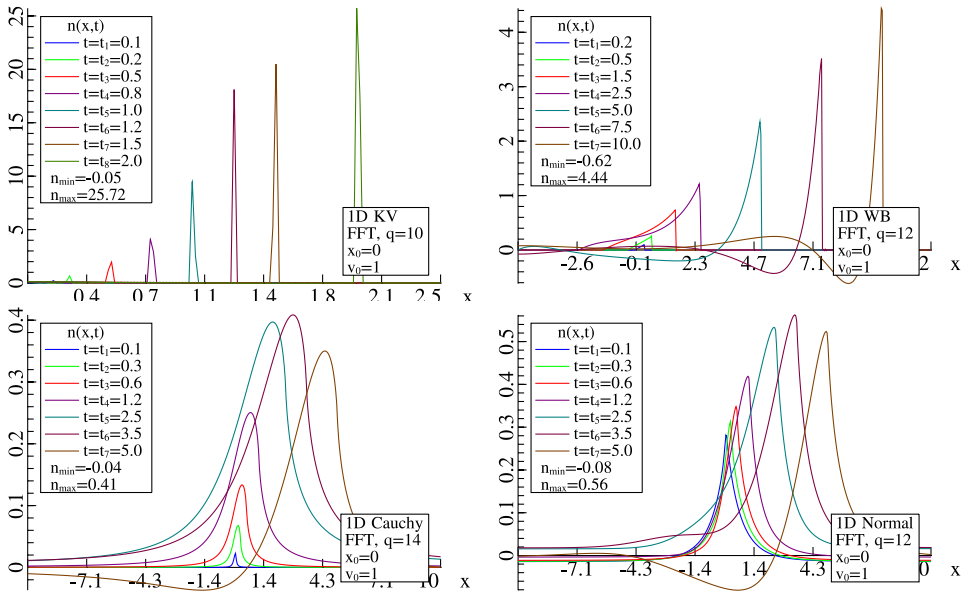

Figure 5: The density $n(\vec{\mathsf{x}}, \mathsf{t})$ for the KV, WB, normal, and Cauchy distributions in 1D space.

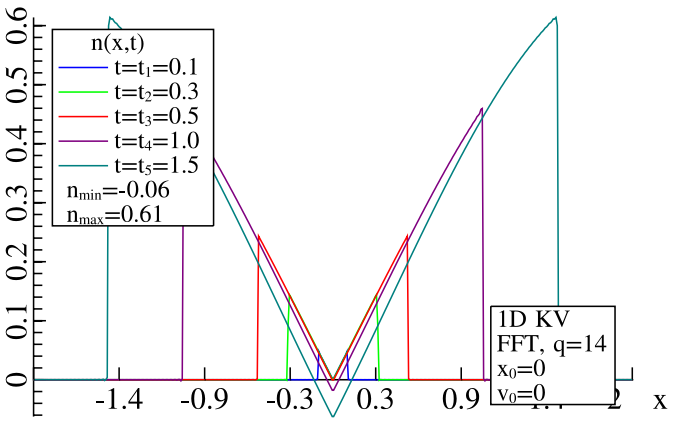

Figure 6: The density $n(\vec{\mathsf{x}}, \mathsf{t})$ for the 1D KV for $\mathsf{v}_0 = 0$.

charge of the same sign as the external charge occurs. For the normal equilibrium distribution, the perturbation is skewed and spiked resembling the shape of the α-stable distribution. For the Cauchy case, the perturbation is also skewed and spiked for $\mathsf{v}_0 \approx 10^{-1}$, as illustrated in Fig. 4. While all other distributions exhibit a symmetric peak around the external charge for $\mathsf{v}_0 = 0$, the KV distribution has two peaks that spread out with time, as shown in Fig. 6; with the increase of the velocity, the relative sizes of the peaks change, and, for $\mathsf{v}_0 = 1$, the left peak almost disappears and the right one looks almost like delta-function, as evidenced in Fig. 5.

In Fig. 7, the lines of equal densities, for a certain set of times, for all 2D distributions considered, are shown for $\mathsf{v}_0 = 4$. For the 2D KV distribution, we see spreading out delta function-like "fronts", similar to the 1D case for $\mathsf{v}_0 = 0$. For the 2D WB distribution, the lines are triangular with a peak following the charge. For the 2D Cauchy distribution, outer lines are almost circular; for the normal distribution, they have a bit more complicated shape. For the smaller velocities, the profiles are less directed toward the charge.

In Fig. 8, the lines of equal densities in certain planes, i.e., in three planes, each of which is parallel to the two out of the three coordinate axes, are illustrated. The shape of the lines for every distribution has the same features as the ones for 1D and 2D cases.

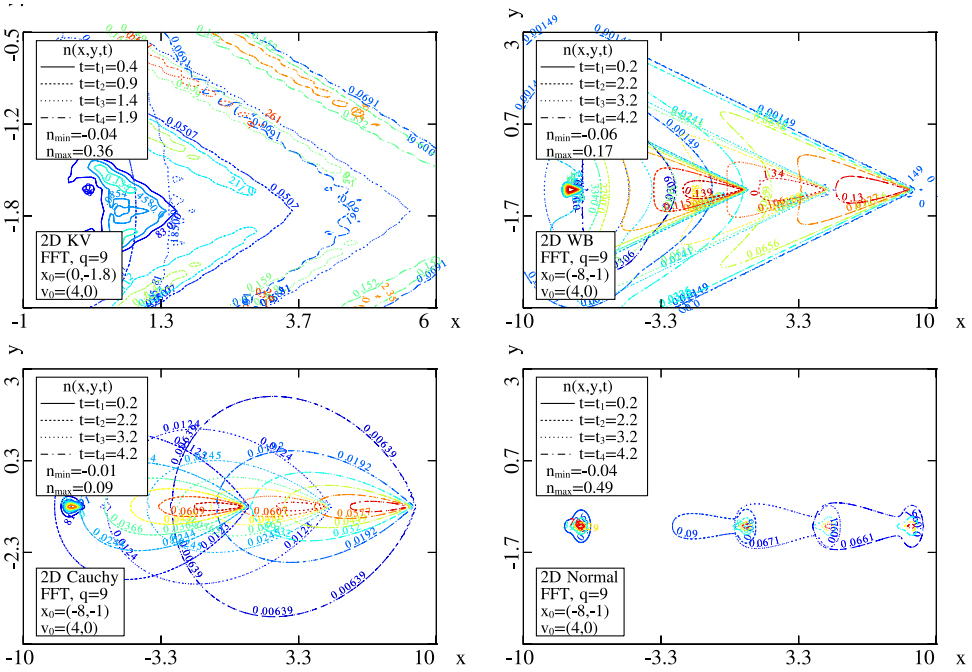

Figure 7: The density $n(\vec{\mathsf{x}}, \mathsf{t})$ for the KV, WB, normal, and Cauchy distributions in 2D space.

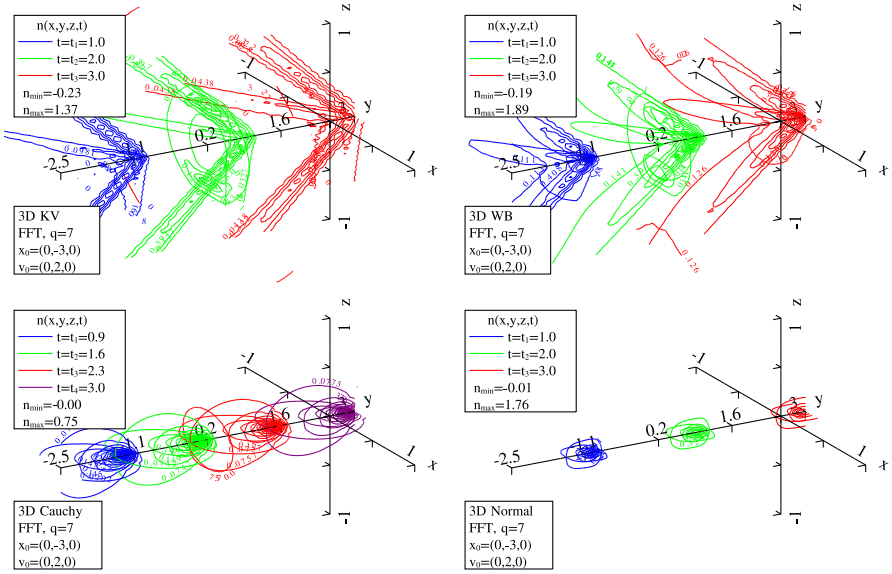

Figure 8: The density $n(\vec{\mathsf{x}}, \mathsf{t})$ for the KV, WB, normal, and Cauchy distributions in 3D space.

2.3.3 Discussion

Figure 3 compares the density perturbation for the 1D Cauchy distribution computed using the analytical expression (72) and the density obtained numerically via (60) using the FFT techniques that we detail in the appendix A. This plot shows that values obtained numerically via the FFT agree perfectly with the exact values. We use the same numerical methods to invert the integral transforms in (250) in our method for the Laplace-Fredholm equation.

In Fig. 5, plots for the density obtained via the expression (60) numerically for the 1D KV, WB, Cauchy and normal distributions are shown. For some time values, we see negative and smaller additional positive peaks. The main positive peaks follow the external charge with some delay.

In Fig. 3, for the density perturbation for the 1D Cauchy distribution, for $\mathsf{t} = 10.61$, we see a negative peak behind the main positive peak and another smaller positive peak behind the negative one; for $\mathsf{t} = 12.54$, we see a larger negative peak. Negative and small positive peaks can also be seen in Fig. 5 for the normal distribution for $\mathsf{t} = 5.0$ and for the WB distribution.

These are standard plasma oscillations, which are caused by appearance of the external charge in plasma.

An initial wave-like disturbance in plasma results in a damped traveling wave – this is well-known Landau damping [28]. Any disturbance can be represented as a superposition of such disturbances via Fourier integral, that means that Landau damping should be present in the solution of the test charge problem as well. However, unlike in classical Landau's consideration, in our case, the external excitation (charge) doesn't disappear immediately, but continues to exist in plasma. As a result, the Landau damping will lead to decay of the oscillations of the maximum of the perturbation, as we see in Fig. 3, and stationary perturbation will be established at infinity, as it was discussed in subsection 1.1.2.

In subsection 4.5, we shall see the results for the confined plasma, which also have these qualitative features.

2.3.4 The code

The method we discussed herein was implemented as an object-oriented program in C++. The solution is stored as a multidimensional array over some grid in space-time; for further usage, it can be evaluated for any point using interpolation. The program is easily expendable for other external charge densities and equilibrium distributions and, in particular, can deal with the empirical ones. The visualization is also very flexible: it is possible to adjust time values, the number of equal density lines, set the particular values of interest, and look at different projections and cross-sections of the 2D and 3D densities.

2.3.5 Application to the Proof-of-principle experiment

As it was mentioned in the introduction, the proof-of-principle (PoP) experiment is planned at Brookhaven National Laboratory and the corresponding facility is currently under construction [5]. In this subsection, we describe how the results can be applied to the modulator of the real device. To recover the dimensional quantities, we need the Debye radius and the plasma frequency; for the PoP, we have $r_{\mathrm{D}} = 4.65 \cdot 10^{-5}\,\mathrm{m}$ and $\omega_{\mathrm{p}} = 6.436 \cdot 10^{9}\,\mathrm{s}^{-1}$. We obtain for the dimensional density perturbation:

$$n_1\left(\vec{x},t\right) = \frac{1}{r_{\mathrm{D}}^d}\mathsf{n}_1\left(\frac{1}{r_{\mathrm{D}}}\vec{x},\omega_{\mathrm{p}}t\right), \tag{107}$$

where d is a spatial dimension of the problem, for the real 3D case, $d = 3$. For the PoP experiment, the modulator is constructed such that the interaction time is about one half of the plasma period, it depends on the hadron's velocity, as the modulator length is constant. The velocity is measured in units of v_{rms}, in the PoP experiment, we have $v_{\text{rms}} = 3.0 \cdot 10^5 \, \frac{\text{m}}{\text{s}}$. Our computations, shown in Fig. 5, demonstrate that extending the modulator up to a few plasma oscillations can significantly increase the density perturbation, i.e., its maximum will be up to four times greater. Further increasing of the modulation time doesn't increase the perturbation, as the modulator saturates, as shown in Fig. 5. The amplification of the perturbation in the FEL section is limited by the FEL saturation. For the model-independent description of the FEL saturation and its application to the theory of CeC, see [29] and [30], respectively. These considerations provide limitations on a possible amplified perturbation that we can get, which, in their turn, determine the performance of the CeC device.

2.4 Conclusion

In this section, we considered a possible way to model the modulator section of the coherent electron cooling, i.e., we developed a method for evaluating the dynamical shielding of an external charge in an infinite electron plasma; for the certain case, we found analytical solution. The software package that we developed gives reliable results for a variety of equilibrium distributions and initial conditions.

It is possible to use the same numerical methods to model other sections of the CeC. We derived formulae for the amplified density perturbations in the FEL section in terms of the inverse integral transforms. We will describe them in the next section.

3 FEL section

In the FEL section, the perturbations generated in the modulator are amplified via the high gain FEL. We apply the 1D FEL theory [20, 22, 18] to derive an expression for the amplified perturbation density and the density corresponding to the self-amplified spontaneous emission (SASE), which can be used to estimate the saturation length, providing the limitations on the density perturbations amplification, and, as a result, on a performance of the whole CeC machine. We start with the coordinate transformation from the modulator to the FEL section, then describe the FEL system of equations, and then solve it for the initial conditions corresponding to the perturbation from the modulator and the SASE.

3.1 From the modulator to the FEL amplifier

The modulator is described in a system of reference moving with the electron beam, however, the FEL theory is written in a laboratory frame, thus, we need to perform the Lorentz transformation, then we shift coordinates such that the hadron have coordinates $(z,t)=(0,0)$ by the end of the modulator section, then we introduce the standard independent variables in the FEL theory, (θ, z), a phase and a coordinate along the beam, via:

$$\begin{cases} \theta(z,t) = (k_1+k_u)z + ck_1 t, \\ z(z,t) = z, \end{cases} \tag{108}$$

the phase θ is the position relative to the bunch center, k_u and k_1 are wavevectors defined in (19) and (21), and c is a speed of light. The "reference electron" is the one that has $\theta = 0$, it has the same position as the hadron. It is well-known that the phase-space density is Lorentz-invariant, thus, if we assume that the velocity distribution of the density perturbation is $\delta(v)$ and using the relation $\eta = \frac{v}{c}$ ($\eta = \frac{\gamma-\gamma_r}{\gamma_r}$) – the relative energy deviation from the resonance [22]), valid for the ultra-relativistic beams, we obtain the following relation between the density perturbation $\mathsf{n}_1^{(\mathrm{lab})}(\theta, \mathsf{z})$ in the frame, which will be used as the initial perturbation in the FEL section, and the density perturbation $\mathsf{n}_1(\vec{\mathsf{z}}', \mathsf{t}')$ in the beam's frame:

$$\mathsf{n}_1^{(\mathrm{lab})}(\theta, \mathsf{z}) = \mathsf{n}_1\big(\mathsf{z}'(\theta, \mathsf{z}), \mathsf{t}'(\theta, \mathsf{z})\big), \tag{109}$$

and the discussed coordinate transformation is

$$\begin{cases} \mathsf{z}'(\theta,\mathsf{z}) & = \gamma\left(\mathsf{z}+\mathsf{L}_m-\beta\left(\frac{\theta-(\mathsf{k}_1+\mathsf{k}_u)\mathsf{z}}{\mathsf{k}_1}+\mathsf{ct}_i\right)\right), \\ \mathsf{t}'(\theta,\mathsf{z}) & = \frac{\gamma}{\mathsf{c}}\left(\frac{\theta-(\mathsf{k}_1+\mathsf{k}_u)\mathsf{z}}{\mathsf{k}_1}+\mathsf{ct}_i-\beta(\mathsf{z}+\mathsf{L}_m)\right), \end{cases} \tag{110}$$

where t_i is the time spent by the hadron in the modulator, typically, it is of the order of $\frac{1}{2}$ of the plasma osicllation:

$$\mathsf{t}_i \equiv \mathsf{t}_i(\vec{\mathsf{v}}_0') = \mathsf{L}_m\frac{\mathsf{c}+\beta\vec{\mathsf{v}}_0'}{\vec{\mathsf{v}}_0'\mathsf{c}+\beta\mathsf{c}^2}, \tag{111}$$

L_m is the length of the modulator and $\vec{\mathsf{v}}_0'$ is the hadron's velocity. In all these formulas we used the dimensionless units introduced before and all vectors are one-dimensional.

3.2 The 1D Maxwell-Vlasov system

In this subsection, we derive expression for the amplified density perturbation in the framework of the 1D FEL theory [19]. The slowly varying frequency domain amplitude of the radiation field $E_\nu(z)$ and the electron density distribution function $F(\theta,\eta,z)$, represented as a sum of a smooth background and a perturbation:

$$F(\theta,\eta,z) = F_0(\eta)+\delta F(\theta,\eta,z), \tag{112}$$

are governed by the 1D Maxwell-Vlasov equations:

$$\begin{cases} \left(\frac{\partial}{\partial z}+i\Delta\nu k_u\right)E_\nu(z) = -\chi_2 n_e\int d\eta\delta F_\nu(\eta,z), \\ \left(\frac{\partial}{\partial z}+2k_u\eta\frac{\partial}{\partial\theta}\right)\delta F(\theta,\eta,z) = -\chi_1\int E_\nu(z)\mathrm{e}^{i\theta\nu}d\nu\frac{d}{d\eta}F_0(\eta), \end{cases} \tag{113}$$

where we wrote $\delta F(\theta,\eta,z)$ in the Maxwell equation, as the smooth background doesn't contribute to the electric field. We refrer to appendix D.3 for explanations of the notations and derivation of the 1D FEL Maxwell-Vlasov system (113). The continuity equation can be solved via the method of unperturbed orbits:

$$\delta F(\theta,\eta,z) = \delta F(\theta^{(0)}(0),\eta,0)-\chi_1\int\limits_0^z\int E_\nu(z_1)\mathrm{e}^{i\theta^{(0)}(z_1)\nu}d\nu dz_1\frac{d}{d\eta}F_0(\eta), \tag{114}$$

where the unperturbed orbit is given by:

$$\theta^{(0)}\left(z_1\right) = \theta + 2k_u\eta\left(z_1 - z\right). \tag{115}$$

Then we insert this expression into the Maxwell equation and solve it via the Laplace transform:

$$E_\nu(z) = \frac{1}{2\pi i}\int\limits_{\sigma-i\infty}^{\sigma+i\infty}\frac{\mathrm{e}^{sz}}{D(s)}\Big[E_\nu(0) -$$

$$-\frac{\chi_2 n_e}{2\pi}\int\limits_0^\infty\int\int\int \mathrm{e}^{-i\nu\theta - sz_2}\delta F(\theta^{(0)}(0),\eta,0)d\theta d\eta dz_2\Big]ds, \tag{116}$$

where

$$D(s) = s + i\Delta\nu k_u - \bar{\rho}^3\int\frac{i\nu}{(s+2ik_u\eta\nu)^2}F_0(\eta)d\eta, \tag{117}$$

and $E_\nu(0)$ is the initial field, which we set to zero. To obtain the expression for the dynamics of the density perturbation we insert expression (116) for $E_\nu(z)$ into expression (114) for $\delta F(\theta,\eta,z)$. As the initial perturbation we can either consider the Klimontovich distribution function or the density perturbation formed in the modulator section. The first case corresponds to the SASE and the second one will give dynamics of the amplification of the perturbation in the FEL section. We consider them in order.

3.3 The SASE

As the initial perturbation we consider the Klimontovich function:

$$\delta F(\theta^{(0)}(0),\eta,0) = \frac{1}{N_\lambda}\sum_{j=1}^{N_e}\delta\big(\theta^{(0)}(0) - \theta_j\big)\delta\big(\eta - \eta_j\big), \tag{118}$$

where $N_\lambda = \lceil\lambda_1\frac{I}{ec}\rceil$ is the number of electrons on one radiation wavelength and N_e is the number of electrons in a bunch. θ_j and η_j are the initial phases and energies of the electrons. For the θ-independent background distribution, θ_j is distributed uniformly over the bunch and η_j are the random variables with the cumulative distribution function $F_0(\eta)$. Following the

route described in the previous subsection we obtain for the SASE density perturbation:

$$\delta\mathsf{n}(\theta,\mathsf{z}) = \frac{1}{N_\lambda}\sum_{j=1}^{N_e}\delta\big(\theta - 2\mathsf{k}_u\eta_j\mathsf{z} - \theta_j\big) -$$

$$-\frac{\Gamma^3}{N_\lambda}\mathsf{F}^{-1}_{\nu,\theta}\mathsf{L}^{-1}_{\mathsf{s},\mathsf{z}}\sum_{j=1}^{N_e}\frac{i\mathrm{e}^{-i\nu\hat{\theta}_j(0)}}{2i\nu\mathsf{k}_u\hat{\eta}_j(0)+\mathsf{s}}\frac{\nu\mathrm{e}^{-\mathsf{sz}}}{\mathsf{D}(\mathsf{s})}\mathcal{I}_1(\mathsf{s},\mathsf{z},\nu,\mathsf{k}_u), \tag{119}$$

where

$$\mathcal{I}_1(\mathsf{s},\mathsf{z},\nu,\mathsf{k}_u) = \int\frac{1-\mathrm{e}^{\mathsf{z}(\mathsf{s}+2i\mathsf{k}_u\eta\nu)}+\mathsf{sz}+2i\mathsf{k}_u\mathsf{z}\eta\nu}{\mathrm{e}^{2i\mathsf{k}_u\mathsf{z}\eta\nu}(\mathsf{s}+2i\mathsf{k}_u\eta\nu)^2}F_0(\eta)d\eta, \tag{120}$$

$$\mathcal{I}_2(\mathsf{s},\nu,\mathsf{k}_u) = \int\frac{i\nu}{(\mathsf{s}+2i\mathsf{k}_u\eta\nu)^2}F_0(\eta)d\eta, \tag{121}$$

$$\mathsf{D}(\mathsf{s}) = \mathsf{s} + i\Delta\nu\mathsf{k}_u - \Gamma^3\mathcal{I}_2(\mathsf{s},\nu,\mathsf{k}_u), \tag{122}$$

and Γ is our equivalent of the Pierce parameter defined via

$$\Gamma = (2\chi_1\chi_2 r_{\mathrm{D}}^{-1}\mathsf{n}_e\mathsf{k}_u)^{\frac{1}{3}}, \tag{123}$$

this definition is different from the conventional one. In formula (119), we used the dimensionless units. The saturation is reached when the SASE perturbation is of the order of $\frac{N_e}{N_\lambda}$. This solution can be used for any equilibrium distribution $F_0(\eta)$. Here we apply it for the KV distribution $F_0(\eta) = \delta(\eta)$ and obtain:

$$\delta\mathsf{n}(\theta,\mathsf{z}) = \frac{1}{N_\lambda}\sum_{j=1}^{N_e}\delta\big(\theta - 2\mathsf{k}_u\eta_j\mathsf{z} - \theta_j\big) -$$

$$-\frac{\Gamma^3}{N_\lambda}\mathsf{F}^{-1}_{\nu,\theta}\mathsf{L}^{-1}_{\mathsf{s},\mathsf{z}}\sum_{j=1}^{N_e}\frac{\mathrm{e}^{-i\nu\hat{\theta}_j(0)}}{\mathsf{s}}\frac{i\nu\mathrm{e}^{-\mathsf{sz}}}{\mathsf{D}(\mathsf{s})}\frac{(1-\mathrm{e}^{\mathsf{zs}}+\mathsf{sz})}{\mathsf{s}^2}, \tag{124}$$

$$\mathsf{D}(\mathsf{s}) = \mathsf{s} + i\Delta\nu\mathsf{k}_u - \Gamma^3\frac{i\nu}{\mathsf{s}^2}, \tag{125}$$

the inverse Laplace transform can be easily computed as the sum over the residues at the roots of the denominator and the inverse Fourier transform can be computed numerically via the FFT.

3.4 The smooth density perturbation

As the initial perturbation we can also use the perturbation formed in the modulator:

$$\delta n(\theta,0) = \mathsf{n}_1^{(\mathrm{lab})}(\theta, \mathsf{z}=0)\,, \tag{126}$$

and

$$\delta F(\theta^{(0)}(0),\eta,0) = \delta n\big(\theta - 2k_u\eta z, 0\big) F_0(\eta). \tag{127}$$

Following the procedure described in the beginning of this section, after quite lengthy computations we obtain:

$$\begin{aligned}
\delta\mathsf{n}(\theta,\mathsf{z}) &= \mathsf{n}_1\left(\mathsf{z}'(\theta - 2\mathsf{k}_u\eta\mathsf{z},0), \mathsf{t}'(\theta-2\mathsf{k}_u\eta\mathsf{z},0)\right) + \\
&+ \frac{\tilde{\chi}_{12}\mathsf{n}_e}{i}\mathsf{L}^{-1}_{\mathsf{s},\mathsf{z}}\mathsf{F}^{-1}_{\nu,\theta}\mathsf{F}^{-1}_{\vec{\mathsf{k}},\frac{L_m}{r_{\mathrm{D}}\gamma}}\Big\{\int \frac{\mathsf{M}(\vec{\mathsf{k}},\mathsf{s}_1^*(\vec{\mathsf{k}}))\mathrm{e}^{i\nu\mathsf{k}_1(\mathsf{ct}_i-\beta\mathsf{L}_m)}}{\frac{2\mathsf{k}_u\eta\gamma}{\mathsf{k}_1}\left(\frac{\mathsf{s}_1^*(\vec{\mathsf{k}})}{\mathsf{c}}+\vec{\mathsf{k}}\beta\right)+\mathsf{s}}\times \\
&\times \frac{F_0(\eta)}{\mathsf{D}(\mathsf{s})}d\eta\int\frac{1-\mathrm{e}^{2i\eta_1\mathsf{k}_u\nu\mathsf{z}-\mathsf{sz}}}{2i\eta_1\mathsf{k}_u\nu+\mathsf{s}}\frac{d}{d\eta_1}F_0(\eta_1)d\eta_1\Big\},
\end{aligned} \tag{128}$$

where $\tilde{\chi}_{12}$ and n_e are the dimensionless equivalents of $\chi_1\chi_2$ and n_e, the electron volume density, respectively, $\mathsf{M}(\vec{\mathsf{k}},\mathsf{s})$ is just the expression in square brackets in (60), $\mathsf{s}_1^*(\vec{\mathsf{k}})$ is defined via:

$$\mathsf{s}_1^*(\vec{\mathsf{k}}) = \frac{it_{\mathrm{p}}ck_1}{\gamma}\left(\frac{\vec{\mathsf{k}}\gamma\beta}{r_{\mathrm{D}}k_1}+\nu\right) = i\nu\frac{t_{\mathrm{p}}ck_1}{\gamma}+i\vec{\mathsf{k}}\frac{t_{\mathrm{p}}c\beta}{r_{\mathrm{D}}}, \tag{129}$$

$\mathsf{D}(\mathsf{s})$ is the same as in (122). $\mathsf{F}^{-1}_{\vec{\mathsf{k}},\frac{L_m}{r_{\mathrm{D}}\gamma}}$ denotes the inverse Fourier transform over $\vec{\mathsf{k}}$ evaluated at $\frac{L_m}{r_{\mathrm{D}}\gamma}$. Expressions for the perturbation formed in the modulator and for $\mathsf{M}(\vec{\mathsf{k}},\mathsf{s})$ for different distributions can be found in appendix D.2.

The expression (128) is valid for any equilibrium distribution $F_0(\eta)$. For the KV distribution $F_0(\eta)=\delta(\eta)$, we have:

$$\begin{aligned}
\delta\mathsf{n}(\theta,\mathsf{z}) &= \mathsf{n}_1\left(\mathsf{z}'(\theta,0),\mathsf{t}'(\theta,0)\right) - \\
&- \Gamma^3\mathsf{F}^{-1}_{\nu,\theta}\mathsf{L}^{-1}_{\mathsf{s},\mathsf{z}}\mathsf{F}^{-1}_{\vec{\mathsf{k}},\frac{\mathsf{L}_m}{\gamma}}\left[\frac{(1+\mathsf{sz})\mathrm{e}^{-\mathsf{sz}}-1}{\mathsf{s}^3\mathsf{D}(\mathsf{s})}\mathsf{M}\left(\vec{\mathsf{k}},i\nu\frac{\mathsf{ck}_1}{\gamma}+i\vec{\mathsf{k}}\mathsf{c}\beta\right)\nu\mathrm{e}^{i\nu\mathsf{k}_1(\mathsf{ct}_i-\beta\mathsf{L}_m)}\right],
\end{aligned} \tag{130}$$

as for the SASE case, the inverse Laplace transform can be easily computed as the sum over the residues at the roots of the denominator and the inverse Fourier transforms can be computed numerically via the FFT.

3.5 The kicker

In the kicker, hadrons interact with the electric field produced by their own amplified density perturbations. Mathematically, the problem is very similar to the one solved for the modulator, but, in the kicker, as initial density perturbation we have the hadron's charge and the amplified electron density from the FEL section. Solving for the Fourier image of the density perturbation, we can easily obtain the potential of the field in the Fourier domain. And then, doing the inverse Fourier transform we can compute the potential in the space domain.

3.6 Results and discussion

In this section we described the FEL section in the framework of the 1D FEL theory, it is possible to extend this description to the 3D FEL theory. The expressions for the amplified density perturbation and the SASE contribution are derived. Both of them are written using the inverse integral transforms, which can be computed numerically in the same way as it was done for the modulator section. The computation of the SASE contribution allows one to estimate the limitations of the amplification of the density modulation in the FEL section. The kicker can be described in a very similar way as the modulator. The numerical methods required for the computations for the every section are thoroughly tested in the modulator section and, undoubtedly, can be applied in other sections.

4 Shielding of a charge in the confined plasma

In this section, we present main results of the thesis. Here, we thoroughly study dynamical test charge problem for the confined plasma. We start with the Vlasov-Poisson system of equations. Then we transform it to the Fredholm integral equation of the second type for the Laplace image of the unknown perturbation, i.e., Laplace-Fredholm equation for the unknown perturbation. Then we describe and test numerical methods for such equations. The 3D physical problem requires a lot of computational resources. We describe parallelization of the algorithms and their optimizations. We conclude the section with numerical results for a model problem and describe physics of the results. The ideas of this method was first presented on IPAC 2012 [31] and then published in a present form in [32].

4.1 The test charge problem for a confined plasma

An interaction of a colisionless anisotropic plasma with an external charge with an electron density $d(\vec{x},t)$ in a center-of-momentum frame of the plasma can be described by the Vlasov-Poisson [25] system of equations:

$$\frac{\partial f}{\partial t}+\vec{v}\cdot\frac{\partial f}{\partial \vec{x}}+\frac{d\vec{p}}{dt}\cdot\frac{\partial f}{\partial \vec{p}}=0,\qquad f\equiv f(\vec{x},\vec{v},t), \tag{131}$$

$$\vec{v}=\frac{\partial H}{\partial \vec{p}},\qquad \frac{d\vec{p}}{dt}=-\frac{\partial H}{\partial \vec{x}},\qquad H=H_0+eU(\vec{x},t), \tag{132}$$

$$H\equiv H(\vec{x},\vec{p},t),\qquad H_0\equiv H_0(\vec{x},\vec{p}), \tag{133}$$

$$H_0=\sum_{i,j}x_i\alpha_{ij}x_j+\sum_{i,j}p_i\beta_{ij}p_j\equiv\vec{x}\cdot\hat{\alpha}\vec{x}+\vec{p}\cdot\hat{\beta}\vec{p}, \tag{134}$$

$$\frac{\partial^2}{\partial\vec{x}^2}U(\vec{x},t)=-\frac{e}{\epsilon_0}\left(n_1(\vec{x},t)+d(\vec{x},t)\right), \tag{135}$$

where the dynamics of the plasma's phase-space electron density $f(\vec{x},\vec{v},t)$ is governed by the Vlasov equation (131), and the electric potential $U(\vec{x},t)$ – by the Poisson equation (135); the charge density can be obtained by multiplying the electron density by an electron charge e: $\rho(\vec{x},t)=en(\vec{x},t)$.

$n_1(\vec{x},t)$ is a plasma's electron density perturbation, caused by an interaction with the external charge, that we are going to evaluate; it is related to the plasma's phase-space electron density perturbation $f_1(\vec{x},\vec{v},t)$ via

$$n_1(\vec{x},t) = \int f_1(\vec{x},\vec{v},t)d\vec{v}. \tag{136}$$

Also, we employ the Hamilton's equations (132), in which H is a total Hamiltonian that includes unperturbed equilibrium Hamiltonian H_0 and the contribution $eU(\vec{x},t)$, caused by the external charge and the plasma's electron density perturbation. In the unperturbed Hamiltonian H_0, the second term is a kinetic energy and $\hat{\beta}$ characterizes the plasma's anisotropy, while the first term is responsible for spatial confining of the plasma. In accelerator physics, $\hat{\alpha}$ is determined by the focusing magnetic fields in an accelerator. We consider the problem with a moving point charge with a density

$$d(\vec{x},t) = -Z\delta(\vec{x}-\vec{y}(t)), \tag{137}$$

where $\vec{y}(t)$ is its trajectory; we assume that the trajectory is unaffected by the space charge fields.

The Vlasov-Poisson system (131)-(135) differs from the one for the infinite plasma [10] only by the $\hat{\alpha}$-term in H_0. This term makes $\frac{\partial H_0}{\partial \vec{x}}$ nonzero and an extra term appears in the Vlasov equation, which makes it unsolvable by the methods that worked for the infinite plasma.

We consider the diagonal matrices in the unperturbed Hamiltonian H_0:

$$\alpha_{ij} = \alpha_i\delta_{ij}, \quad \beta_{ij} = \beta_i\delta_{ij}, \tag{138}$$

where δ_{ij} is the Kronecker delta. In this case,

$$H_0 = \sum_i \alpha_i x_i^2 + \sum_i \beta_i p_i^2, \tag{139}$$

$$\vec{v} = \frac{\partial H}{\partial \vec{p}}, \quad v_i = 2\beta_i p_i, \quad \vec{v} = \hat{\gamma}\vec{p}, \tag{140}$$

$$\text{where } \gamma_{ij} = \frac{\partial v_j}{\partial p_i} = 2\beta_i\delta_{ij}, \tag{141}$$

and,

$$\frac{d\vec{p}}{dt} = -\frac{\partial H}{\partial \vec{x}}, \quad -\frac{\partial H_0}{\partial x_i} = -2\alpha_i x_i, \quad \text{or} \quad -\frac{\partial H_0}{\partial \vec{x}} = -\hat{\eta}\vec{x}, \tag{142}$$

where $\eta_{ij} = 2\alpha_i\delta_{ij}$. Thus, we have

$$H_0 = \sum_i \alpha_i x_i^2 + \sum_i \frac{v_i^2}{4\beta_i}. \tag{143}$$

Introducing new notations

$$a_i = \alpha_i, \quad b_i = \frac{1}{4\beta_i}, \tag{144}$$

we rewrite the unperturbed Hamiltonian in a form:

$$H_0 = \sum_i a_i x_i^2 + \sum_i b_i v_i^2. \tag{145}$$

For the diagonal matrices, we have

$$\gamma_{ij} = \gamma_i\delta_{ij}, \quad \eta_{ij} = \eta_i\delta_{ij}, \quad \frac{\partial f}{\partial \vec{p}} = \hat{\gamma}\frac{\partial f}{\partial \vec{v}}. \tag{146}$$

For a fully confined symmetric 1D, 2D, or 3D plasmas, we have:

$$\alpha_i = \alpha, \;\; \beta_i = \frac{1}{2m_0}, \;\; b_i = \frac{m_0}{2}, \;\; \gamma_i = \frac{1}{m_0}, \eta_i = 2\alpha. \tag{147}$$

All our considerations are applicable to the 1D, 2D and 3D spaces. The only differences are in the expressions for the Green's function for the Poisson's equation (135) and in the units of the dimensional constants. These aspects are discussed in subsections 4.2.5 and 4.2.7, respectively.

4.2 Integral equation for the test charge problem

In the present subsection, we describe how the Vlasov-Poisson (131)-(135) system can be transformed into the Fredholm integral equation of the second type for the Laplace image of the density perturbation $n_1(\vec{x}, t)$. We use the method of unperturbed orbits to solve the linearized Vlasov equation, and then insert into the obtained equation an expression for the potential in the form of an integral of the Green's function multiplied by the electron density and $\frac{e}{\epsilon_0}$. We derived two different integral equations. The first one is for general orbits; the second is for periodic orbits only (for the fully confined plasma), but it involves integrals that can be evaluated faster. We describe these two methods in order.

4.2.1 Method for general orbits

We represent the phase-space electron density f, $f \equiv f(\vec{x}, \vec{v}, t_1)$, in a form $f = f_0 + f_1$, where f_0, $f_0 \equiv f_0(\vec{x}, \vec{v})$ is an equilibrium electron density and f_1, $f_1 \equiv f_1(\vec{x}, \vec{v}, t_1)$, is the unknown electron density perturbation, which satisfies the linearized Vlasov equation:

$$\frac{\partial f_1}{\partial t_1} + \vec{v} \cdot \frac{\partial f_1}{\partial \vec{x}} - \frac{\partial H_0}{\partial \vec{x}} \hat{\gamma} \frac{\partial f_1}{\partial \vec{v}} = e \frac{\partial U}{\partial \vec{x}} \hat{\gamma} \frac{\partial f_0}{\partial \vec{v}}, \tag{148}$$

where we denoted the time variable as t_1 just for future convenience and introduced the notation:

$$\vec{a}\, \hat{b}\, \vec{c} \equiv \sum_i a_i b_{i,i} c_i = \vec{a} \cdot \hat{b} \vec{c}, \tag{149}$$

where $\hat{b}$ is a diagonal matrix. The third term in equation (148) represents interaction of the perturbation with the focusing fields and the term in the right-hand side represents interaction of the unknown perturbation and external charge with the equilibrium space-charge filed; it will be clear from (155). After substituting

$$\begin{array}{c} \vec{x} = \vec{X}_0 (t_1), \\ \vec{v} = \vec{V}_0 (t_1), \end{array} \tag{150}$$

where $\vec{X}_0 (t_1)$, $\vec{V}_0 (t_1)$ are the unperturbed orbits, the solutions of the following Hamilton's system:

$$\dot{\vec{X}}_0 (t_1) = \vec{V}_0 (t_1), \quad \dot{\vec{V}}_0 (t_1) = -\hat{\gamma} \frac{\partial H_0}{\partial \vec{X}_0 (t_1)}, \tag{151}$$

with the initial conditions:

$$\vec{X}_0 (t) = \vec{x}, \quad \vec{V}_0 (t) = \vec{v}, \tag{152}$$

into the equation (148), terms in its left-hand side will be equal to a full time derivative of f_1:

$$\frac{d}{dt_1} f_1 (\vec{x}, \vec{v}, t_1) = e \left. \frac{\partial U}{\partial \vec{x}} \hat{\gamma} \frac{\partial f_0}{\partial \vec{v}} \right|_{\begin{array}{c} \vec{x} = \vec{X}_0 (t_1) \\ \vec{v} = \vec{V}_0 (t_1) \end{array}}. \tag{153}$$

With a reasonable initial condition $f_1(\vec{x},\vec{v},0) = 0$, this equation can be integrated:

$$f_1(\vec{x},\vec{v},t) = e\int_0^t \frac{\partial U}{\partial \vec{x}}\hat{\gamma}\frac{\partial f_0}{\partial \vec{v}}\Bigg|_{\substack{\vec{x}=\vec{X}_0(t_1)\\ \vec{v}=\vec{V}_0(t_1)}} dt_1. \tag{154}$$

When plasma oscillations are considered [33], an equation analogous to (154) is already a solution, since in this case, U is a known quantity and doesn't depend on f_1. In our case, this is not a solution yet, since U depends on f_1.

Assuming boundary conditions at infinity, we have for the electric potential:

$$U(\vec{x},t_1) = U_1(\vec{x},t_1) + U_2\big(\vec{x},t_1\big) = \tag{155}$$

$$= \frac{e}{\epsilon_0}\int n_1(\vec{x}^{\,\prime},t_1)G(\vec{x},\vec{x}^{\,\prime})d\vec{x}^{\,\prime} - Z\frac{e}{\epsilon_0}G\big(\vec{x},\vec{Y}(t_1)\big), \tag{156}$$

where $G(\vec{x},\vec{x}^{\,\prime})$ is the Green's function for the Poisson equation, $U_1(\vec{x})$ is a potential of the plasma's electron density perturbation, and $U_2(\vec{x})$ is a potential of the hadron and $\vec{Y}(t_1)$ is its trajectory. Inserting (156) into (154) and integrating over $\vec{v}$, we obtain

$$n_1(\vec{x},t) = \frac{e^2}{\epsilon_0}\int_0^t\int n_1\big(\vec{x}^{\,\prime},t_1\big)\int \frac{\partial G(\vec{x},\vec{x}^{\,\prime})}{\partial \vec{x}}\hat{\gamma}\frac{\partial f_0}{\partial \vec{v}}\Bigg|_{\substack{\vec{x}=\vec{X}_0(t_1)\\ \vec{v}=\vec{V}_0(t_1)}} d\vec{v}d\vec{x}^{\,\prime}dt_1 +$$

$$+e\int_0^t\int \frac{\partial U_2\big(\vec{x},t_1\big)}{\partial \vec{x}}\hat{\gamma}\frac{\partial f_0}{\partial \vec{v}}\Bigg|_{\substack{\vec{x}=\vec{X}_0(t_1)\\ \vec{v}=\vec{V}_0(t_1)}} d\vec{v}dt_1. \tag{157}$$

The first term in the right-hand side can be considered as a convolution over time, since the unperturbed orbits are functions of $(t-t_1)$, as we shall show in subsection 4.2.2. Applying the Laplace transform over t, and taking into account that the Laplace image of a convolution of two functions equals a

product of their Laplace images, we obtain

$$N_1(\vec{x},s)=\frac{e^2}{\epsilon_0}\int N_1\big(\vec{x}^{'},s\big)\mathcal{L}\int\frac{\partial G(\vec{x},\vec{x}^{'})}{\partial\vec{x}}\hat{\gamma}\frac{\partial f_0}{\partial\vec{v}}\Bigg|_{\substack{\vec{x}=\vec{X}_0(0)\\ \vec{v}=\vec{V}_0(0)}} d\vec{v}d\vec{x}^{'}+$$

$$+e\mathcal{L}\int_0^t\int\frac{\partial U_2\big(\vec{x},t_1\big)}{\partial\vec{x}}\hat{\gamma}\frac{\partial f_0}{\partial\vec{v}}\Bigg|_{\substack{\vec{x}=\vec{X}_0(t_1)\\ \vec{v}=\vec{V}_0(t_1)}} d\vec{v}dt_1, \quad (158)$$

where $\mathcal{L}$ is a Laplace transform operator and

$$N_1(\vec{x},s)\equiv\mathcal{L}n_1(\vec{x},t) \quad (159)$$

is a Laplace image of the unknown function $n_1(\vec{x},t)$. Equation (158) is the Fredholm integral equation of the second type with a kernel

$$K\big(\vec{x},\vec{x}^{'},s\big)=\mathcal{L}\int\frac{\partial G(\vec{x},\vec{x}^{'})}{\partial\vec{x}}\hat{\gamma}\frac{\partial f_0}{\partial\vec{v}}\Bigg|_{\substack{\vec{x}=\vec{X}_0(0)\\ \vec{v}=\vec{V}_0(0)}} d\vec{v}, \quad (160)$$

and a left-hand side

$$F(\vec{x},s)=-Z\frac{e^2}{\epsilon_0}\mathcal{L}\int_0^t\int\frac{\partial G\big(\vec{x},\vec{Y}(t_1)\big)}{\partial\vec{x}}\hat{\gamma}\frac{\partial f_0}{\partial\vec{v}}\Bigg|_{\substack{\vec{x}=\vec{X}_0(t_1)\\ \vec{v}=\vec{V}_0(t_1)}} d\vec{v}dt_1. \quad (161)$$

With these notations, the equation can be written in a standard form:

$$F(\vec{x},s)=N_1\big(\vec{x},s\big)-\lambda\int N_1\big(\vec{x}^{'},s\big)K\big(\vec{x},\vec{x}^{'},s\big)d\vec{x}^{'}, \quad (162)$$

where $\lambda=\frac{e^2}{\epsilon_0}$.

4.2.2 Unperturbed orbits

In some cases, the Hamilton's equations (151) with the initial conditions (152) can be solved exactly. For example, for the Hamiltonian (143), we have

$$X_{0i}(t_1)=x_i\cos\left(\omega_i\left(t-t_1\right)\right)-\frac{v_i}{\omega_i}\sin\left(\omega_i\left(t-t_1\right)\right), \quad (163)$$

$$V_{0i}(t_1)=v_i\cos\left(\omega_i\left(t-t_1\right)\right)+x_i\omega_i\sin\left(\omega_i\left(t-t_1\right)\right), \quad (164)$$

where $\omega_i = \sqrt{\gamma_i \eta_i}$ and i is a vector index, $i = 1, \ldots, d$, where d is a dimensionality of the space. The Hamilton's system (151) with the initial conditions (152) defines a map from the phase space to the space of trajectories:

$$(\vec{x}, \vec{v}, t) \longmapsto \left(\dot{\vec{X}}_0 (\cdot), \dot{\vec{V}}_0 (\cdot) \right). \tag{165}$$

We call the orbits (163), (164) elliptical; and spherical, if all ω_i are equal.

When H_0 does not depend on $\vec{x}$, all ω_i equal zero, and we obtain orbits for the infinite plasma:

$$X_{0i} (t_1) = x_i - v_i (t - t_1), \tag{166}$$

$$V_{0i} (t_1) = v_i. \tag{167}$$

For an electron beam finite in the transverse direction, and infinite in longitudinal, we have the orbits (163), (164) for the transverse directions and (166), (167) for the longitudinal one. We will call the unperturbed orbits simply orbits or trajectories.

4.2.3 On integration domain

Generally, the domain of the integral equation is $\mathbb{R}^3$. However, the numerical methods for integral equation are developed for a finite domain, so we need to transform these infinite regions to finite ones. In this subsection, we describe changes of variables, which can transform an integral equation with infinite domain to the one with the finite.

Suppose, we have an equation with semi-infinite domain:

$$n (x) = \int_0^\infty n(x') K(x, x') dx'. \tag{168}$$

Introducing a function

$$x (y) = \frac{1 - y}{y}, \tag{169}$$

we have

$$m (y) = \int_0^1 m\big(y'\big) K\big(x\big(y\big), x\big(y'\big)\big) \frac{1}{y'^2} dy', \tag{170}$$

and

$$n\left(x\right)=m\left(y\left(x\right)\right),\quad y\left(x\right)\equiv x^{-1}\left(x\right)=\frac{1}{x+1}, \tag{171}$$

this transforms domain [0, ∞] to [0, 1].

For double-infinite domain, we have

$$n\left(x\right)=\int\limits_{-\infty}^{\infty}n\left(x^{'}\right)K\left(x,x^{'}\right)dx^{'}, \tag{172}$$

here we take

$$x\left(y\right)=\tan y, \tag{173}$$

and

$$m\left(y\right)=\int\limits_{-\frac{\pi}{2}}^{\frac{\pi}{2}}m\left(y^{'}\right)K\left(x\left(y\right),x\left(y^{'}\right)\right)\frac{1}{\cos^{2}y^{'}}dy^{'}, \tag{174}$$

and

$$n\left(x\right)=m\left(y\left(x\right)\right),\quad y\left(x\right)\equiv x^{-1}\left(x\right)=\arctan x, \tag{175}$$

this transforms domain [$-\infty$, ∞] to [$-\frac{\pi}{2}$, $\frac{\pi}{2}$].

In our physical problem, in the kernel, there is an equilibrium distribution, which tends to zero quite fast, and it is possible just to cut the tails of the distribution, since they do not contribute. For example, if we have normal distribution, we can safely consider "four-sigma" interval instead of infinite domain, we will discuss it in more detail in subsection 4.5.

4.2.4 Method for periodic orbits

In this subsection, we describe a method suitable for the periodic orbits with the same periods in all dimensions, spherical orbits fall into this category. Instead of integrating from 0 to t, as in (154), for the case of periodic trajectories, we can integrate the linearized Vlasov equation from t to $t+\frac{2\pi}{\omega}$,

where $\frac{2\pi}{\omega}$ is the orbits' period. We start with the linearized Vlasov equation (148), as before:

$$\frac{\partial f_1}{\partial t_1} + \vec{v} \cdot \frac{\partial f_1}{\partial \vec{x}} = \frac{\partial H_0}{\partial \vec{x}} \hat{\gamma} \frac{\partial f_1}{\partial \vec{v}} + e \frac{\partial U}{\partial \vec{x}} \hat{\gamma} \frac{\partial f_0}{\partial \vec{v}}, \tag{176}$$

then, taking into account

$$\mathcal{L} \frac{\partial f_1(t_1)}{\partial t_1} = sF_1(s) - f_1(0), \text{ in our case } f_1(0) = 0, \tag{177}$$

where $f_1(t_1) \equiv f_1$ and F_1 is the Laplace image of f_1, $F_1 \equiv F_1(s) \equiv F_1(\vec{x}, \vec{v}, s)$, we do the Laplace transform of the equation and then multiply it by $\mathrm{e}^{t_1 s}$:

$$sF_1 \mathrm{e}^{t_1 s} + \vec{v} \cdot \frac{\partial F_1}{\partial \vec{x}} \mathrm{e}^{t_1 s} = \frac{\partial H_0}{\partial \vec{x}} \hat{\gamma} \frac{\partial F_1}{\partial \vec{v}} \mathrm{e}^{t_1 s} + e \frac{\partial \bar{U}}{\partial \vec{x}} \hat{\gamma} \frac{\partial f_0}{\partial \vec{v}} \mathrm{e}^{t_1 s}. \tag{178}$$

Taking into account that

$$\frac{\partial}{\partial t_1} \left(F_1(s) \mathrm{e}^{t_1 s} \right) = sF_1(s) \mathrm{e}^{t_1 s}, \tag{179}$$

we obtain

$$\begin{aligned} \frac{\partial}{\partial t_1} \left(F_1(s) \mathrm{e}^{t_1 s} \right) + \vec{v} \cdot \frac{\partial}{\partial \vec{x}} \left(F_1(s) \mathrm{e}^{t_1 s} \right) = \\ = \frac{\partial H_0}{\partial \vec{x}} \hat{\gamma} \frac{\partial}{\partial \vec{v}} \left(F_1(s) \mathrm{e}^{t_1 s} \right) + e \frac{\partial \left(\bar{U}(s) \mathrm{e}^{t_1 s} \right)}{\partial \vec{x}} \hat{\gamma} \frac{\partial f_0}{\partial \vec{v}}; \end{aligned} \tag{180}$$

then, doing substitution

$$\begin{aligned} \vec{x} &= \vec{X}_0(t_1), \\ \vec{v} &= \vec{V}_0(t_1), \end{aligned} \tag{181}$$

where $\vec{X}_0(t_1)$, $\vec{V}_0(t_1)$ are the unperturbed orbits, we obtain

$$\frac{d}{dt_1} \left(F_1(\vec{X}_0(t_1), \vec{V}_0(t_1), s) \mathrm{e}^{t_1 s} \right) = e \left. \frac{\partial \left(\bar{U}(\vec{x}, s) \mathrm{e}^{t_1 s} \right)}{\partial \vec{x}} \hat{\gamma} \frac{\partial f_0(\vec{x}, \vec{v})}{\partial \vec{v}} \right|_{\substack{\vec{x} = \vec{X}_0(t_1) \\ \vec{v} = \vec{V}_0(t_1)}}. \tag{182}$$

Then we integrate this equation over t_1:

$$F_1(\vec{X}_0(t+\frac{2\pi}{\omega}),\vec{V}_0(t+\frac{2\pi}{\omega}),s)\mathrm{e}^{\left(t+\frac{2\pi}{\omega}\right)s} - F_1(\vec{X}_0(t),\vec{V}_0(t),s)\mathrm{e}^{ts} = \\ = e\int\limits_t^{t+\frac{2\pi}{\omega}} \frac{\partial\left(\bar{U}(\vec{x},s)\mathrm{e}^{t_1 s}\right)}{\partial\vec{x}}\hat{\gamma}\frac{\partial f_0(\vec{x},\vec{v})}{\partial\vec{v}}\Bigg|_{\substack{\vec{x}=\vec{X}_0(t_1)\\ \vec{v}=\vec{V}_0(t_1)}} dt_1, \qquad (183)$$

where $\bar{U}(\vec{x},s)$ is the Laplace image of the potential. Using periodicity of the trajectories and initial conditions (152), we obtain

$$F_1(\vec{x},\vec{v},s) = e\frac{\mathrm{e}^{-ts}}{\mathrm{e}^{\frac{2\pi}{\omega}s}-1}\int\limits_t^{t+\frac{2\pi}{\omega}} \frac{\partial\bar{U}(\vec{x},s)}{\partial\vec{x}}\hat{\gamma}\frac{\partial f_0(\vec{x},\vec{v})}{\partial\vec{v}}\Bigg|_{\substack{\vec{x}=\vec{X}_0(t_1)\\ \vec{v}=\vec{V}_0(t_1)}} \mathrm{e}^{t_1 s}dt_1, \quad (184)$$

where t is some free constant that can be set to any number, t is also present in trajectories, as it is evident from (163) and (164); for example, it can be set to 0 without any loss of generality. For the potential, we use expressions (155), (156) and obtain for $\bar{U}(\vec{x},s)$:

$$\bar{U}(\vec{x},s) = \bar{U}_1(\vec{x},s) + \bar{U}_2(\vec{x},s) = \qquad (185)$$

$$= \frac{e}{\epsilon_0}\int N_1(\vec{x}^{'},s)G(\vec{x},\vec{x}^{'})d\vec{x}^{'} - \frac{eZ}{\epsilon_0}\mathcal{L}_{t_2,s}G(\vec{x},\vec{Y}(t_2)). \qquad (186)$$

Inserting this into the equation (184) and integrating it over $\vec{v}$, we obtain the same equation as in the previous case:

$$F(\vec{x},s) = N_1\big(\vec{x},s\big) - \lambda\int N_1\big(\vec{x}^{'},s\big)K\big(\vec{x},\vec{x}^{'},s\big)d\vec{x}^{'}, \qquad (187)$$

but with the different expressions for the kernel and left-hand side:

$$K\big(\vec{x},\vec{x}^{'},s\big) = \frac{\mathrm{e}^{-ts}}{\mathrm{e}^{\frac{2\pi}{\omega}s}-1}\int\int\limits_t^{t+\frac{2\pi}{\omega}} \frac{\partial G(\vec{x},\vec{x}^{'})}{\partial\vec{x}}\hat{\gamma}\frac{\partial f_0(\vec{x},\vec{v})}{\partial\vec{v}}\Bigg|_{\substack{\vec{x}=\vec{X}_0(t_1)\\ \vec{v}=\vec{V}_0(t_1)}} \mathrm{e}^{t_1 s}dt_1 d\vec{v}, \qquad (188)$$

$$F\left(\vec{x},s\right)=-Z\frac{e^2}{\epsilon_0}\frac{\mathrm{e}^{-ts}}{\mathrm{e}^{\frac{2\pi}{\omega}s}-1}\int\limits_0^{\infty}\int\limits_t^{t+\frac{2\pi}{\omega}}\frac{\partial G(\vec{x},\vec{Y}\left(t_2\right))}{\partial\vec{x}}\cdot$$
$$\cdot\,\hat{\gamma}\frac{\partial f_0(\vec{x},\vec{v})}{\partial\vec{v}}\Bigg|_{\substack{\vec{x}=\vec{X}_0\left(t_1\right)\\ \vec{v}=\vec{V}_0\left(t_1\right)}}\mathrm{e}^{(t_1-t_2)s}dt_1dt_2d\vec{v}, \tag{189}$$

and $\lambda=\frac{e^2}{\epsilon_0}$.

4.2.5 Introducing dimensionless variables

The dimensionless units that we define for the confined plasma slightly differ from the ones that we used for the infinite one [10]. There, we used the following dimensionless variables:

$$\vec{\mathsf{x}}=\frac{\vec{x}}{r_{\mathrm{D}}},\quad \vec{\mathsf{v}}=\frac{\vec{v}}{v_{\mathrm{rms}}},\quad \mathsf{t}=\frac{t}{t_{\mathrm{p}}}\equiv t\omega_{\mathrm{p}}, \tag{190}$$

$$\vec{\mathsf{k}}=\vec{k}r_{\mathrm{D}},\quad \mathsf{s}=\frac{s}{\omega_{\mathrm{p}}}\equiv st_{\mathrm{p}}, \tag{191}$$

where we used sans-serif font to denote them, and the root mean square velocity v_{rms}, plasma frequency ω_{p}, plasma period t_{p}, and Debye radius r_{D} were defined as follows

$$v_{\mathrm{rms}}=\sqrt{\frac{1}{\rho}\int v^2f_0(\vec{v})d\vec{v}},\quad \omega_{\mathrm{p}}=\sqrt{\frac{e^2\rho}{m_0\epsilon_0}}=\frac{1}{t_{\mathrm{p}}}, \tag{192}$$

$$r_{\mathrm{D}}=\frac{v_{\mathrm{rms}}}{\omega_{\mathrm{p}}}=v_{\mathrm{rms}}t_{\mathrm{p}}. \tag{193}$$

The vacuum permittivity ϵ_0 has different units in the 1D, 2D, and 3D cases, i.e.,

$$[\epsilon_0]=\frac{C^2T^2}{L^dM}, \tag{194}$$

where d is a dimensionality of the space, and C, T, L, and M are the charge, time, length and mass units, respectively. And we used the dimensionless equilibrium density $\mathsf{f}_0(\vec{\mathsf{v}})$ defined via:

$$f_0(\vec{v})=\rho f_d\mathsf{f}_0(\vec{\mathsf{v}}), \tag{195}$$

where $[\rho] = [n(\vec{x}, t)] = L^{-d}$, and $[f_d] = [v_{\text{rms}}]^{-d}$.

For the confined plasma, the equilibrium distribution also depends on $\vec{x}$, thus we have

$$f_0(\vec{x}, \vec{v}) = \rho f_d \mathsf{f}_0(\vec{\mathsf{x}}, \vec{\mathsf{v}}),\ [\rho] = 1,\ [f_d] = [v_{\text{rms}} r_{\text{D}}]^{-d}. \tag{196}$$

In this case, ρ has different units; we redefine plasma frequency accordingly:

$$\omega_{\text{p}} = \sqrt{\frac{e^2 \rho r_{\text{D}}^{-d}}{m_0 \epsilon_0}}. \tag{197}$$

In subsection 4.2.8, we rewrite the integral equations for the test charge problem using these units. In the next subsection, we detail the equilibrium distributions.

4.2.6 Equilibrium distributions

Since any function of the unperturbed Hamiltonian is a solution of the unperturbed Vlasov equation, we consider equilibrium distributions that are functions of the unperturbed Hamiltonian, i.e., $f_0(H_0)$. For H_0, we have

$$H_0 = \sum_i a_i x_i^2 + \sum_i b_i v_i^2. \tag{198}$$

We consider the normal and Cauchy distributions. The latter was very useful for the infinite plasma, since it has a simpler density, and hence, the computations were faster. We normalize the distributions such that

$$\int f_0(\vec{x}, \vec{v}) d\vec{x} d\vec{v} = \rho. \tag{199}$$

Normal distribution For the normal distribution, we have

$$f(\vec{x}, \vec{v}) = \rho \frac{\left(\prod_i a_i b_i\right)^{\frac{1}{2}}}{H_c^d \pi^d} \mathrm{e}^{-\sum_i \frac{a_i}{H_c} x_i^2 - \sum_i \frac{b_i}{H_c} v_i^2} \tag{200}$$

and we obtain for v_{rms}^2 via (192):

$$v_{\text{rms}}^2 = \frac{H_c}{2} \frac{\sum_{j=1}^{d} \prod_{i=1, i\neq j}^{d} b_i}{\prod_{i=1}^{d} b_i}, \tag{201}$$

or, for the isotropic case ($b_i = b$, for all i),

$$v_{\rm rms}^2 = \frac{H_c}{2}\frac{d}{b}. \tag{202}$$

We will not use this $v_{\rm rms}$, though; rather, we define $v_{{\rm rms},i}$ for each spatial dimension, it turns out that they are given by:

$$v_{{\rm rms},i} = \sqrt{\frac{H_c}{2b_i}}, \tag{203}$$

and, for the isotropic plasma, we have

$$v_{\rm rms} = \sqrt{\frac{H_c}{2b}}. \tag{204}$$

While it is possible to consider general anisotropic case, this leads to more dimensionless parameters in the dimensionless density; thus, for simplicity, we consider isotropic case with the Hamiltonian

$$\mathsf{H}_0 = \sum_i \mathsf{a}_i \mathsf{x}_i^2 + \frac{1}{2}\sum_i \mathsf{v}_i^2. \tag{205}$$

We have for the distribution:

$$\mathsf{f}_0(\vec{\mathsf{x}}, \vec{\mathsf{v}}) = \frac{1}{\pi^d} \mathrm{e}^{-\sum_i \mathsf{a}_i \mathsf{x}_i^2 - \frac{1}{2}\sum_i \mathsf{v}_i^2}; \tag{206}$$

the conventions we used here are slightly different from those used in [10], and

$$f_d = \left(\frac{b}{H_c}\right)^{\frac{d}{2}} \prod_i \sqrt{\frac{a_i}{H_c}}. \tag{207}$$

Alternatively, we can consider $v_{\rm rms} = \sqrt{\frac{H_c}{b}}$, this gives

$$\mathsf{f}_0(\vec{\mathsf{x}}, \vec{\mathsf{v}}) = \frac{1}{\pi^d} \mathrm{e}^{-\sum_i \mathsf{a}_i \mathsf{x}_i^2 - \sum_i \mathsf{v}_i^2}, \tag{208}$$

by setting $\mathsf{a}_i = 1$ for all i and integrating over $\vec{\mathsf{x}}$, this distribution can be reduced to the same velocity distribution that we considered in [10] for the infinite plasma. We have for the derivative:

$$\frac{\partial \mathsf{f}_0(\vec{\mathsf{x}}, \vec{\mathsf{v}})}{\partial \vec{\mathsf{v}}} = -2\,\vec{\mathsf{v}}\,\mathsf{f}_0(\vec{\mathsf{x}}, \vec{\mathsf{v}}). \tag{209}$$

In next subsections, we will need plasma's spatial size. Integrating the distribution (208) over $\vec{\mathsf{v}}$, we obtain

$$\int \mathsf{f}_0(\vec{\mathsf{x}},\vec{\mathsf{v}})d\vec{\mathsf{v}} = \frac{1}{\pi^{\frac{d}{2}}}\mathrm{e}^{-\sum\limits_i \mathsf{a}_i\mathsf{x}_i^2}. \tag{210}$$

The variance of this integrated distribution in a certain direction j is

$$\sigma_j^2 = \frac{1}{2}\left(\prod_i \mathsf{a}_i\right)^{-\frac{1}{2}}\frac{1}{\mathsf{a}_j}, \tag{211}$$

It is well-known that approximately 99.9% of the values of the 1D, 2D and 3D normally distributed random variables lie within a "four sigma" interval. Thus, we assume that the plasma with the normal spatial distribution lies within a closed interval $[-4\sigma_j, 4\sigma_j]$ in dimension j. If we assume that for all j, $\mathsf{a}_j = 1$, all σ_j equal $2^{-\frac{1}{2}} \approx 0.707$ and $4\sigma_j \approx 2.83$ for all j. For the case when all σ_j are equal, we introduce σ:

$$\sigma = \sqrt{2}\sigma_j, \tag{212}$$

which equals one, when all a_j equal one; we will use σ to characterize plasmas' sizes in section 4.5.

Cauchy distribution All of the considerations for the normal distribution also can be applied to other distributions. For example, for the Cauchy distribution, we have

$$f_0\left(\vec{x},\vec{v}\right) = \rho\frac{\left(\prod\limits_i a_i b_i\right)^{\frac{1}{2}}}{H_c^d\pi^d}\frac{\Gamma(\frac{1+d}{2})}{\Gamma(\frac{1}{2})\pi^{\frac{d}{2}}}\left(1+\sum_i \frac{a_i}{H_c}x_i^2 + \sum_i \frac{b_i}{H_c}v_i^2\right)^{-\frac{1+d}{2}}, \tag{213}$$

where $\Gamma(z)$ is the gamma function [27]; in this case, v_{rms} cannot be computed, since the corresponding integral is divergent; we use

$$v_{\mathrm{rms}} = \sqrt{\frac{H_c}{b}}. \tag{214}$$

Considering an isotropic plasma ($b_i = b$, for all i), we obtain

$$\mathsf{f}_0(\vec{\mathsf{x}},\vec{\mathsf{v}}) = \frac{\Gamma(\frac{1+d}{2})}{\Gamma(\frac{1}{2})\pi^{\frac{d}{2}}}\frac{1}{\left(1+\sum\limits_i \mathsf{a}_i\mathsf{x}_i^2 + \sum\limits_i \mathsf{v}_i^2\right)^{\frac{1+d}{2}}}, \tag{215}$$

and

$$f_d = \left(\sqrt{\frac{b}{H_c}}\right)^d \prod_i \sqrt{\frac{a_i}{H_c}}, \tag{216}$$

and for the derivative:

$$\frac{\partial \mathsf{f}_0(\vec{\mathsf{x}}, \vec{\mathsf{v}})}{\partial \vec{\mathsf{v}}} = -\frac{(1+d)\,\vec{\mathsf{v}}\,\mathsf{f}_0(\vec{\mathsf{x}}, \vec{\mathsf{v}})}{1 + \sum\limits_i \mathsf{a}_i \mathsf{x}_i^2 + \sum\limits_i \mathsf{v}_i^2}. \tag{217}$$

For an infinite plasma [10], the Cauchy distribution is very useful, since with it the formulae are much simpler and the equation was even exactly solvable in the 1D case; in higher dimensional cases, computations were much faster than for the normal. Using this distribution for the confined plasma does not offer any advantages; thus, we focus on a realistic normal distribution.

4.2.7 The Green's functions

In this subsection, we write the well-known expressions for the Poisson's equation Green's functions in the 1D, 2D and 3D spaces and their gradients. Using the introduced dimensionless units, we have

$$\mathsf{G}(\vec{\mathsf{x}}, \vec{\mathsf{x}}') = -\frac{1}{2}|\vec{\mathsf{x}} - \vec{\mathsf{x}}'|, \qquad \frac{\partial}{\partial \vec{\mathsf{x}}}\mathsf{G}(\vec{\mathsf{x}}, \vec{\mathsf{x}}') = -\frac{1}{2}\mathrm{sign}(\vec{\mathsf{x}} - \vec{\mathsf{x}}'), \tag{218}$$

$$\mathsf{G}(\vec{\mathsf{x}}, \vec{\mathsf{x}}') = -\frac{1}{2\pi}\ln|\vec{\mathsf{x}} - \vec{\mathsf{x}}'|, \qquad \frac{\partial}{\partial \vec{\mathsf{x}}}\mathsf{G}(\vec{\mathsf{x}}, \vec{\mathsf{x}}') = -\frac{1}{2\pi}\frac{\vec{\mathsf{x}} - \vec{\mathsf{x}}'}{|\vec{\mathsf{x}} - \vec{\mathsf{x}}'|^2}, \tag{219}$$

$$\mathsf{G}(\vec{\mathsf{x}}, \vec{\mathsf{x}}') = \frac{1}{4\pi}\frac{1}{|\vec{\mathsf{x}} - \vec{\mathsf{x}}'|}, \qquad \frac{\partial}{\partial \vec{\mathsf{x}}}\mathsf{G}(\vec{\mathsf{x}}, \vec{\mathsf{x}}') = -\frac{1}{4\pi}\frac{\vec{\mathsf{x}} - \vec{\mathsf{x}}'}{|\vec{\mathsf{x}} - \vec{\mathsf{x}}'|^3}, \tag{220}$$

for the 1D, 2D, and 3D spaces, respectively.

4.2.8 Dimensionless units for the integral equation

Using the dimensionless units, we rewrite the integral equation (187) as follows:

$$\mathsf{F}(\vec{\mathsf{x}}, \mathsf{s}) = \mathsf{N}_1(\vec{\mathsf{x}}, \mathsf{s}) - \int \mathsf{N}_1(\vec{\mathsf{x}}', \mathsf{s})\mathsf{K}\big(\vec{\mathsf{x}}, \vec{\mathsf{x}}', \mathsf{s}\big)d\vec{\mathsf{x}}'. \tag{221}$$

To simplify the expressions, we introduce the following notation:

$$\mathsf{R}\big(\vec{\mathsf{x}},\vec{\mathsf{x}}',\vec{\mathsf{v}}\big)=F_{\mathrm{d}}\frac{\partial\mathsf{G}(\vec{\mathsf{x}},\vec{\mathsf{x}}')}{\partial\vec{\mathsf{x}}}\frac{\partial\mathsf{f}_0(\vec{\mathsf{x}},\vec{\mathsf{v}})}{\partial\vec{\mathsf{v}}}, \tag{222}$$

where F_{d} is a dimensionless constant, $F_{\mathrm{d}}=f_d v_{\mathrm{rms}}^d r_{\mathrm{D}}^d$; the derivatives in this expression are given by equations (218)-(220), (209), and (217). For the method for general orbits, we have

$$\mathsf{K}\big(\vec{\mathsf{x}},\vec{\mathsf{x}}',\mathsf{s}\big)=\int\limits_0^\infty\int\mathsf{R}\big(\vec{\mathsf{X}}_0\left(0\right),\vec{\mathsf{x}}',\vec{\mathsf{V}}_0\left(0\right)\big)d\vec{\mathsf{v}}\mathrm{e}^{-\mathsf{st}}d\mathsf{t}, \tag{223}$$

$$\mathsf{F}\left(\vec{\mathsf{x}},\mathsf{s}\right)=-Z\int\int\limits_0^\infty\int\limits_0^{\mathsf{t}}\mathsf{R}\big(\vec{\mathsf{X}}_0\left(\mathsf{t}_1\right),\vec{\mathsf{Y}}\left(\mathsf{t}_1\right),\vec{\mathsf{V}}_0\left(\mathsf{t}_1\right)\big)\mathrm{e}^{-\mathsf{st}}d\mathsf{t}_1d\mathsf{t}d\vec{\mathsf{v}}, \tag{224}$$

and, for the method for periodic orbits,

$$\mathsf{K}_{\mathsf{t}}\big(\vec{\mathsf{x}},\vec{\mathsf{x}}',\mathsf{s}\big)=\frac{\mathrm{e}^{-\mathsf{ts}}}{\mathrm{e}^{\frac{2\pi}{\tilde{\omega}}\mathsf{s}}-1}\int\limits_{\mathsf{t}}^{\mathsf{t}+\frac{2\pi}{\omega}}\int\mathsf{R}\big(\vec{\mathsf{X}}_0\left(\mathsf{t}_1\right),\vec{\mathsf{x}}',\vec{\mathsf{V}}_0\left(\mathsf{t}_1\right)\big)\mathrm{e}^{\mathsf{st}_1}d\vec{\mathsf{v}}d\mathsf{t}_1, \tag{225}$$

$$\mathsf{F}_{\mathsf{t}}\left(\vec{\mathsf{x}},\mathsf{s}\right)=-Z\frac{\mathrm{e}^{-\mathsf{ts}}}{\mathrm{e}^{\frac{2\pi}{\tilde{\omega}}\mathsf{s}}-1}\int\limits_0^\infty\int\limits_{\mathsf{t}}^{\mathsf{t}+\frac{2\pi}{\omega}}\int\mathsf{R}\big(\vec{\mathsf{X}}_0\left(\mathsf{t}_1\right),\vec{\mathsf{Y}}\left(\mathsf{t}_1\right),\vec{\mathsf{V}}_0\left(\mathsf{t}_1\right)\big)\mathrm{e}^{(\mathsf{t}_1-\mathsf{t}_2)\mathsf{s}}d\vec{\mathsf{v}}d\mathsf{t}_1d\mathsf{t}_2, \tag{226}$$

where t, as mentioned, is a free constant that can be set to zero.

4.2.9 On integration domain

To apply numerical methods, which will be described in subsection 4.3, to the equation (221), we have to transform its domain to a finite rectangular domain. Let us assume that we have an equation in Cartesian coordinates:

$$\mathsf{F}\left(\vec{\mathsf{x}},\mathsf{s}\right)=\mathsf{N}_1(\vec{\mathsf{x}},\mathsf{s})-\int\limits_{\mathbb{R}^d}\mathsf{N}_1(\vec{\mathsf{x}}',\mathsf{s})\mathsf{K}\big(\vec{\mathsf{x}},\vec{\mathsf{x}}',\mathsf{s}\big)d\vec{\mathsf{x}}'. \tag{227}$$

We can use change of variables (173) to do the required transformation:

$$\mathsf{F}\left(\tan\vec{\mathsf{x}},\mathsf{s}\right) = \mathsf{N}_1(\tan\vec{\mathsf{x}},\mathsf{s}) - \\ - \int\limits_{\left[-\frac{\pi}{2},\frac{\pi}{2}\right]^d} \mathsf{N}_1(\tan\vec{\mathsf{x}}',\mathsf{s})\mathsf{K}\big(\tan\vec{\mathsf{x}},\tan\vec{\mathsf{x}}',\mathsf{s}\big)\frac{1}{\prod\limits_i \cos^2(\mathsf{x}_i')}d\vec{\mathsf{x}}'. \quad (228)$$

Then we solve the following equation for $\bar{\mathsf{N}}_1(\vec{\mathsf{x}},\mathsf{s})$:

$$\bar{\mathsf{F}}\left(\vec{\mathsf{x}},\mathsf{s}\right) = \bar{\mathsf{N}}_1(\vec{\mathsf{x}},\mathsf{s}) - \int\limits_{\left[-\frac{\pi}{2},\frac{\pi}{2}\right]^d} \bar{\mathsf{N}}_1(\vec{\mathsf{x}},\mathsf{s})\bar{\mathsf{K}}\big(\vec{\mathsf{x}},\vec{\mathsf{x}}',\mathsf{s}\big)d\vec{\mathsf{x}}', \quad (229)$$

where

$$\bar{\mathsf{K}}\big(\vec{\mathsf{x}},\vec{\mathsf{x}}',\mathsf{s}\big) = \mathsf{K}\big(\tan\vec{\mathsf{x}},\tan\vec{\mathsf{x}}',\mathsf{s}\big)\frac{1}{\prod\limits_i \cos^2(\mathsf{x}_i')}, \quad (230)$$

$$\bar{\mathsf{F}}\left(\vec{\mathsf{x}},\mathsf{s}\right) = \mathsf{F}\left(\tan\vec{\mathsf{x}},\mathsf{s}\right). \quad (231)$$

We get solution of the initial equation via:

$$\mathsf{N}_1(\vec{\mathsf{x}},\mathsf{s}) = \bar{\mathsf{N}}_1(\arctan\vec{\mathsf{x}},\mathsf{s}). \quad (232)$$

Another way is to use spherical coordinates and compactify the radial coordinate, but the approach we just described seems simpler.

4.3 Numerical Methods

In the previous subsection, we derived the Laplace-Fredholm integral equation for the test charge problem for the confined plasma. In this subsection, we describe a numerical method to solve such equation and the software that we developed. The method has two main steps: solving the Fredholm integral equation for the Laplace image of the unknown function and then doing the inverse Laplace transform. We detail these steps in order. Then we describe our program, discuss parallelization of the algorithm and optimizations.

The complete source code of our program is distributed under the terms of the GNU General Public License at [34]. The code includes a stand-alone solver for the multidimensional Fredholm integral equations of the second type, a solver for the Laplace-Fredholm equations and the kernel and left-hand side classes for the test charge problem. The codes for all particular cases considered in subsection 4.5 are included.

4.3.1 Numerical solution of the Fredholm equation

Numerical methods for the Fredholm equations are very well developed [35], however, there are no publicly available codes implementing them. In this subsection, we review the piecewise polynomial collocation method (PPCM), emphasizing implementation details; for the mathematical details, such as the existence theorems and accuracy estimates, we refer to [35]. The idea of the method is to split the equation's domain, which should be a d-dimensional rectangle, into rectangular sub-domains and then to represent the solution in each sub-domain as polynomial series. The polynomials should be of some special form to transform the integral equation into a system of linear equations for the coefficients of these expansions, when polynomial solution is inserted into the equation and evaluated at some special points.

Let us consider an integral equation

$$\mathsf{F}\left(\vec{\mathsf{x}}\right) = \mathsf{N}_1(\vec{\mathsf{x}}) - \int\limits_G \mathsf{N}_1(\vec{\mathsf{x}}')\mathsf{K}\left(\vec{\mathsf{x}},\vec{\mathsf{x}}'\right)d\vec{\mathsf{x}}', \tag{233}$$

defined on a d-dimensional rectangular domain

$$G = \prod_{i=1}^{d}[0,\mathsf{b}_i]. \tag{234}$$

In every dimension k, we introduce $2N_k+1$ grid points:

$$\mathsf{x}_k^j = \frac{\mathsf{b}_k}{2}\left(\frac{j}{N_k}\right)^r,\ j=0,\ldots,N_k, \tag{235}$$

$$\mathsf{x}_k^{N_k+j} = \mathsf{b}_k - \mathsf{x}_k^{N_k-j},\ j=1,\ldots,N_k, \tag{236}$$

where r is a constant, $r \geq 1$, that characterizes uniformity of the grid, i.e., for $r > 1$, the grid becomes denser towards the boundaries of the domain, and, for $r = 1$, it is uniform. Using these grid points, we partition G into the closed cells:

$$G_{j_1,\ldots,j_d} = \{\vec{\mathsf{x}} \in \mathbb{R}^d : \mathsf{x}_k^{j_k} \leq \mathsf{x}_k \leq \mathsf{x}_k^{j_k+1},\ k=1,\ldots,d\}, \tag{237}$$

for all $j_k = 0,\ldots,2N_k$ for all $k = 1,\ldots,d$. We then introduce d-dimensional multi-index $\mathbf{j}$, $\mathbf{j} = (j_1,\ldots,j_d)$, such that $G_{j_1,\ldots,j_d} \equiv G_{\mathbf{j}}$ and

$$G = \bigcup_{\mathbf{j}} G_{\mathbf{j}}. \tag{238}$$

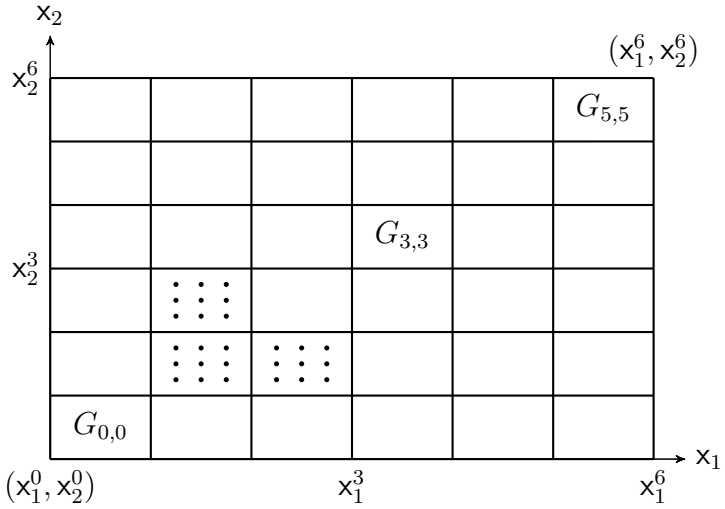

Figure 9: Cells and collocation points for the PPCM for $d = 2$, $N_1 = N_2 = 3$, $m = 3$, $r = 1$. The collocation points are shown only in three cells, while, of course, they exist in all of them.

Then we choose m interpolation points in $[-1, 1]$: $-1 \leq \xi^1 < \cdots < \xi^m \leq 1$ and map them into every dimension of all partitions, thereby obtaining collocation points in each cell $G_{\mathbf{j}}$. We denote the collocation points as $\boldsymbol{\xi}^{\mathbf{j},\mathbf{l}}$; it is a d-dimensional vector with two multi-indexes, where $\mathbf{j}$ characterizes the cell the collocation point belongs to and components of $\mathbf{l}$ runs from 1 to m characterizing the mapped interpolation point. In Fig. 9, we depict this construction for $d = 2$.

Then, we introduce the interpolating polynomials of degree $(m-1)^d$ that has two multi-indexes:

$$\boldsymbol{\phi}^{\mathbf{j},\mathbf{m}}(\vec{\mathsf{x}}) = \prod_{i=1}^{d} \prod_{q=1\ldots m}^{q \neq m_i} \frac{\left(\mathsf{x}_i - \xi_i^{j_i,q}\right)}{\left(\xi_i^{j_i,m_i} - \xi_i^{j_i,q}\right)}, \ \vec{\mathsf{x}} \in G_{\mathbf{j}}, \tag{239}$$

where the first multi-index characterizes the cell, to which the polynomial belongs, and the second, each component of which runs from 1 to m, characterizes the collocation point used to build the polynomial. For example, for $m = 1$, the polynomials will be just constants. The polynomials satisfy the

following important property:

$$\boldsymbol{\phi}^{\mathbf{j},\mathbf{m}}\left(\boldsymbol{\xi}^{\mathbf{j},\mathbf{l}}\right) = \delta_{\mathbf{m},\mathbf{l}}, \tag{240}$$

where $\delta_{\mathbf{m},\mathbf{l}}$ is the Kronecker delta, defined for the multi-indexes via

$$\delta_{\mathbf{m},\mathbf{l}} = \prod_{i=1}^{d} \delta_{m_i,l_i}. \tag{241}$$

We look for a solution in the following form:

$$\mathsf{N}_1(\vec{\mathsf{x}}) = \sum_{\mathbf{m}} c_{\mathbf{j}}^{\mathbf{m}} \boldsymbol{\phi}^{\mathbf{j},\mathbf{m}}\left(\vec{\mathsf{x}}\right), \;\; \vec{\mathsf{x}} \in G_{\mathbf{j}}, \tag{242}$$

where the summation runs over all possible values of multi-index $\mathbf{m}$. We emphasize that unknown coefficients and polynomials are different in each cell $G_{\mathbf{j}}$.

Then we insert the solution (242) into the equation (233), and, using the condition that the equation is satisfied at the collocation points and property (240), we reduce the integral equation to the system of linear equations for $c_{\mathbf{j}}^{\mathbf{m}}$:

$$c_{\mathbf{i}}^{\mathbf{l}} = \sum_{\mathbf{j}} \sum_{\mathbf{m}} a_{\mathbf{i},\mathbf{j}}^{\mathbf{l},\mathbf{m}} c_{\mathbf{j}}^{\mathbf{m}} + \mathsf{F}(\boldsymbol{\xi}^{\mathbf{i},\mathbf{l}}), \tag{243}$$

where

$$a_{\mathbf{i},\mathbf{j}}^{\mathbf{l},\mathbf{m}} = \int_{G_{\mathbf{j}}} K(\boldsymbol{\xi}^{\mathbf{i},\mathbf{l}}, \vec{y}) \boldsymbol{\phi}^{\mathbf{j},\mathbf{m}}(\vec{y}) d\vec{y}, \tag{244}$$

and $\mathsf{F}(\boldsymbol{\xi}^{\mathbf{i},\mathbf{l}})$ is just $\mathsf{F}\left(\vec{\mathsf{x}}\right)$ evaluated at the collocation point $\boldsymbol{\xi}^{\mathbf{i},\mathbf{l}}$. Equations (243) ensure that the numerical solution (242) equals the unknown true solution at all collocation points; at other points, the numerical solution is interpolated by polynomials. Obviously, the matrix $a_{\mathbf{i},\mathbf{j}}^{\mathbf{l},\mathbf{m}}$, vector $\mathsf{F}(\boldsymbol{\xi}^{\mathbf{i},\mathbf{l}})$ and the unknown vector of coefficients $c_{\mathbf{i}}^{\mathbf{l}}$ can be represented as a matrix with two scalar indexes and two vectors with one scalar index, i.e., $\mathbf{A}$, $\vec{f}$, and $\vec{c}$, respectively, and standard methods to solve systems of linear equations can be applied. With these notations, the system (243) looks as follows:

$$(\mathbf{I} - \mathbf{A})\vec{c} = \vec{f}, \tag{245}$$

where $\mathbf{I}$ is an identity matrix. Dimension of matrix $\mathbf{A}$ is

$$\prod_{k=1}^{d}(2N_k m_k). \tag{246}$$

The system of linear equations (245) can be solved using standard numerical methods such as "LU decomposition". We will discuss the algorithm and its parallelization scheme in appendix F.

It is worth to note that this method can deal with integral equations with weakly singular kernels, meaning that the kernels can have singularities, but they must be integrable [35], i.e., the integral in (244) must be convergent.

We developed our own multidimensional integrators to compute integrals in (244). Multidimensional integral can be computed recursively using one-dimensional integrators. At each step of recursion, we use as an integrand the initial integral corresponding to this step, but with lowered by one number of integration variables. We also store the values of this step's integration variables and pass them to further steps. When dimension of the integral is one, the recursive integrator takes function as an integrand and evaluates it at the values of the integration variables, which were stored in previous steps of the recursion. To perform one-dimensional integration, we implemented the adaptive Gauss-Kronrod algorithm. We also used this integrator to evaluate integrals in expressions for the kernel and the left-hand side of the integral equations corresponding to the test charge problem. For more details on numerical integration, we refer to appendix E.

4.3.2 Numerical solution of the Laplace-Fredholm equation

The integral equation for the test charge problem (221) is slightly more complicated than the Fredholm equation (233), i.e., we have the Fredholm equation

$$\mathsf{F}\left(\vec{\mathsf{x}},\mathsf{s}\right)=\mathsf{N}_1(\vec{\mathsf{x}},\mathsf{s})-\int \mathsf{N}_1(\vec{\mathsf{x}}',\mathsf{s})\mathsf{K}\big(\vec{\mathsf{x}},\vec{\mathsf{x}}',\mathsf{s}\big)d\vec{\mathsf{x}}', \tag{247}$$

but for the Laplace image of the quantity of interest. It is well-known that the inverse Laplace transform of a known function $\tilde{f}\left(s\right)$ can be computed using discrete Fourier transform (323):

$$f\left(t_j\right)=\mathrm{e}^{\sigma t_j}C_j\mathrm{DFT}_j\left[\{\tilde{f}\left(\sigma+ik_n\right)\left(-1\right)^n\}_{0\leq n\leq N-1}\right], \tag{248}$$

this formula is derived and all notations are explained in appendix A; for more details, we refer to [10], where numerical tests were also performed. The discrete Fourier transform can be computed numerically using the fast Fourier transform (FFT) algorithm. For any value of s, we can obtain the numerical solution of the integral equation (247) via the PPCM described in previous subsection. To invert the Laplace transform numerically, we need to solve the equation (247) for $\mathsf{s} = \sigma + i\mathsf{k}_n$ for some set $\{\mathsf{k}_n\}_{0\le n\le N-1}$. Then, we store these solutions for d-dimensional array of $\vec{\mathsf{x}}$ values of interest; thereafter, for each value of $\vec{\mathsf{x}}$, we invert the Laplace transform via (248). After solving equations (247) for the set of s, we have the following $(d+1)$-dimensional array of solutions:

$$\{\mathsf{N}_1(\mathsf{x}_{i_1},\dots,\mathsf{x}_{i_d},\sigma+i\mathsf{k}_n)\}_{0\le n\le N-1,\,0\le i_j\le N_j^{(x)},\,0\le j\le d-1}, \tag{249}$$

where $N_j^{(x)}$ is the number of grid points in dimension j. Inverting the Laplace transform via (248), we obtain the space-time solution:

$$\mathsf{n}_1(\vec{\mathsf{x}}_{\mathbf{i}},t_j) = \mathrm{e}^{\sigma t_j} C_j \mathrm{DFT}_j\left[\{\mathsf{N}_1(\vec{\mathsf{x}}_{\mathbf{i}},\sigma+i\mathsf{k}_n)\,(-1)^n\}_{0\le n\le N-1}\right], \tag{250}$$

where $\vec{\mathsf{x}}_{\mathbf{i}} = (\mathsf{x}_{i_1},\dots,\mathsf{x}_{i_d})$. The discrete Fourier transform in this formula can be evaluated via the FFT; the numerical test of this procedure is discussed in subsection 4.4.

Thus, being able to solve equation (247) over some grid of complex numbers for s, we can obtain the space-time density $\mathsf{n}_1(\vec{\mathsf{x}},t)$ via (250). For complex values of s, equation (247) turns into a system of equations for $\mathrm{Re}\,\mathsf{N}_1(\vec{\mathsf{x}}',\mathsf{s})$ and $\mathrm{Im}\,\mathsf{N}_1(\vec{\mathsf{x}}',\mathsf{s})$:

$$\begin{pmatrix}\mathrm{Re}\,\mathsf{F}\\ \mathrm{Im}\,\mathsf{F}\end{pmatrix} = \begin{pmatrix}\mathrm{Re}\,\mathsf{N}_1\\ \mathrm{Im}\,\mathsf{N}_1\end{pmatrix} - \int\limits_G \begin{pmatrix}\mathrm{Re}\,\mathsf{K} & -\mathrm{Im}\,\mathsf{K}\\ \mathrm{Im}\,\mathsf{K} & \mathrm{Re}\,\mathsf{K}\end{pmatrix}\begin{pmatrix}\mathrm{Re}\,\mathsf{N}_1\\ \mathrm{Im}\,\mathsf{N}_1\end{pmatrix} d\vec{\mathsf{x}}', \tag{251}$$

wherein, for brevity, we omitted arguments of functions. The PPCM can be applied to this system as well. Looking for solution in a form similar to (242),

$$\begin{pmatrix}\mathrm{Re}\,\mathsf{N}_1(\vec{\mathsf{x}})\\ \mathrm{Im}\,\mathsf{N}_1(\vec{\mathsf{x}})\end{pmatrix} = \sum_{\mathbf{m}} \begin{pmatrix}c_{\mathbf{j}}^{\mathbf{m}}\\ d_{\mathbf{j}}^{\mathbf{m}}\end{pmatrix} \boldsymbol{\phi}^{\mathbf{j},\mathbf{m}}(\vec{\mathsf{x}}),\ \ \vec{\mathsf{x}}\in G_{\mathbf{j}}, \tag{252}$$

we obtain a system of linear equations analogous to (245):

$$\begin{pmatrix} \mathbf{I}-\mathbf{A} & \mathbf{B} \\ -\mathbf{B} & \mathbf{I}-\mathbf{A} \end{pmatrix} \begin{pmatrix} \vec{c} \\ \vec{d} \end{pmatrix} = \begin{pmatrix} \vec{f} \\ \vec{g} \end{pmatrix}, \tag{253}$$

where $\mathbf{A}$ and $\vec{f}$ have the same meaning as in (245), but for the real parts of the corresponding quantities, and $\mathbf{B}$ and $\vec{g}$ – for the imaginary parts; vectors $\vec{c}$ and $\vec{d}$ are the unknown vectors corresponding to solution (252). The dimension of the matrix of the system (253) is

$$\prod_{k=1}^{d}(4N_k m_k). \tag{254}$$

The system of linear equations (253) is a standard system of linear equation and can be easily solved using, for example, "LU decomposition", which is discussed in appendix F.

4.3.3 Implementation and tests

The algorithm described in the previous section we implemented as a parallel object-oriented program. Our solver deals with abstract classes for the kernel and for the left-hand side of an integral equation. By defining sub-classes of these classes and supplying them to the solver, we can solve equations corresponding to different problems. The diagram of this design is depicted in Fig. 10. This design completely separates the solver and a particular equation it solves, i.e., the solver only deals with interfaces, which are defined by the abstract classes for the kernel and left-hand side. That means that we can test the solver with some simple exactly solvable equation and be sure that it solves correctly any other integral equation of the same type.

It is easy to construct an exactly solvable integral equation by taking some functions for the solution and for the kernel, and then, the left-hand side can be obtained via substituting these functions into the equation. For example, a d-dimensional equation

$$\mathsf{F}\left(\vec{\mathsf{x}},\mathsf{s}\right) = \mathsf{N}(\vec{\mathsf{x}},\mathsf{s}) - \int\limits_{[-\pi,\pi]^d} \mathsf{N}(\vec{\mathsf{x}}',\mathsf{s})\mathsf{K}\left(\vec{\mathsf{x}},\vec{\mathsf{x}}',\mathsf{s}\right)d\vec{\mathsf{x}}' \tag{255}$$

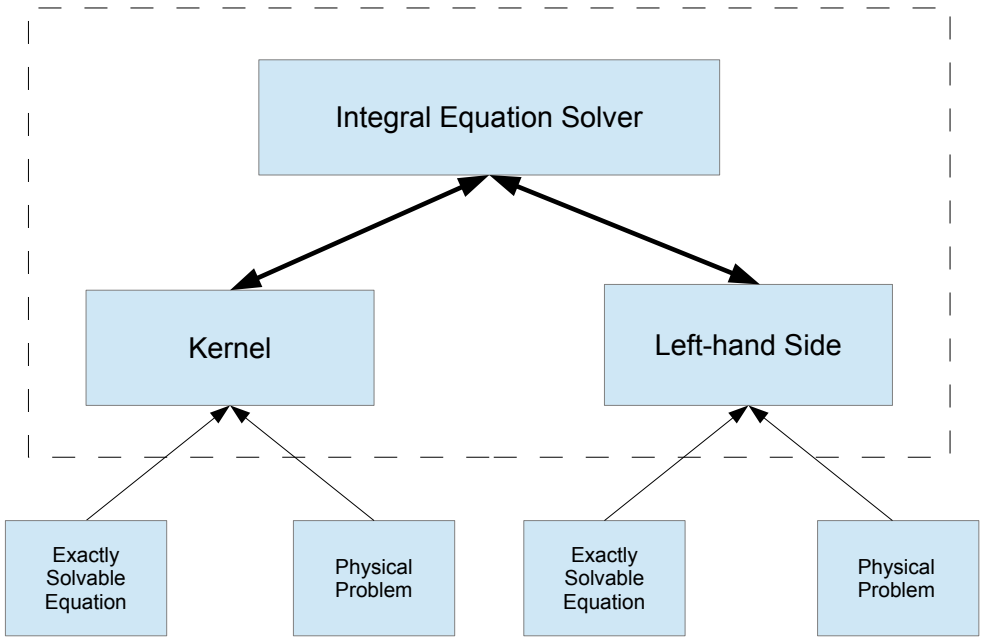

Figure 10: Design of the integral equation solver. The solver deals only with abstract classes for the kernel and left-hand side.

with a kernel

$$\mathsf{K}\left(\vec{\mathsf{x}},\vec{\mathsf{x}}',\mathsf{s}\right)=\mathsf{s}^2\prod_{i=1}^{d}\cos\mathsf{x}_i'\sin\mathsf{x}_i, \tag{256}$$

and a left-hand side

$$\mathsf{F}\left(\vec{\mathsf{x}},\mathsf{s}\right)=\frac{1}{\mathsf{s}^2}\prod_{i=1}^{d}\sin\mathsf{x}_i \tag{257}$$

has an exact solution

$$\mathsf{N}(\vec{\mathsf{x}},\mathsf{s})=\frac{1}{\mathsf{s}^2}\prod_{i=1}^{d}\sin\mathsf{x}_i, \tag{258}$$

and in the time domain:

$$\mathsf{n}(\vec{\mathsf{x}},\mathsf{t}) = \mathsf{t}\prod_{i=1}^{d}\sin \mathsf{x}_i,\ \ \mathsf{t} \geq 0. \tag{259}$$

In Fig. 11, we show numerical solution in the time domain of this equation

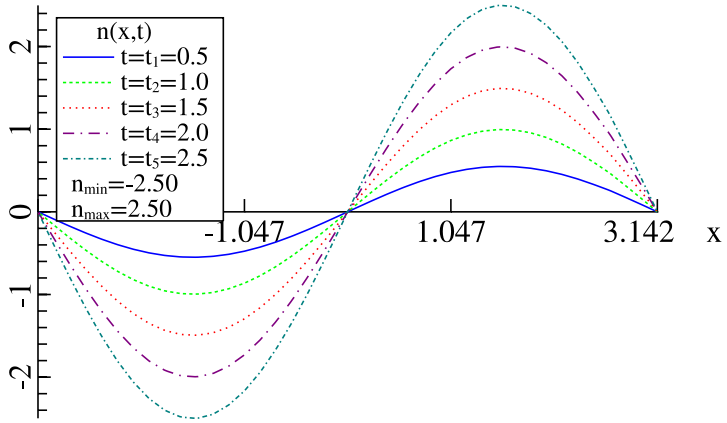

Figure 11: Numerical solution of the exactly solvable 1D Laplace-Fredholm equation (255) with kernel (256) and left-hand side(257) obtained via the PPCM and Laplace transform inversion via FFT.

obtained by our program for $d = 1$. It is indistinguishable from the exact solution (259), the extrema of the curves equal the corresponding time values, as they should accordingly to (259). We also completed the same tests for higher dimensions. From this test we can conclude that our solver will solve any equation of this type correctly.

The solver is implemented in C++ using MPI for parallelization. The results shown in Fig. 11 were obtained on Hopper machine at the National Energy Research Scientific Computing Center (NERSC); Hopper is a Cray XE6 supercomputer with 6,384 nodes, which are two twelve-core AMD 'Magny-Cours' 2.1 GHz processors. We utilized 256 nodes (6,144 cores), it took 2.52 seconds to solve this exactly solvable Laplace-Fredholm equation; individual Fredholm equations (for a given s) were solved in 0.02 seconds.

4.3.4 Parallel algorithm for the Fredholm equation

In this subsection, we describe parallel algorithm for the Fredholm equation. There are two natural ways to parallelize the algorithm. To do the Laplace transform in (250), we need to have the solutions of the integral equation (247) for different values of the parameter s, which are independent and can be obtained in parallel. The most time-consuming part of solving the individual integral equation is the evaluation of the matrix elements of $\mathbf{A}$, or, in complex case, of the matrix of the system of linear equations (253); for simplicity, we will denote this matrix as $\mathbf{a}$ in this subsection in both cases. Each matrix element is a multidimensional integral (244) and they are also independent of each other; thus, they can be evaluated in parallel. We consider two cases of real or complex kernel simultaneously; for the real case $\mathbf{a}$ has $r_d \times r_d$ elements, in the complex case it has $2r_d \times 2r_d$ elements, where r_d is a dimension of the matrix for the real kernel, "real dimension". We want to distribute all these integral between available processes. Let us assume that we have I_c integrals:

$$\begin{cases} I_c = r_d \times r_d, & \text{for real kernel,} \\ I_c = 2r_d \times r_d, & \text{for complex kernel.} \end{cases} \tag{260}$$

In addition, we compute vector $\mathbf{f}$ corresponding to the right-hand side of the equation, this vector is r_d-dimensional in the real case, and $2r_d$-dimensional in the complex one:

$$\begin{cases} d_c = r_d, & \text{for real kernel,} \\ d_c = 2r_d, & \text{for complex kernel,} \end{cases} \tag{261}$$

Let us say that we have K processes. On root process we crate a full matrix $\mathbf{a}$, ($r_d \times r_d$ or $2r_d \times 2r_d$). And we have a loop computing integrals indexed by $i \in [0, r_d \times r_d)$.

We consider three cases:

1. $K > I_c$. In this case, there exist positive integers b, M, such that

$$K = MI_c + b,\ b < I_c. \tag{262}$$

   We form a group of I_c processes and assign for each integral each own process, i.e., we assign integral i to process k, iff $i = k$. In case of

complex kernel, we assign "imaginary" i-th integral to the process k, iff $i + r_d \times r_d = k$. On the non-root processes we create 1×1 matrices $\mathbf{a}$. For the left-hand side (LHS), we assign i-th integral to process k, iff $i = k$. In the complex case, we assign "imaginary" i-th LHS to the process k, iff $i + r_d = k$. On the non-root processes with ranks less than d_c, we create 1×1 matrices $\mathbf{f}$.

2. $K > I_c/2$. We consider this case only for the complex kernels. Analogously, we find positive integers b, M:

$$K = M\frac{I_c}{2} + b,\ b < \frac{I_c}{2}, \tag{263}$$

and form a group of $\frac{I_c}{2}$ processes, and for each process we assign two integrals corresponding for the real and imaginary parts of the kernel, i.e., we assign both real and imaginary i-th integrals to process k, iff $i = k$, thus on non-root processes we create 1×2 matrices $\mathbf{a}$. For the LHS, we assign real i-th LHS to process k, iff $i = k$, and we assign imaginary i-th LHS to the process k, iff $i + r_d = k$. On the non-root processes with ranks less than d_c, we create 1×1 matrices $\mathbf{f}$.

3. $K < I_c$ for the real case and $K < \frac{I_c}{2}$ for the complex. In this case we define

$$\begin{cases} \tilde{I}_c = I_c = r_d \times r_d, & \text{for real kernel,} \\ \tilde{I}_c = \frac{I_c}{2} = r_d \times r_d, & \text{for complex kernel,} \end{cases} \tag{264}$$

and find positive integers $\tilde{M}$, $\tilde{b}$ such that

$$\tilde{I}_c = \tilde{M}K + \tilde{b},\ \tilde{b} < K, \tag{265}$$

thus, we form a group of K processes and assign to each process computation of $\tilde{M}+1$ integrals, i.e., we compute i-th integral on the process k, iff $i \equiv k (\mathrm{mod}\, K)$, and for the complex integral $i + r_d \times r_d \equiv k (\mathrm{mod}\, K)$. In this way, we actually compute $(\tilde{M} + 1)K$ integrals in the real case, and $2(\tilde{M} + 1)K$ in the complex. We create $1 \times (\tilde{M} + 1)$ matrices $\mathbf{a}$ on non-root processes for the real case, and, for the complex case, we create $2 \times (\tilde{M} + 1)$ matrices $\mathbf{a}$ and store real integrals in the first row and imaginary ones in the second.

For the LHS, we define

$$\begin{cases} \tilde{d_c} = d_c = r_d, & \text{for real kernel,} \\ \tilde{d_c} = \frac{I_c}{2} = r_d, & \text{for complex kernel,} \end{cases} \tag{266}$$

and find positive integers $\tilde{M_f}$, $\tilde{b_f}$ such that

$$\tilde{d_c} = \tilde{M_f} K + \tilde{b_f},\ \tilde{b_f} < K, \tag{267}$$

on each process we compute $\tilde{M_f} + 1$ integrals in the real case and $2(\tilde{M_f} + 1)$ in the complex, i.e., we compute i-th LHS on a process k, iff $i \equiv k (\mathrm{mod}\ K)$, and, for the imaginary LHS, $i + r_d \equiv k (\mathrm{mod}\ K)$. In this way, we actually compute $(\tilde{M_f} + 1)K$ LHSs in the real case, and $2(\tilde{M_f} + 1)K$ in the complex. We create $1 \times (\tilde{M_f} + 1)$ matrices $\mathbf{f}$ on non-root processes for the real case, and, for the complex case, we create $2 \times (\tilde{M_f} + 1)$ matrices $\mathbf{f}$ and store real integrals in the first row and imaginary in the second.

Then we have to collect all the data to the matrix on the root process. In the real case, we have $r_d \times r_d$ matrix and there is a one-to-one correspondence between integrals and matrix elements, in the complex case we have $2r_d \times 2r_d$ matrix, and the real integrals go into upper left and lower right $r_d \times r_d$ block, and the complex integrals go into upper right and lower left blocks. As for integrals we have a loop with index i running from 0 to $r_d \times r_d - 1$. We have the same three cases:

1. $K > I_c$. For the real case, we gather all 1×1 matrices into the $r_d \times r_d$ matrix to the root process. In the complex case, we gather all 1×1 matrices into an upper left corner of the $2r_d \times 2r_d$ matrix $\mathbf{a}$ on the root process, i.e., we form an auxiliary array on a root process of the dimension r_d, collect the data from first r_d processes to it, then write the data into $\mathbf{a}$, then read from the second group of processes of the size r_d and then write that data into the second row of the matrix $\mathbf{a}$. In this way, we read all real integrals. Then we continue with imaginary, but write them to the lower right corner of $\mathbf{a}$. For the LHS, we just gather all 1×1 matrices to the LHS matrix on the root process.

2. $K > I_c/2$. We consider this case only for the complex kernels. In this case, we form an auxiliary array of the size $2r_d$, we collect real data

from r_d processes into the first half of the array, and imaginary into the second. Then, we write first half into the upper left corner of $\mathbf{a}$ and second into the lower left corner. For the LHS, we just gather all 1×1 matrices to the LHS matrix on the root process.

3. $K < I_c$ for the real case, and $K < \frac{I_c}{2}$ for the complex. In this case, we have $\tilde{M} + 1$ gathering steps. At each step, we collect one (two) number(s) and write numbers corresponding to the real case into the upper left corner of $\mathbf{a}$, in the complex case, we also write complex contribution into the lower right corner of the matrix.

4.3.5 Optimized solver

The solver, whose design is depicted in Fig. 10, is implemented using abstract classes, pure virtual functions, and, since it is equation-independent, it doesn't take advantage of a certain equation. This implementation is very important for testing, but it's too slow for the realistic 3D test charge problem.

The most time consuming part of the algorithm is evaluation of the multidimensional integral in the expression for the matrix elements of the system of linear equations (244). It is a multidimensional integral of the kernel of the equation, which is also a multidimensional integral. For the physical problem that we consider, it is possible to rearrange integrals and precompute some inner integrals providing significant speed-up of the whole computation. In next paragraphs, we detail this procedure for both methods, i.e., for the method with periodic orbits and for the general one.

Evaluation of $a_{\mathbf{i},\mathbf{j}}^{\mathbf{l},\mathbf{m}}$ for the method with periodic orbits We need to compute the following expression (244):

$$a_{\mathbf{i},\mathbf{j}}^{\mathbf{l},\mathbf{m}}(\mathsf{s}) = \int_{G_{\mathbf{j}}} K(\boldsymbol{\xi}^{\mathbf{i},\mathbf{l}}, \vec{\mathsf{y}}, \mathsf{s}) \boldsymbol{\phi}^{\mathbf{j},\mathbf{m}}(\vec{\mathsf{y}}) d\vec{y}, \tag{268}$$

with the kernel (225). Inserting into the equation (225) the expression (222) for $\mathsf{R}\big(\vec{\mathsf{x}}, \vec{\mathsf{x}}', \vec{\mathsf{v}}\big)$, changing infinite domain of the integral over $\vec{\mathsf{v}}$ to $\left[-\frac{\pi}{2}, \frac{\pi}{2}\right]^d$ via

change of variables, and putting $\mathsf{t}=0$, we have

$$\mathsf{K}_0\big(\vec{\mathsf{x}},\vec{\mathsf{x}}',\mathsf{s}\big)=F_{\mathrm{d}}\frac{1}{\mathrm{e}^{\frac{2\pi}{\tilde{\omega}}\mathsf{s}}-1}\int\limits_{\left[-\frac{\pi}{2},\frac{\pi}{2}\right]^d}\int\limits_0^{\frac{2\pi}{\tilde{\omega}}}\left(\frac{\partial}{\partial\vec{\mathsf{X}}_0\left(\mathsf{t}_1\right)}\mathsf{G}(\vec{\mathsf{X}}_0\left(\mathsf{t}_1\right),\vec{\mathsf{x}}')\cdot\right.$$
$$\left.\cdot\ \frac{\partial\mathsf{f}_0(\vec{\mathsf{X}}_0\left(\mathsf{t}_1\right),\vec{\mathsf{V}}_0\left(\mathsf{t}_1\right))}{\partial\vec{\mathsf{V}}_0\left(\mathsf{t}_1\right)}\right)\Bigg|_{\mathsf{v}_i=\tan\mathsf{v}_i}\mathrm{e}^{\mathsf{s}\mathsf{t}_1}d\mathsf{t}_1\frac{d\vec{\mathsf{v}}}{\prod_i\cos^2(\mathsf{v}_i)}. \tag{269}$$

Let us look at the integrand. We have the following expressions for the orbits:

$$\begin{cases}\mathsf{X}_{0i}\left(\mathsf{t}_1\right)=\mathsf{x}_i\cos\left(\tilde{\omega}\mathsf{t}_1\right)+\frac{\mathsf{v}_i}{\tilde{\omega}_i}\sin\left(\tilde{\omega}\mathsf{t}_1\right),\\ \mathsf{V}_{0i}\left(\mathsf{t}_1\right)=\mathsf{v}_i\cos\left(\tilde{\omega}\mathsf{t}_1\right)-\mathsf{x}_i\tilde{\omega}_i\sin\left(\tilde{\omega}\mathsf{t}_1\right),\end{cases} \tag{270}$$

and for the equilibrium distribution:

$$\mathsf{f}_0(\vec{\mathsf{x}},\vec{\mathsf{v}})=\frac{1}{\pi^d}\mathrm{e}^{-\sum\limits_i\mathsf{a}_i\mathsf{x}_i^2-\frac{1}{2}\sum\limits_i\mathsf{v}_i^2}, \tag{271}$$

and its derivative:

$$\frac{\partial\mathsf{f}_0(\vec{\mathsf{X}}_0\left(\mathsf{t}_1\right),\vec{\mathsf{V}}_0\left(\mathsf{t}_1\right))}{\partial\vec{\mathsf{V}}_0\left(\mathsf{t}_1\right)}=-2\mathsf{f}_0(\vec{\mathsf{x}},\vec{\mathsf{v}})\vec{\mathsf{V}}_0\left(\mathsf{t}_1\right). \tag{272}$$

Thus, we obtain for the kernel:

$$\mathsf{K}_0\big(\vec{\mathsf{x}},\vec{\mathsf{x}}',\mathsf{s}\big)=-2F_{\mathrm{d}}\frac{1}{\mathrm{e}^{\frac{2\pi}{\tilde{\omega}}\mathsf{s}}-1}\int\limits_{\left[-\frac{\pi}{2},\frac{\pi}{2}\right]^d}\int\limits_0^{\frac{2\pi}{\tilde{\omega}}}\left(\frac{\partial\mathsf{G}}{\partial\vec{\mathsf{x}}}\big(\vec{\mathsf{x}}\cos\left(\tilde{\omega}\mathsf{t}_1\right)+\frac{\vec{\mathsf{v}}}{\tilde{\omega}_i}\sin\left(\tilde{\omega}\mathsf{t}_1\right),\vec{\mathsf{x}}'\big)\ \times\right.$$
$$\left.\times\ \left(\vec{\mathsf{v}}\cos\left(\tilde{\omega}\mathsf{t}_1\right)-\vec{\mathsf{x}}\tilde{\omega}_i\sin\left(\tilde{\omega}\mathsf{t}_1\right)\right)\mathsf{f}_0(\vec{\mathsf{x}},\vec{\mathsf{v}})\right)\big|_{\mathsf{v}_i=\tan\mathsf{v}_i}\mathrm{e}^{\mathsf{s}\mathsf{t}_1}d\mathsf{t}_1\frac{d\vec{\mathsf{v}}}{\prod_i\cos^2(\mathsf{v}_i)}. \tag{273}$$

In expression (268), the kernel should be integrated with the polynomials:

$$\boldsymbol{\phi}^{\mathbf{j},\mathbf{m}}\left(\vec{\mathsf{y}}\right)=\prod_{i=1}^d\prod_{r=1\ldots m}^{r\neq m_i}\frac{\left(\mathsf{y}_i-\xi_i^{j_i,r}\right)}{\left(\xi_i^{j_i,m_i}-\xi_i^{j_i,r}\right)}= \tag{274}$$
$$=\prod_{i=1}^d\prod_{r=1\ldots m}^{r\neq m_i}\frac{1}{\left(\xi_i^{j_i,m_i}-\xi_i^{j_i,r}\right)}\times\prod_{i=1}^d\prod_{r=1\ldots m}^{r\neq m_i}\left(\mathsf{y}_i-\xi_i^{j_i,r}\right), \tag{275}$$

i.e.,

$$a_{\mathbf{i},\mathbf{j}}^{\mathbf{l},\mathbf{m}}(\mathsf{s}) = \frac{1}{\prod_{i=1}^{d}\prod_{r=1\ldots m}^{r\neq m_i}\left(\xi_i^{j_i,m_i} - \xi_i^{j_i,r}\right)} \int_{G_{\mathbf{j}}} K(\boldsymbol{\xi}^{\mathbf{i},\mathbf{l}}, \vec{\mathsf{y}}, \mathsf{s}) \prod_{i=1}^{d}\prod_{r=1\ldots m}^{r\neq m_i}\left(\mathsf{y}_i - \xi_i^{j_i,r}\right) d\vec{y}. \tag{276}$$

We change the order of integration and obtain:

$$a_{\mathbf{i},\mathbf{j}}^{\mathbf{l},\mathbf{m}}(\mathsf{s}) = g(\mathsf{s}) \int_{G_{\mathbf{j}}} \int_{0}^{\frac{2\pi}{\omega}} \int_{[-L_v, L_v]^d} F^{\mathbf{j},\mathbf{m}}(\xi^{\mathbf{i},\mathbf{l}}, \vec{\mathsf{y}}, \vec{\mathsf{v}}, \mathsf{t}_1) d\vec{\mathsf{v}} \mathrm{e}^{\mathsf{s}\mathsf{t}_1} d\mathsf{t}_1 d\vec{\mathsf{y}},$$

where

$$g(\mathsf{s}) = \frac{1}{\mathrm{e}^{\frac{2\pi}{\omega}\mathsf{s}} - 1}, \tag{277}$$

and what is denoted by $F^{\mathbf{j},\mathbf{m}}(\xi^{\mathbf{i},\mathbf{l}}, \vec{\mathsf{y}}, \vec{\mathsf{v}}, \mathsf{t}_1)$ is clear from the expression (276). We pre-compute and store the boxed integral:

$$a_{\mathbf{i},\mathbf{j}}^{\mathbf{l},\mathbf{m}}(\mathsf{s}) = g(\mathsf{s}) \int_{0}^{\frac{2\pi}{\omega}} \boxed{\int_{G_{\mathbf{j}}} \int_{[-L_v, L_v]^d} F^{\mathbf{j},\mathbf{m}}(\xi^{\mathbf{i},\mathbf{l}}, \vec{\mathsf{y}}, \vec{\mathsf{v}}, \mathsf{t}_1) d\vec{\mathsf{v}} d\vec{\mathsf{y}}} \mathrm{e}^{\mathsf{s}\mathsf{t}_1} d\mathsf{t}_1.$$

For the equilibrium distribution, we precompute $\vec{\mathsf{v}}$-related factors and $\vec{\mathsf{x}}$-related factors separately:

$$\mathsf{f}_0(\boldsymbol{\xi}^{\mathbf{i},\mathbf{l}}, \vec{\mathsf{v}}) = \frac{1}{\pi^d} \mathrm{e}^{-\sum_j \mathsf{a}_i \xi_j^{\mathbf{i},\mathbf{l}^2} - \frac{1}{2}\sum_i \mathsf{v}_i^2} \equiv \mathrm{e}^{\mathbf{i},\mathbf{l}} \prod_{i=1}^{d} \mathrm{e}^{-\frac{1}{2}\mathsf{v}_i^2}. \tag{278}$$

We obtain the final expression for the matrix element:

$$a_{\mathbf{i},\mathbf{j}}^{\mathbf{l},\mathbf{m}}(\mathsf{s}) = g(\mathsf{s}) \int\limits_0^{\frac{2\pi}{\omega}} \Bigg[\frac{-2d_f F_{\mathrm{d}} \mathrm{e}^{\mathbf{i},\mathbf{l}}}{\prod\limits_{i=1}^{d} \prod\limits_{r=1\ldots m}^{r\neq m_i} \left(\xi_i^{j_i,m_i} - \xi_i^{j_i,r}\right)} \times$$
$$\times \int_{G_{\mathbf{j}}} \int\limits_{[-L_v,L_v]^d} \frac{\boldsymbol{\xi}^{\mathbf{i},\mathbf{l}} \cos\left(\tilde{\omega}\mathsf{t}_1\right) + \frac{\vec{\mathsf{v}}}{\tilde{\omega}_i} \sin\left(\tilde{\omega}\mathsf{t}_1\right) - \vec{\mathsf{y}}}{\left| \boldsymbol{\xi}^{\mathbf{i},\mathbf{l}} \cos\left(\tilde{\omega}\mathsf{t}_1\right) + \frac{\vec{\mathsf{v}}}{\tilde{\omega}_i} \sin\left(\tilde{\omega}\mathsf{t}_1\right) - \vec{\mathsf{y}} \right|^d} \cdot$$
$$\cdot \left(\vec{\mathsf{v}} \cos\left(\tilde{\omega}\mathsf{t}_1\right) - \boldsymbol{\xi}^{\mathbf{i},\mathbf{l}} \tilde{\omega}_i \sin\left(\tilde{\omega}\mathsf{t}_1\right)\right) \prod_{i=1}^{d} \mathrm{e}^{-\frac{1}{2}\mathsf{v}_i^2} d\vec{\mathsf{v}} \prod_{i=1}^{d} \prod_{r=1\ldots m}^{r\neq m_i} \left(\mathsf{y}_i - \xi_i^{j_i,r}\right) d\vec{\mathsf{y}} \Bigg] \mathrm{e}^{\mathsf{s}\mathsf{t}_1} d\mathsf{t}_1, \tag{279}$$

where d is a dimensionality of space and d_f is a constant factor in the expression for derivative of the Green's function. Denoting expression in square brackets as $\tilde{a}_{\mathbf{i},\mathbf{j}}^{\mathbf{l},\mathbf{m}}(\mathsf{t}_1)$, we have:

$$a_{\mathbf{i},\mathbf{j}}^{\mathbf{l},\mathbf{m}}(\mathsf{s}) = g(\mathsf{s}) \int\limits_0^{\frac{2\pi}{\omega}} \tilde{a}_{\mathbf{i},\mathbf{j}}^{\mathbf{l},\mathbf{m}}(\mathsf{t}_1) \mathrm{e}^{\mathsf{s}\mathsf{t}_1} d\mathsf{t}_1.$$

We pre-compute $\tilde{a}_{\mathbf{i},\mathbf{j}}^{\mathbf{l},\mathbf{m}}(\mathsf{t}_1)$ for the nodes of the integral over t_1 and store them, it will be a vector of matrices. Similarly we proceed with the left-hand side:

$$\mathsf{F}_0\left(\vec{\mathsf{x}},\mathsf{s}\right) = ZF_{\mathrm{d}} \frac{2}{\mathrm{e}^{\frac{2\pi}{\tilde{\omega}}\mathsf{s}} - 1} \int\limits_{[-L_v,L_v]^d} \int\limits_0^{\frac{2\pi}{\omega}} \int\limits_0^1 \frac{\frac{\partial \mathsf{G}}{\partial \vec{\mathsf{x}}} \left(\vec{\mathsf{X}}_0\left(\mathsf{t}_1\right), \vec{\mathsf{Y}}\left(\frac{1-\mathsf{t}_2}{\mathsf{t}_2}\right)\right)}{\mathrm{e}^{\left(\frac{1-\mathsf{t}_2}{\mathsf{t}_2}\right)\mathsf{s}-\mathsf{t}_1\mathsf{s}}} \frac{d\mathsf{t}_2}{\mathsf{t}_2^2} \times$$
$$\times \left(\vec{\mathsf{v}} \cos\left(\tilde{\omega}\mathsf{t}_1\right) - \vec{\mathsf{x}}\tilde{\omega}_i \sin\left(\tilde{\omega}\mathsf{t}_1\right)\right) \mathsf{f}_0(\vec{\mathsf{x}},\vec{\mathsf{v}}) d\mathsf{t}_1 d\vec{\mathsf{v}}, \tag{280}$$

$$\mathsf{F}_0(\boldsymbol{\xi}^{\mathbf{i,l}},\mathsf{s}) = \frac{1}{\mathrm{e}^{\frac{2\pi}{\tilde{\omega}}\mathsf{s}}-1}\int\limits_0^{\frac{2\pi}{\omega}}\int\limits_0^1$$
$$2Zd_fF_{\mathrm{d}}\mathrm{e}^{\mathbf{i,l}}\int\limits_{[-L_v,L_v]^d}\frac{\boldsymbol{\xi}^{\mathbf{i,l}}\cos(\tilde{\omega}\mathsf{t}_1)+\frac{\vec{\mathsf{v}}}{\tilde{\omega}_i}\sin(\tilde{\omega}\mathsf{t}_1)-\vec{\mathsf{x}}_0-\vec{\mathsf{v}}_0\frac{1-\mathsf{t}_2}{\mathsf{t}_2}}{\left|\boldsymbol{\xi}^{\mathbf{i,l}}\cos(\tilde{\omega}\mathsf{t}_1)+\frac{\vec{\mathsf{v}}}{\tilde{\omega}_i}\sin(\tilde{\omega}\mathsf{t}_1)-\vec{\mathsf{x}}_0-\vec{\mathsf{v}}_0\frac{1-\mathsf{t}_2}{\mathsf{t}_2}\right|^d}\cdot$$
$$\cdot\left(\vec{\mathsf{v}}\cos(\tilde{\omega}\mathsf{t}_1)-\boldsymbol{\xi}^{\mathbf{i,l}}\tilde{\omega}_i\sin(\tilde{\omega}\mathsf{t}_1)\right)\prod_{i=1}^{d}\mathrm{e}^{-\frac{1}{2}\mathsf{v}_i^2}d\vec{\mathsf{v}}\frac{1}{\mathsf{t}_2^2}\mathrm{e}^{-\left(\frac{1-\mathsf{t}_2}{\mathsf{t}_2}\right)\mathsf{s}}d\mathsf{t}_2\mathrm{e}^{\mathsf{t}_1\mathsf{s}}d\mathsf{t}_1. \tag{281}$$

We denote the integral over $\vec{\mathsf{v}}$ multiplied by a constant and $\frac{1}{\mathsf{t}_2^2}$ as $\tilde{\mathsf{F}}(\boldsymbol{\xi}^{\mathbf{i,l}},\mathsf{t}_1,\mathsf{t}_2)$ and obtain:

$$\mathsf{F}_0(\boldsymbol{\xi}^{\mathbf{i,l}},\mathsf{s}) = g(\mathsf{s})\int\limits_0^{\frac{2\pi}{\omega}}\int\limits_0^1\tilde{\mathsf{F}}(\boldsymbol{\xi}^{\mathbf{i,l}},\mathsf{t}_1,\mathsf{t}_2)\mathrm{e}^{-\left(\frac{1-\mathsf{t}_2}{\mathsf{t}_2}\right)\mathsf{s}}d\mathsf{t}_2\mathrm{e}^{\mathsf{t}_1\mathsf{s}}d\mathsf{t}_1. \tag{282}$$

We precompute $\tilde{\mathsf{F}}(\boldsymbol{\xi}^{\mathbf{i,l}},\mathsf{t}_1,\mathsf{t}_2)$ for nodes of integrals over t_1 and t_2.

With precomputed $\tilde{a}_{\mathbf{i,j}}^{\mathbf{l,m}}(\mathsf{t}_1)$ and $\tilde{\mathsf{F}}(\boldsymbol{\xi}^{\mathbf{i,l}},\mathsf{t}_1,\mathsf{t}_2)$, integrals for the system of linear equations can be evaluated much faster.

Evaluation of $a_{\mathbf{i,j}}^{\mathbf{l,m}}$ for the method for non-periodic orbits In this case, we need to compute

$$a_{\mathbf{i,j}}^{\mathbf{l,m}}(\mathsf{s}) = \int_{G_{\mathbf{j}}}K(\boldsymbol{\xi}^{\mathbf{i,l}},\vec{\mathsf{y}},\mathsf{s})\boldsymbol{\phi}^{\mathbf{j,m}}(\vec{\mathsf{y}})d\vec{y} \tag{283}$$

with the kernel given by equation (223). Doing the same transformations as in the previous paragraph, we obtain

$$\mathsf{K}\left(\vec{\mathsf{x}},\vec{\mathsf{x}}',\mathsf{s}\right) = -2F_{\mathrm{d}}\int\limits_0^1\int\limits_{\mathbb{R}^d}\frac{\partial\mathsf{G}}{\partial\vec{\mathsf{x}}}(\vec{\mathsf{x}}\cos(\tilde{\omega}\mathsf{t})-\frac{\vec{\mathsf{v}}}{\tilde{\omega}_i}\sin(\tilde{\omega}\mathsf{t}),\vec{\mathsf{x}}')\times$$
$$\times\left(\vec{\mathsf{v}}\cos(\tilde{\omega}\mathsf{t})+\vec{\mathsf{x}}\tilde{\omega}_i\sin(\tilde{\omega}\mathsf{t})\right)\mathsf{f}_0(\vec{\mathsf{x}},\vec{\mathsf{v}})|_{\mathsf{t}=\frac{1-\mathsf{t}}{\mathsf{t}}}\frac{1}{\mathsf{t}^2}\mathrm{e}^{-\mathsf{s}\left(\frac{1-\mathsf{t}}{\mathsf{t}}\right)}d\vec{\mathsf{v}}d\mathsf{t}. \tag{284}$$

The kernel should be integrated with polynomials:

$$a_{\mathbf{i,j}}^{\mathbf{l,m}}(\mathsf{s}) = \int_{G_{\mathbf{j}}}K(\boldsymbol{\xi}^{\mathbf{i,l}},\vec{\mathsf{y}},\mathsf{s})\boldsymbol{\phi}^{\mathbf{j,m}}(\vec{\mathsf{y}})d\vec{\mathsf{y}}, \tag{285}$$

$$\boldsymbol{\phi}^{\mathbf{j},\mathbf{m}}\left(\vec{\mathsf{y}}\right)=\prod_{i=1}^{d}\prod_{r=1\ldots m}^{r\neq m_i}\frac{\left(\mathsf{y}_i-\xi_i^{j_i,r}\right)}{\left(\xi_i^{j_i,m_i}-\xi_i^{j_i,r}\right)}= \tag{286}$$

$$=\prod_{i=1}^{d}\prod_{r=1\ldots m}^{r\neq m_i}\frac{1}{\left(\xi_i^{j_i,m_i}-\xi_i^{j_i,r}\right)}\times\prod_{i=1}^{d}\prod_{r=1\ldots m}^{r\neq m_i}\left(\mathsf{y}_i-\xi_i^{j_i,r}\right), \tag{287}$$

$$a_{\mathbf{i},\mathbf{j}}^{\mathbf{l},\mathbf{m}}(\mathsf{s})=\frac{1}{\prod\limits_{i=1}^{d}\prod\limits_{r=1\ldots m}^{r\neq m_i}\left(\xi_i^{j_i,m_i}-\xi_i^{j_i,r}\right)}\int_{G_{\mathbf{j}}}K(\boldsymbol{\xi}^{\mathbf{i},\mathbf{l}},\vec{\mathsf{y}},\mathsf{s})\prod_{i=1}^{d}\prod_{r=1\ldots m}^{r\neq m_i}\left(\mathsf{y}_i-\xi_i^{j_i,r}\right)d\vec{y}. \tag{288}$$

We exchange integration order, precompute and store boxed integral:

$$a_{\mathbf{i},\mathbf{j}}^{\mathbf{l},\mathbf{m}}(\mathsf{s})=\int_0^1\boxed{\int_{G_{\mathbf{j}}}\int_{[-L_v,L_v]^d}F^{\mathbf{j},\mathbf{m}}(\xi^{\mathbf{i},\mathbf{l}},\vec{\mathsf{y}},\vec{\mathsf{v}},\mathsf{t})d\vec{\mathsf{v}}d\vec{\mathsf{y}}}\,\mathrm{e}^{-\mathsf{s}\left(\frac{1-\mathsf{t}}{\mathsf{t}}\right)}d\mathsf{t}, \tag{289}$$

what is denoted by $F^{\mathbf{j},\mathbf{m}}(\xi^{\mathbf{i},\mathbf{l}},\vec{\mathsf{y}},\vec{\mathsf{v}},\mathsf{t})$ clear from the expression (289). For the equilibrium distribution, we precompute $\vec{\mathsf{v}}$-related factors and $\vec{\mathsf{x}}$-related factors separately:

$$\mathsf{f}_0(\boldsymbol{\xi}^{\mathbf{i},\mathbf{l}},\vec{\mathsf{v}})=\frac{1}{\pi^{d-1}}\mathrm{e}^{-\sum\limits_{j\neq1}\mathsf{a}_i\xi_j^{\mathbf{i},\mathbf{l}^2}-\frac{1}{2}\sum\limits_i\mathsf{v}_i^2}\equiv\mathrm{e}^{\mathbf{i},\mathbf{l}}\prod_{i=1}^{d}\mathrm{e}^{-\frac{1}{2}\mathsf{v}_i^2}, \tag{290}$$

with that, we have:

$$\begin{aligned}a_{\mathbf{i},\mathbf{j}}^{\mathbf{l},\mathbf{m}}(\mathsf{s})=\int_0^1\Bigg[&-2d_fF_{\mathrm{d}}\mathrm{e}^{\mathbf{i},\mathbf{l}}\prod_{i=1}^{d}\prod_{r=1\ldots m}^{r\neq m_i}\left(\xi_i^{j_i,m_i}-\xi_i^{j_i,r}\right)^{-1}\times\\&\times\int_{G_{\mathbf{j}}}\int_{[-L_v,L_v]^d}\frac{\boldsymbol{\xi}^{\mathbf{i},\mathbf{l}}\cos\left(\tilde{\omega}\mathsf{t}_1\right)+\frac{\vec{\mathsf{v}}}{\tilde{\omega}_i}\sin\left(\tilde{\omega}\mathsf{t}_1\right)-\vec{\mathsf{y}}}{\left|\boldsymbol{\xi}^{\mathbf{i},\mathbf{l}}\cos\left(\tilde{\omega}\mathsf{t}_1\right)+\frac{\vec{\mathsf{v}}}{\tilde{\omega}_i}\sin\left(\tilde{\omega}\mathsf{t}_1\right)-\vec{\mathsf{y}}\right|^d}\cdot\\&\cdot\left(\vec{\mathsf{v}}\cos\left(\tilde{\omega}\mathsf{t}_1\right)-\boldsymbol{\xi}^{\mathbf{i},\mathbf{l}}\tilde{\omega}_i\sin\left(\tilde{\omega}\mathsf{t}_1\right)\right)\prod_{i=1}^{d}\mathrm{e}^{-\frac{1}{2}\mathsf{v}_i^2}d\vec{\mathsf{v}}\times\\&\times\prod_{i=1}^{d}\prod_{r=1\ldots m}^{r\neq m_i}\left(\mathsf{y}_i-\xi_i^{j_i,r}\right)d\vec{\mathsf{y}}\frac{1}{\mathsf{t}^2}\Bigg]\mathrm{e}^{-\mathsf{s}\left(\frac{1-\mathsf{t}}{\mathsf{t}}\right)}d\mathsf{t},\end{aligned} \tag{291}$$

where d is a dimensionality of space and d_f is a constant factor in the expression for derivative of the Green's function. Denoting expression in square brackets as $\tilde{a}^{\mathbf{l},\mathbf{m}}_{\mathbf{i},\mathbf{j}}(\mathsf{t})$, we have:

$$a^{\mathbf{l},\mathbf{m}}_{\mathbf{i},\mathbf{j}}(\mathsf{s}) = \int\limits_0^1 \tilde{a}^{\mathbf{l},\mathbf{m}}_{\mathbf{i},\mathbf{j}}(\mathsf{t}) \mathrm{e}^{-\mathsf{s}\left(\frac{1-\mathsf{t}}{\mathsf{t}}\right)} \frac{1}{\mathsf{t}^2} d\mathsf{t}.$$

We precompute $\tilde{a}^{\mathbf{l},\mathbf{m}}_{\mathbf{i},\mathbf{j}}(\mathsf{t})$ for the nodes of the integral over t and store them, it will be a vector of matrices. Similarly we proceed with the left-hand side. In this case, it is given by:

$$\begin{aligned}\mathsf{F}\left(\vec{\mathsf{x}},\mathsf{s}\right) =& 2F_{\mathrm{d}} Z \int\limits_0^{\infty}\int\limits_0^{\mathsf{t}} \frac{\partial \mathsf{G}}{\partial \vec{\mathsf{x}}}\left(\vec{\mathsf{X}}_0\left(\mathsf{t}_1\right), \vec{\mathsf{Y}}\left(\frac{1-\mathsf{t}_2}{\mathsf{t}_2}\right)\right) \times \\ & \times \left(\vec{\mathsf{v}}\cos\left(\tilde{\omega}\mathsf{t}_1\right) - \vec{\mathsf{x}}\tilde{\omega}_i \sin\left(\tilde{\omega}\mathsf{t}_1\right)\right) \mathsf{f}_0(\vec{\mathsf{x}},\vec{\mathsf{v}}) \mathrm{e}^{-\mathsf{st}} d\mathsf{t}_1 d\mathsf{t} d\vec{\mathsf{v}}. \end{aligned} \tag{292}$$

In the same way as in the previous paragraph, we expand it:

$$\begin{aligned}\mathsf{F}(\boldsymbol{\xi}^{\mathbf{i},\mathbf{l}},\mathsf{s}) = & \int\limits_0^1\int\limits_0^{\mathsf{t}} \int\limits_{[-L_v,L_v]^d} \frac{\boldsymbol{\xi}^{\mathbf{i},\mathbf{l}}\cos\left(\tilde{\omega}\mathsf{t}_1\right) + \frac{\vec{\mathsf{v}}}{\tilde{\omega}_i}\sin\left(\tilde{\omega}\mathsf{t}_1\right) - \vec{\mathsf{x}}_0 - \vec{\mathsf{v}}_0\frac{1-\mathsf{t}_2}{\mathsf{t}_2}}{\left|\boldsymbol{\xi}^{\mathbf{i},\mathbf{l}}\cos\left(\tilde{\omega}\mathsf{t}_1\right) + \frac{\vec{\mathsf{v}}}{\tilde{\omega}_i}\sin\left(\tilde{\omega}\mathsf{t}_1\right) - \vec{\mathsf{x}}_0 - \vec{\mathsf{v}}_0\frac{1-\mathsf{t}_2}{\mathsf{t}_2}\right|^d} \cdot \\ & \cdot \left(\vec{\mathsf{v}}\cos\left(\tilde{\omega}\mathsf{t}_1\right) - \boldsymbol{\xi}^{\mathbf{i},\mathbf{l}}\tilde{\omega}_i\sin\left(\tilde{\omega}\mathsf{t}_1\right)\right) 2Z d_f F_{\mathrm{d}} \prod_{i=1}^{d} \mathrm{e}^{-\frac{1}{2}\mathsf{v}_i^2} d\vec{\mathsf{v}} \mathrm{e}^{\mathbf{i},\mathbf{l}} d\mathsf{t}_1 \mathrm{e}^{-\mathsf{s}\left(\frac{1-\mathsf{t}}{\mathsf{t}}\right)} \frac{1}{\mathsf{t}^2} d\mathsf{t}. \end{aligned} \tag{293}$$

We denote the integral over $\vec{\mathsf{v}}$ multiplied by a constant as $\tilde{\mathsf{F}}(\boldsymbol{\xi}^{\mathbf{i},\mathbf{l}},\mathsf{t},\mathsf{t}_1)$ and obtain:

$$\mathsf{F}(\boldsymbol{\xi}^{\mathbf{i},\mathbf{l}},\mathsf{s}) = \int\limits_0^1\int\limits_0^{\mathsf{t}} \tilde{\mathsf{F}}(\boldsymbol{\xi}^{\mathbf{i},\mathbf{l}},\mathsf{t},\mathsf{t}_1) d\mathsf{t}_1 \mathrm{e}^{-\mathsf{s}\left(\frac{1-\mathsf{t}}{\mathsf{t}}\right)} \frac{1}{\mathsf{t}^2} d\mathsf{t}, \tag{294}$$

we precompute $\tilde{\mathsf{F}}(\boldsymbol{\xi}^{\mathbf{i},\mathbf{l}},\mathsf{t},\mathsf{t}_1)$ for nodes of integrals over t and t_1.

Summary This pre-computation allows to compute elements of the system of linear equations much faster. For sparse grids, we tested this faster method and obtained exactly same results for the physical problem, as we obtained using the general solver, which was tested on exactly solvable equations. We conclude that our solver works correctly and provides an opportunity to solve the realistic 3D problem with fine grids.

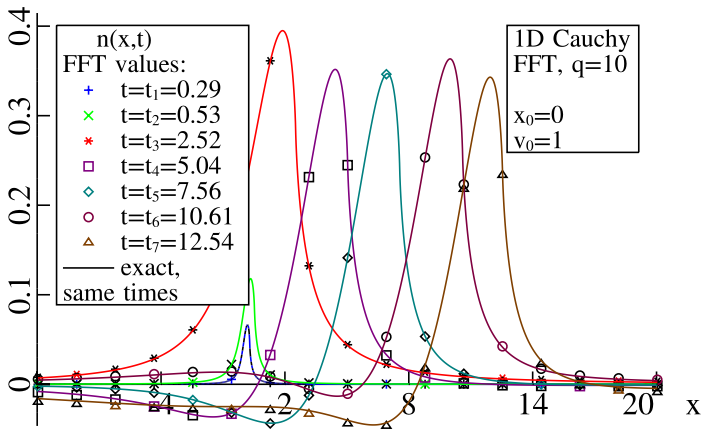

Figure 12: The density $\mathsf{n}_1(\vec{\mathsf{x}}, \mathsf{t})$ for the infinite plasma with the 1D Cauchy velocity distribution obtained via exact formula (72) and numerically via the FFT.

4.4 Test charge problem for an infinite plasma

Before discussing our numerical results for the confined plasma, we remind the reader our results for the infinite plasma, which was detailed in section 2. All the features of shielding in the infinite plasma can be seen in the case of 1D Cauchy distribution, which is depicted in Fig. 12.

For the infinite plasma, we observe a density peak, which follows the charge with a little delay. Due to infiniteness of the plasma's charge, for small time values, we observe positive peak without any negative peaks. Then, size of the peak increases, and negative and additional positive peaks appear – these are standard plasma oscillations. Then we observe saturation, i.e., peak stops growing and its hight oscillates around some value; these oscillations disappear at infinity due to Landau damping.

4.5 Numerical results

In subsection 4.2, we derived two different integral equations for the test charge problem in a confined plasma. One equation can deal with both confined and infinite plasmas; the kernel and the left-hand side are given by the formulae (223) and (224), respectively. Although, this method can deal

with infinite plasmas, the numerical method that we described in subsection 4.3 is only for compact domains; some modifications are required to solve the equations with infinite domains, which we are not going to discuss here. For infinite plasmas, there are much simpler methods that are thoroughly developed in [10]. The second integral equation with the kernel and the left-hand side given by (225) and (226) can deal only with a spherical confined plasma; however, it has simpler integrals over time that can be computed faster. We did numerical tests of both methods for a confined plasma and obtained the same results, this confirms that the methods are equivalent for spherical plasmas, as they should be according to our theory.

In this subsection, we focus on a confined spherical plasma with the normal (Maxwell) velocity and spatial distributions given by (208). The components of vector $\vec{\mathsf{a}}$ in the expression for the equilibrium distribution characterize the plasma's size; for example, when they all equal one, σ also equals one, and more than 99.9% of the plasma lie within a ball of radius 3, accordingly to considerations in subsection 4.2.6.

We will graphically present our results obtained via the second method. We show plots for some time values, but we would like to emphasize that, when solution is obtained, it is available for all time points in a certain predefined range. We consider the 1D, 2D and 3D cases in order. Then we will discuss our results.

We also assume that perturbation is zero outside of the d-dimensional rectangle $\prod_{j=1}^{d}[-4\sigma_j, 4\sigma_j]$, where σ_j is defined via (211), and take this rectangle as a domain of the integral equations. In all plots, the time and distance are measured in units of inverse plasma frequency and the Debye radius, defined in (192) and (193), respectively.

Since in the 1D case, the time dependence is quite simple, we depicted the densities with time step 0.5. In the 2D and 3D cases, it is more complicated; hence, we plotted it with a time step 0.1 and depicted for the values, for which important features of the dynamics of the density are more pronounced.

For simplicity, we did computations for the external charges moving with a constant velocity along straight lines; however, the method and our software can deal with charges moving along any trajectory.

All computations were performed on Edison machine at NERSC. Edison is a Cray XC30 supercomputer with 5,576 nodes, which are two twelve-core Intel "Ivy Bridge" 2.4 GHz processors with 64 GB of RAM. The 1D case

was computed on 2,048 cores in 14 seconds. The 2D case was computed on 4,096 cores in 14 minutes and 12 seconds. Computation of the 3D case was split into two steps: evaluation the matrix and right-hand side of the system (253), and solving this system via LU decomposition. The first step was done on 16,392 cores (16,392 MPI tasks, 683 nodes) in 2 hours, and the second step was done on 3,072 cores (256 MPI tasks, two tasks per node or one task per 12 cores – we needed more memory on each task) in 36 minutes. Computation of the second step can be accelerated approximately by a factor of 10 by using parallel LU decomposition reducing computation of the whole 3D problem to almost 2 hours. The great advantage of our program is its ability to utilize effectively thousands of cores available on modern supercomputers.

4.5.1 Numerical results for 1D plasma

In this case, we consider an external charge starting moving with velocity $\mathsf{v}_0 = 1$ from the center of the plasma, $\mathsf{x}_0 = 0$, and moving with the same velocity, but from outside of the plasma, i.e., $\mathsf{x}_0 = -4$.

In Fig. 13, we show our results for the "$\mathsf{x}_0 = 0$" case and, in Fig. 14, for "$\mathsf{x}_0 = -4$". They exhibit three main qualitative differences from the results for the infinite plasma shown in Fig. 12; for more plots for the infinite plasma, we refer to [10]. For the infinite plasma, the peak of the perturbation quite closely follows the charge, just with a little delay, while, for the confined plasma, the symmetry of the plasma has much larger affection on the perturbation's density than the charge's position, which only determines location of the positive and negatives peaks relatively to the center of the plasma; this is because the density perturbation is affected by the confining and space-charge fields, which equal zero in the infinite plasma case. Another difference is a compensation of the positive peak, which is around the charge, by a negative one. In the infinite plasma, this compensation occurs only for the large time values, while, for the confined plasma, it always exists. This effect is reasonable, since the total charge of the confined plasma is finite. The last difference lies in the dynamics of the perturbation. In the infinite plasma, the perturbation reaches certain value, i.e., saturates, and then slightly oscillates around this value, as shown in Fig. 3 for the Cauchy velocity distribution, for the results for other distributions, we refer to [10], while for the confined plasma, an amplitude of the oscillations is much larger and they take place around zero. These oscillations are seen for large time

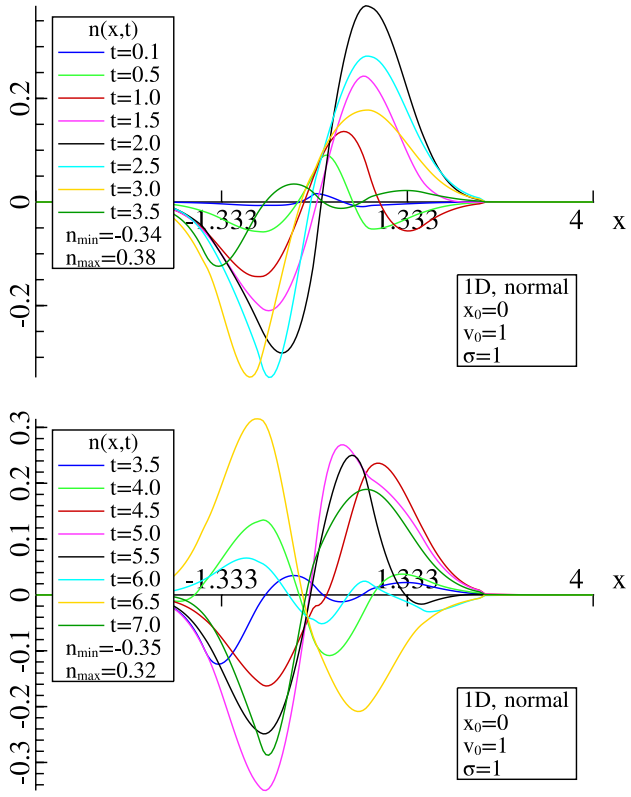

Figure 13: Dynamics of the density $n(\vec{\mathsf{x}}, \mathsf{t})$ for the 1D plasma with the normal spatial and velocity distributions and for a charge starting moving from $\mathsf{x}_0 = 0$.

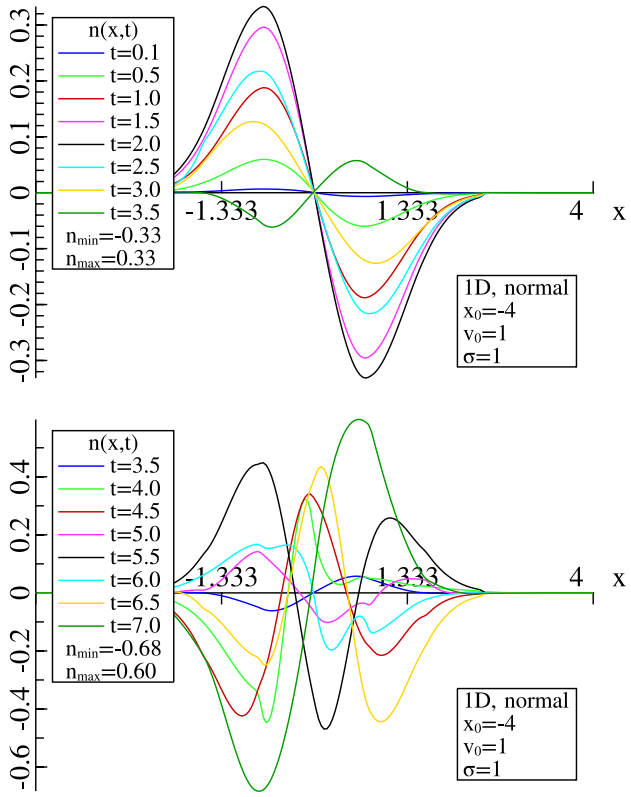

Figure 14: Dynamics of the density $n(\vec{\mathsf{x}}, \mathsf{t})$ for the 1D plasma with the normal spatial and velocity distributions and for a charge starting moving from $\mathsf{x}_0 = -4$.

values in Fig. 13 and Fig. 14.

A point charge in the 1D space corresponds to a charged plane perpendicular to x axis in a 3D plasma with the x-dependent distribution, in our case, the normal distribution along x axis and the uniform with the infinite support (support of a function is a set of points where the function is nonzero) along two other axes. If this plane has equation $x = c$, where c is some constant, the potential and the charge density do not depend on z and y and equations are the same as we have in the 1D case.

4.5.2 Numerical results for 2D plasma

In the 2D case, we consider an and an external charge starting moving from the center of the plasma along x axis with velocity $\vec{v} = (1.0, 0.0)$.

Figure 15 shows the electron density for different values of the time; these are the contour density plots, depicting lines, along which the density is constant; we call them the *equidensity contours*. For some contours, values of the density are shown on the graphs; for others, the values can be obtained via the color bars attached to the plots. As we see from the plots, for times smaller than one half, there is no significant negative peak, and the negative density is spread out around a positive peak, while for the 1D case, both peaks are of the same size from the beginning. Then, the positive peak continues to grow and a negative peak starts to build up, but in front of the positive peak; in the 1D case, it was behind the positive one. For times greater than one, another negative peak appears, now, behind the positive one; and they both become very spiky, then they widen for a time around two. Thereafter, the oscillations continue; for a time about 3.5, the positive peak has negative x coordinate and the negative – positive, and then they widen. These oscillations continue for larger times.

A point charge in the 2D space corresponds to a charged infinite line in a 3D plasma with the z-independent distribution; in our case, it is an infinite cylinder with the normal distribution in transverse directions and uniform with infinite support in longitudinal.

4.5.3 Numerical results for 3D plasma

In the 3D case, we consider the problem with an external charge starting moving from the center of the plasma along y axis with velocity $\vec{v} = (0.0, 1.0, 0.0)$. In this case, we show the results as 3D density plots, which depict equidensity

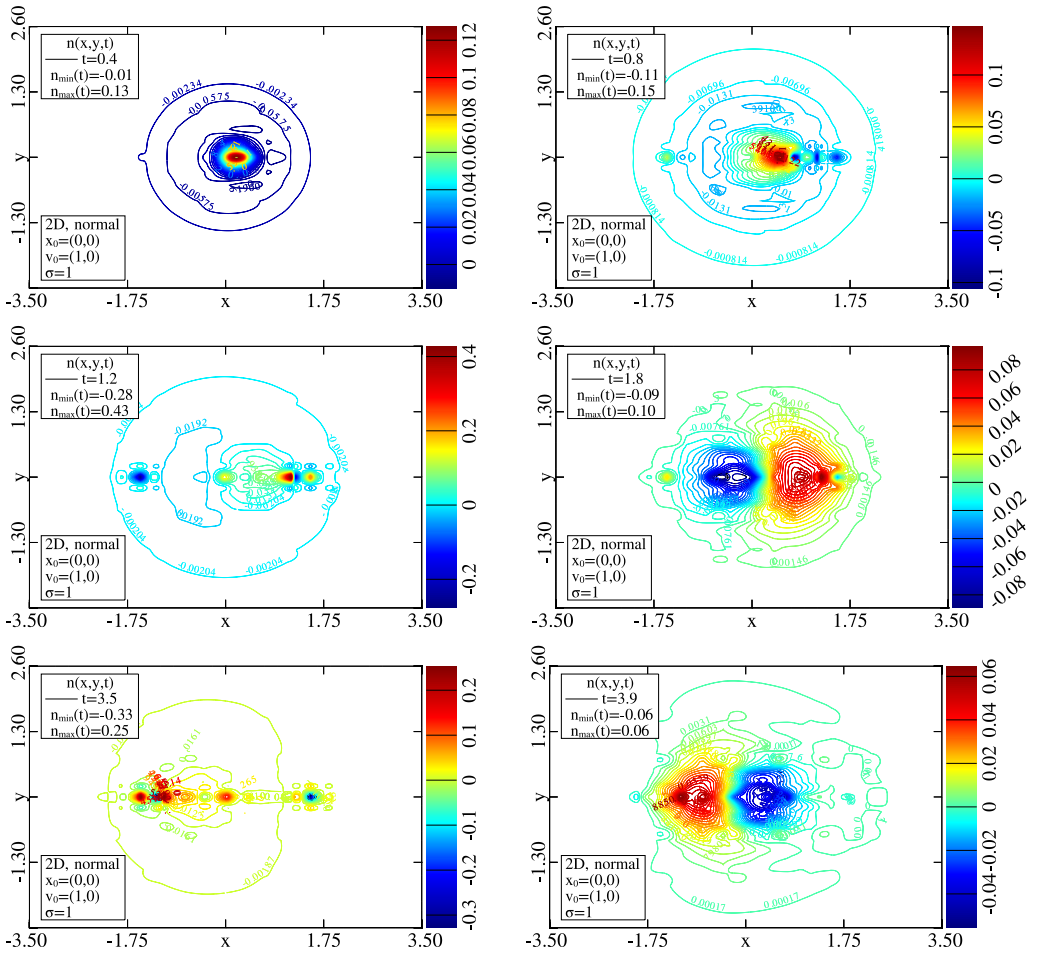

Figure 15: Dynamics of the density $n(\vec{\mathrm{x}}, \mathrm{t})$ for the 2D plasma with normal spatial and velocity distributions for different values of time; the external charge starts moving from $\vec{\mathrm{x}}_0 = (0.0, 0.0)$ with velocity $\vec{\mathrm{v}}_0 = (1.0, 0.0)$; each plot has its own color bar.

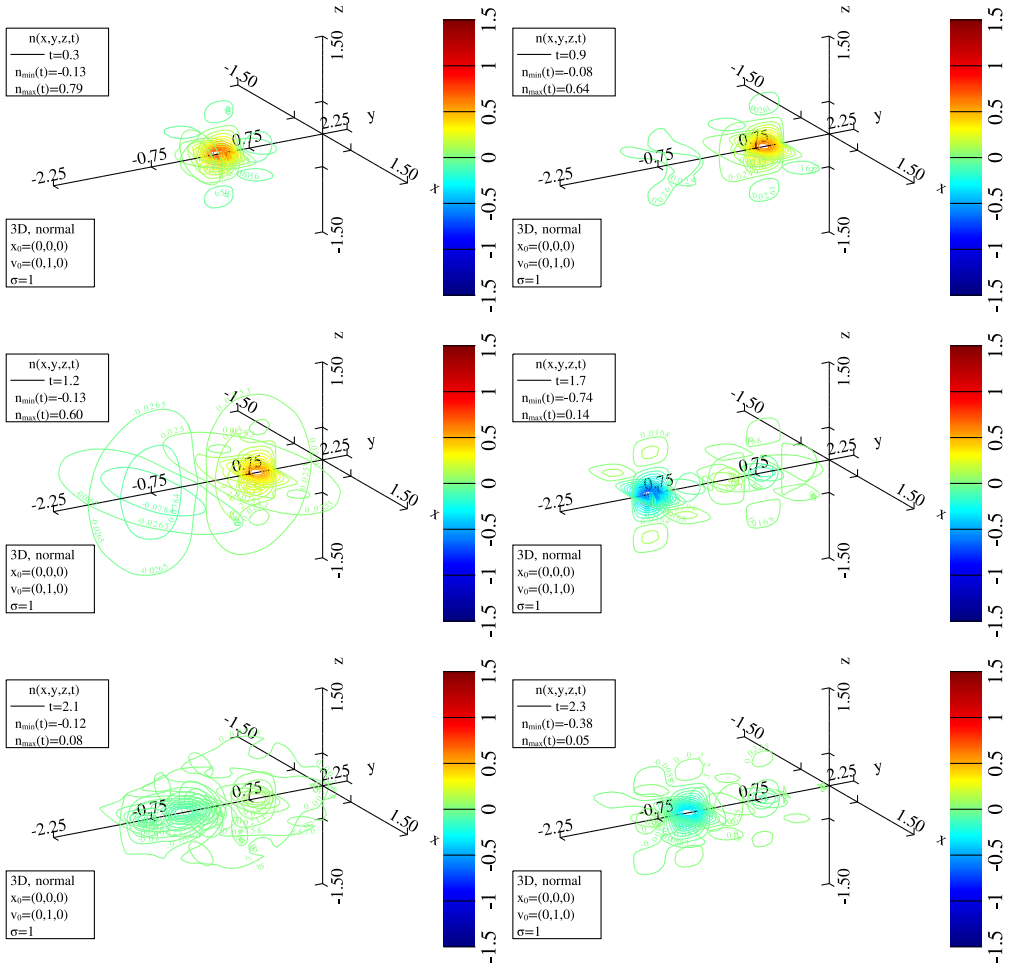

Figure 16: Dynamics of the density $n(\vec{\mathsf{x}}, \mathsf{t})$ for the 3D plasma with normal spatial and velocity distributions for different values of time; the external charge starts moving from $\vec{\mathsf{x}}_0 = (0.0, 0.0, 0.0)$ with velocity $\vec{\mathsf{v}}_0 = (0.0, 1.0, 0.0)$.

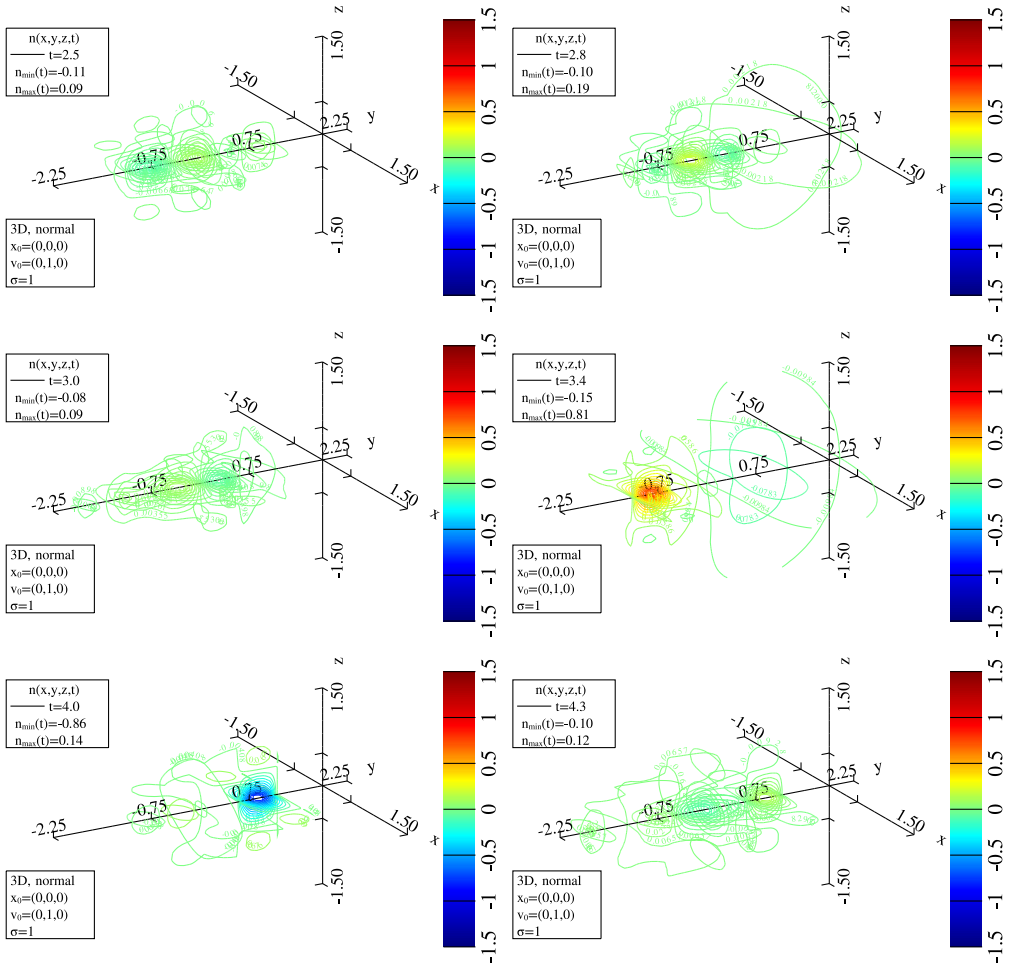

Figure 17: Dynamics of the density $n(\vec{\mathsf{x}}, \mathsf{t})$ for the 3D plasma with normal spatial and velocity distributions for different values of time; the external charge starts moving from $\vec{\mathsf{x}}_0 = (0.0, 0.0, 0.0)$ with velocity $\vec{\mathsf{v}}_0 = (0.0, 1.0, 0.0)$.

contours in the planes $\mathsf{x} = 0$ and $\mathsf{z} = 0$; some plots also have few lines in the plane $\mathsf{y} = 0$.

Figures 16 and 17 depict the densities for different times. The dynamics is quite similar to that in the 2D case. In the beginning, there is a positive peak, which follows the external charge and the negative density is spread around. This peak reaches its maximum height at $\mathsf{t} \approx 0.9$. Then, this peak continues to exist, and its height decreases, until $\mathsf{t} = 1.7$, when it almost disappears and negative peak appears in the negative part of y axis. For $\mathsf{t} = 2.1$, both peaks are relatively small and have almost the same sizes. Thereafter, for $\mathsf{t} = 2.3$, we see the negative peak in a negative part of the y axis; for $\mathsf{t} = 2.5$, the negative and positive peaks are of the same size. Then, a positive peak appears in the negative part of the y axis, and then, the positive and negative peaks have almost same size for $\mathsf{t} = 3.0$. For $\mathsf{t} = 3.4$ and $\mathsf{t} = 4.0$, we see a quite large positive peak in the negative part and negative peak in the positive part, respectively. For $\mathsf{t} = 4.3$, the peaks are almost of the same size. At this time, the charge is outside of the plasma and barely affects its charge distribution. For larger time values, the oscillations continue but with decreasing amplitudes, as we see for the time values $\mathsf{t} = 3.4$ and $\mathsf{t} = 4.0$, similarly to the lower dimensional cases.

In this subsection, we described our results for the test charge problem in a 3D confined plasma. These results can be used to analyze the dynamics of shielding of a charge particle in a bunched electron beam that is needed to model the modulator section of the coherent electron cooling; we will discuss this after explaining physics of the observed effects.

4.5.4 Discussion

Dynamics of the density perturbation caused by interaction of plasma with a moving charged particle has some qualitative features that can be seen in both confined and infinite plasmas. However, there are also differences, which are caused by an interaction with the confining fields.

There is always a main positive peak, which follows the charge, as shown in Figures 5, 7, 8 and 12 for the infinite plasma, and in Figures 13 - 17 for the confined; this peak is caused by attraction between plasma's particles and an external charge. In the infinite plasma (with infinite charge), the charges are coming from infinity and sole positive peaks can occur for small time values, as shown in Figures 5, 7, 8 and 12. In contrast, in the finite plasma, the charge is finite and conserved, and positive peaks are always surrounded by

negative density regions or well-formed negative peaks, as shown in Figures 13 - 17.

For large time values, negative and spurious positive peaks appear in the infinite plasma. For the infinite 1D Cauchy plasma, appearance of additional peaks is confirmed by the exact analytical solution (72) depicted in Fig. 3, for other distributions, it is confirmed by numerical solutions [10]. These are the plasma oscillations (also known as Langmuir waves) induced by sudden appearance and movement of the external charge. These plasma waves are solutions of the Vlasov-Poisson system for both infinite and confined plasmas and they are also seen in Figures 13 - 17 for the confined plasma. Their amplitude decreases because of the Landau damping.

The confined plasma considered doesn't have an actual boundary, however, the confining fields serve as one and we observe reflections of the plasma waves from this effective boundary. In the 1D case, there is only one spatial dimension and reflection of the wave from the boundary leads to decrease of the positive peak and then to its transformation into the negative one. It is seen in Fig. 13: the perturbation reaches its maximum at $\mathsf{t} = 2.0$ and then decreases, then the charge leaves the plasma and we see standing wave with decreasing amplitude. In Fig. 14, the situation is more complicated, since the charge spends more time in the plasma and travels across it, but reflections are also there. In the 2D and 3D cases, the situation is different, since we still have a point (zero-dimensional) charge traveling along a line, which is a 1D object, but the plasma has more spatial dimensions. The plasma waves sourced at the location of the charge travel to the boundary in all directions, then reflect from the boundary and form a negative peak at the location opposite to the location of the charge with respect to center of the plasma. In the 2D and 3D cases, these negative peaks appear at $\mathsf{t} = 1.2$ and $\mathsf{t} = 1.7$, respectively. Thus, confining fields serve as a reflecting boundary, which focuses reflected waves to the position opposite to the location of the initial peak with respect to the origin in the 2D and 3D cases, and just reflects the wave in the 1D case.

Then, in all confined plasmas, we see a standing density waves. These waves are harmonic oscillations of the perturbation's density in the confining fields, which correspond to x-dependent part of the Hamiltonian H_0 (205):

$$\mathsf{H}_0 = \sum_i \mathsf{a}_i \mathsf{x}_i^2 + \frac{1}{2} \sum_i \mathsf{v}_i^2. \tag{295}$$

We consider symmetric case, for which all a_i equal 1; denoting them as a, we

obtain for the dimensionless frequency $\tilde{\omega}_0$:

$$\tilde{\omega}_0 = \sqrt{2\mathsf{a}}. \tag{296}$$

For $\mathsf{a} = 1$, we have for the dimensionless period T_0:

$$\mathsf{T}_0 = \frac{2\pi}{\tilde{\omega}_0} = \sqrt{2}\pi \approx 4.44, \text{ and } \frac{\mathsf{T}_0}{2} \approx 2.22. \tag{297}$$

This value for the half-period is in an agreement with the observed behavior. In the 2D case, the changes of the density profiles between $\mathsf{t} = 1.8$ and $\mathsf{t} = 3.9$, and $\mathsf{t} = 1.2$ and $\mathsf{t} = 3.5$ correspond to half-oscillation and time differences are close to the computed value for the half-period. (We plotted densities with time step 0.1, so the exact equality should not be expected.) Similarly, in the 3D case, we see half-oscillation from $\mathsf{t} = 1.7$ to $\mathsf{t} = 4.0$, and from $\mathsf{t} = 1.2$ to $\mathsf{t} = 3.4$. Since the 1D plasma is not symmetric with respect to charge's trajectory, as the 2D and 3D plasmas, and there is no focusing in the 1D case, the standing wave behaves a bit differently in the 1D plasma case.

In the 2D and 3D case, there is another interesting effect: oscillations of the shape of the peaks of the standing density wave. In the 2D case, we see wide peaks for $\mathsf{t} = 1.8$ and $\mathsf{t} = 3.9$ and spiky peaks for $\mathsf{t} = 1.2$ and $\mathsf{t} = 3.5$. Similarly, in the 3D case, we see wide peaks for $\mathsf{t} = 2.1$ and $\mathsf{t} = 4.3$ and spiky peaks for $\mathsf{t} = 1.7$ and $\mathsf{t} = 4.0$. This effect is caused by reflection and focusing of the standing wave in the confining fields: the wide density profiles reach the boundary and then focuses into spiky peaks, then widen again, etc. In the 1D case, we do not see this widening and shrinking of the peaks, since we do not have focusing, which is responsible for this effect, the wave just reflects.

Another feature is damped oscillations of the maximum of the positive peak for the large time values. This effect is caused by the Landau damping and confirmed for the infinite plasma by the exact solution (72) plotted in Fig. 3. For the large time values, the charge does not leave the plasma and perturbation continues to exist approaching constant nonzero value at infinity [9]. In the confined plasma case, oscillations in the confining fields have much larger amplitude and this effect is not clearly observable. For the large time values, the charge is outside of the plasma and do not affect much the plasma's charge distribution, which is controlled by the space charge fields and confining fields, which damp the perturbation caused by the charge.

4.5.5 Application to the coherent electron cooling

The device for the coherent electron cooling proof of principle (PoP) experiment is being constructed in the Relativistic Heavy Ion Collider (RHIC) at Brookhaven National Laboratory [5]. To apply our results to the modulator section of the device, we need to recover the dimensional quantities. For the PoP experiment, we have the Debye radius $r_{\mathrm{D}} = 4.65 \cdot 10^{-5}\,\mathrm{m}$ and plasma frequency $\omega_{\mathrm{p}} = 6.436 \cdot 10^{9}\,\mathrm{s}^{-1}$. The dimensional electron density perturbation can be obtained as follows:

$$n_1\left(\vec{x}, t\right) = r_{\mathrm{D}}^{-d} \mathsf{n}_1\left(r_{\mathrm{D}}^{-1}\vec{x}, \omega_{\mathrm{p}} t\right), \tag{298}$$

where d is a spatial dimension of the problem; for the real 3D case, $d = 3$. In the PoP experiment, the modulator is designed such that the interaction time is around one half of the plasma period, it is one half in our dimensionless units, and it depends on the hadron's velocity, since the modulator's length is constant. The velocity is measured in units of electron beam's v_{rms}, in the PoP experiment, $v_{\mathrm{rms}} = 3.0 \cdot 10^{5}\,\frac{\mathrm{m}}{\mathrm{s}}$.

Our computations for the 3D confined plasma show that for times around one half of the plasma period the density perturbation follows the charge, and there are no considerable negative peaks, which could cause problems in a CeC device, since they also would be amplified in an FEL and created electric fields that would undesirably accelerate the hadrons. Since the peaks grow with time and we are interested in largest possible ones, the maximum time, for which there are no negative peaks, sets limit on a possible length of the modulator. Although, it is possible to determine the precise time value, for which negative peaks of a certain size appear, it wouldn't make sense, since the modulator's length is constant and hadrons have different velocities, thus their passing through the modulator takes different times. For the 3D ball that we considered, it is $\mathsf{t} \approx 1.2$, this time is larger than the modulation time in the PoP experiment, thus the modulator can even be extended. Moreover, in the actual device, the bunches are not ball-like; their longitudinal size is larger than transversal, and so the hadrons will pass through a much smaller part of the bunch, than in our computations, and these edge effects will not play a role, thus, spurious perturbations will not cause any problems.

Although, we shed some light on the dynamics of the perturbation in the device for the CeC PoP experiment, the main goal was to develop the method and explore the physics of the shielding in the confined plasma.

4.6 Conclusion

In this section, we studied in detail dynamical test charge problem for the confined plasma. We developed a novel method for solving this problem. We considered a collisionless single-species electron plasma; the method can be easily generalized to a multi-species plasma. While other known non-simulation methods are applicable only to the infinite plasma [9, 10], our method is developed for the confined plasmas and can be modified to deal with the infinite plasma as well.

The idea underlying the method is to transform the Vlasov-Poisson system of differential equations to an integral equation for the Laplace image of the density perturbation, and then to solve this equation numerically. To solve the integral equation, we applied the piecewise polynomial collocation method [35] that we reviewed in detail. We used the FFT to compute the inverse Laplace transform.

We developed a stand-alone solver for the Fredholm integral equations, and for the Laplace-Fredholm ones, which are Fredholm equations for the Laplace image of the quantity of interest. Our solver can be used to solve other equations of this type; for example, such equations appear in the three-dimensional theory of high-gain free-electron lasers [21]. All our programs are object-oriented, parallel, and written in C++; the complete source code is available at [34] under the GNU General Public License; all computations were performed on Cray supercomputers at the National Energy Research Scientific Computing Center (NERSC).

Our computations revealed a few important features of the shielding of a charged particle in a confined plasma. Similarly to the case of the infinite plasma, in addition to main positive peak, we see plasma oscillations, i.e., negative and positive peaks of the density perturbation, these peaks can be comparable in size to the main positive peak. For the case of confined plasma, especially, for large time values, the shape of the perturbation is mostly determined by the symmetry of the plasma, and we observe density oscillations in the confining fields that occur around zero, while for the case of the infinite plasma [9, 10], the density oscillates around some saturation value and follows the charge even for large time values. These differences are caused by non-zero confining and space-charge fields in the confined plasma and by the finiteness of its charge. The confining fields create an effective boundary, which reflects plasma waves. For the 2D and 3D plasmas, we observe focusing of these reflected waves and formation of additional peaks

via this mechanism; reflections and focusing also explain oscillations of the shape of the peaks, i.e., spiky and wide peaks are observed. In the 1D plasma, there is no focusing, only reflections, and there are no spiky peaks.

The method developed provides an opportunity to compute shielding effects in confined plasmas, which are realistic models of the corresponding physical systems in accelerator physics, astrophysics and other areas of plasma physics such as physics of dusty plasmas. In particular, these computations will allow to advance further theoretical modeling of the coherent electron cooling.

5 Conclusion

The main result of the present thesis is a development of a new method for solving the dynamical test charge problem for the confined plasma, a realistic model of an electron beam (and other physical systems in astrophysics and physics of dusty plasmas). This problem is important for modeling the coherent electron cooling, a modern hadron beam cooling technique.

We started our considerations with a simpler problem, i.e., the dynamical test charge problem for the infinite plasma. The Vlasov-Poisson system for this problem can be solved via the Fourier and Laplace transforms and the general solution for the arbitrary equilibrium distribution $\mathsf{f}_0\left(\vec{\mathsf{v}}\right)$ and point charge traveling along a straight line can be obtained (60):

$$\mathsf{n}_1\left(\vec{\mathsf{x}},\mathsf{t}\right)=\mathsf{L}^{-1}\mathsf{F}^{-1}\left[\frac{\mathrm{e}^{-i\vec{\mathsf{k}}\cdot\vec{\mathsf{x}}_0}}{\left(\frac{f_d^{-1}v_{\mathrm{rms}}^{-d}}{\mathsf{LF}_{\vec{\mathsf{k}}\mathsf{t}}(\mathsf{tf}_0(\vec{\mathsf{v}}))}+1\right)\left(\mathsf{s}+i\vec{\mathsf{k}}\cdot\vec{\mathsf{v}}_0\right)}\right]. \tag{299}$$

For the 1D Cauchy distribution, (69),

$$\mathsf{f}_0(\vec{\mathsf{v}})=\frac{1}{\pi\left(1+\mathsf{v}^2\right)}, \tag{300}$$

the integral transforms can be inverted analytically and we can obtain exact solution (72):

$$\begin{aligned}\mathsf{n}_1\left(\vec{\mathsf{x}},\mathsf{t}\right)=&\frac{1}{4\pi}\frac{1}{\mathsf{v}_0-i}\left(\mathrm{e}^{-\mathcal{A}_+}\left(\mathrm{Ei}(\mathcal{A}_+)-\mathrm{Ei}(\mathcal{B}_+)\right)+\mathrm{e}^{\mathcal{A}_+}\left(\mathrm{E}_1(\mathcal{A}_+)-\mathrm{E}_1(\mathcal{B}_+)\right)\right)+\\&+\frac{1}{4\pi}\frac{1}{\mathsf{v}_0+i}\left(\mathrm{e}^{-\mathcal{A}_-}\left(\mathrm{Ei}(\mathcal{A}_-)-\mathrm{Ei}(\mathcal{B}_-)\right)+\mathrm{e}^{\mathcal{A}_-}\left(\mathrm{E}_1(\mathcal{A}_-)-\mathrm{E}_1(\mathcal{B}_-)\right)\right),\end{aligned} \tag{301}$$

where

$$\mathcal{A}_\pm=\frac{\mathsf{tv}_0-\mathsf{x}+\mathsf{x}_0}{1\pm i\mathsf{v}_0},\quad \mathcal{B}_\pm=\frac{\mathsf{x}_0-\mathsf{x}\pm i\mathsf{t}}{1\pm i\mathsf{v}_0}, \tag{302}$$

and $\mathrm{E}_1(z)$ and $\mathrm{Ei}(z)$ are the exponential integral functions [27]. For other equilibrium distributions, the integral transforms in must be inverted numerically. We discussed algorithms in appendix A and the results obtained in subsections 2.2 and 2.3.

The Fourier methods developed for the test charge problem for the infinite plasma can be applied to the FEL section of the CeC as well. We discussed this in section 3, where we derived formulas for the amplified density perturbation (124) and SASE contribution (130).

The Vlasov-Poisson system for the test charge problem for the confined plasma contains additional term in the Vlasov equation and cannot be solved using methods that worked for the infinite plasma. We proposed a new solving technique, in which the system is transformed into the Fredholm equation for the Laplace image of the solution, we call such equation the Laplace-Fredholm equation for the density perturbation (221):

$$\mathsf{F}\left(\vec{\mathsf{x}},\mathsf{s}\right)=\mathsf{N}_1(\vec{\mathsf{x}},\mathsf{s})-\int\mathsf{N}_1(\vec{\mathsf{x}}^{\,\prime},\mathsf{s})\mathsf{K}\big(\vec{\mathsf{x}},\vec{\mathsf{x}}^{\,\prime},\mathsf{s}\big)d\vec{\mathsf{x}}^{\,\prime}. \tag{303}$$

For the kernel $\mathsf{K}\big(\vec{\mathsf{x}},\vec{\mathsf{x}}^{\,\prime},\mathsf{s}\big)$ and the left-hand side $\mathsf{F}\left(\vec{\mathsf{x}},\mathsf{s}\right)$, we derived two different expressions one is for general orbits and the other is for periodic. The latter is less general, but faster. These are the expressions (225) and (226) (we set $\mathsf{t}=0$):

$$\mathsf{K}\big(\vec{\mathsf{x}},\vec{\mathsf{x}}^{\,\prime},\mathsf{s}\big)=\frac{1}{\mathrm{e}^{\frac{2\pi}{\omega}\mathsf{s}}-1}\int\limits_0^{\frac{2\pi}{\omega}}\int\mathsf{R}\big(\vec{\mathsf{X}}_0\left(\mathsf{t}_1\right),\vec{\mathsf{x}}^{\,\prime},\vec{\mathsf{V}}_0\left(\mathsf{t}_1\right)\big)\mathrm{e}^{\mathsf{s}\mathsf{t}_1}d\vec{\mathsf{v}}d\mathsf{t}_1, \tag{304}$$

$$\mathsf{F}\left(\vec{\mathsf{x}},\mathsf{s}\right)=-Z\frac{1}{\mathrm{e}^{\frac{2\pi}{\omega}\mathsf{s}}-1}\int\limits_0^{\infty}\int\limits_0^{\frac{2\pi}{\omega}}\int\mathsf{R}\big(\vec{\mathsf{X}}_0\left(\mathsf{t}_1\right),\vec{\mathsf{Y}}\left(\mathsf{t}_1\right),\vec{\mathsf{V}}_0\left(\mathsf{t}_1\right)\big)\mathrm{e}^{(\mathsf{t}_1-\mathsf{t}_2)\mathsf{s}}d\vec{\mathsf{v}}d\mathsf{t}_1d\mathsf{t}_2, \tag{305}$$

where, in orbits, t is also should be set to zero, and $\mathsf{R}\big(\vec{\mathsf{x}},\vec{\mathsf{x}}^{\,\prime},\vec{\mathsf{v}}\big)$ is given by (222):

$$\mathsf{R}\big(\vec{\mathsf{x}},\vec{\mathsf{x}}^{\,\prime},\vec{\mathsf{v}}\big)=F_{\mathrm{d}}\frac{\partial\mathsf{G}(\vec{\mathsf{x}},\vec{\mathsf{x}}^{\,\prime})}{\partial\vec{\mathsf{x}}}\frac{\partial\mathsf{f}_0(\vec{\mathsf{x}},\vec{\mathsf{v}})}{\partial\vec{\mathsf{v}}}, \tag{306}$$

where F_{d} is a dimensionless constant characterizing the equilibrium distribution, $\mathsf{G}(\vec{\mathsf{x}},\vec{\mathsf{x}}^{\,\prime})$ is the Green's function, and $\mathsf{f}_0(\vec{\mathsf{x}},\vec{\mathsf{v}})$ is the equilibrium distribution.

In subsection 4.3, we describe the piecewise polynomial collocation method for the Fredholm equation and our extension of it for the Laplace-Fredholm

equation. We implemented this methods as a parallel object-oriented program written in C++ and available at [34] under GNU GPL License; the program was tested on some exactly solvable equations. Multidimensional integrators is an important part of the program and we describe our integrators in appendix E. We discuss our numerical results in subsection 4.5.

The results obtained can be used to analyze the modulator of the coherent electron cooling. After the modulator, the perturbation created will be amplified in the FEL, thus the larger the perturbation, the better. In the initial analysis of the modulator, its length was suggested to be such that, on average, the hadron spends one half of the plasma period in the modulator.

Our computations suggest that the modulator can be extended. For the infinite plasma, we obtained that the perturbation grows approximately until 3 plasma periods (for the Cauchy and normal distributions), then it saturates and oscillates around this saturation value. For the 3D confined plasma, we obtained that the perturbation grows approximately until 1.2 plasma periods and then it decreases due to edge effects. These two cases are extreme cases; in the real beam, the edge effects will affect the perturbation less than in the confined plasma considered, since the longitudinal size of the actual bunch is greater than of the one considered. Thus, the modulator can be made at least two times longer and the edge effects will not cause any problems.

A Numerical evaluation of the inverse Laplace and Fourier transforms

In this appendix, we provide definitions of the Fourier and Laplace transforms, and corresponding inverse transforms. We discuss their numerical evaluation via converting them to the discrete Fourier transform (DFT). We conclude the section with the fast Fourier transform algorithm for the DFT.

A.1 The Fourier transform

We use the following definition of the Fourier transform:

$$\mathcal{F}f\left(x\right)\equiv\tilde{f}\left(k\right)=\int\limits_{-\infty}^{\infty}f\left(x\right)\mathrm{e}^{-ikx}dx, \tag{307}$$

and the inverse Fourier transform:

$$\mathcal{F}^{-1}\tilde{f}\left(k\right)\equiv f\left(x\right)=\frac{1}{2\pi}\int\limits_{-\infty}^{\infty}\tilde{f}\left(k\right)\mathrm{e}^{ikx}dk. \tag{308}$$

When we write the Fourier transform or its inverse for the dimensionless variables, we use F and F^{-1}, respectively. The discrete Fourier transform (DFT) assigns to the set of points $\{x_n\}_{0\leq n\leq N-1}$ the set of points $\{X_k\}_{0\leq k\leq N-1}$:

$$X_k=\sum_{n=0}^{N-1}x_n\mathrm{e}^{-2\pi i\frac{kn}{N}}, \tag{309}$$

we use the following notation:

$$X_k=\mathrm{DFT}_k\left[\{x_n\}_{0\leq n\leq N-1}\right]. \tag{310}$$

The DFT can be computed numerically using the effective fast Fourier transform (FFT) algorithm, there are parallel algorithms allowing to increase the speed of computations.

A.2 The Laplace transform

The Laplace transform of function $f(t)$ is defined as follows:

$$\mathcal{L}f(t) \equiv \tilde{f}(s) = \int_0^\infty f(t)\mathrm{e}^{-ts}dt, \tag{311}$$

and the inverse:

$$\mathcal{L}^{-1}\tilde{f}(s) \equiv f(t) = \frac{1}{2\pi i}\int_{\sigma-i\infty}^{\sigma+i\infty} \tilde{f}(s)\mathrm{e}^{ts}ds, \tag{312}$$

where σ is a real constant greater than the real parts of all singularities of $\tilde{f}(s)$, we use L and L^{-1} for the dimensionless variables.

A.3 The inverse Fourier transform via the DFT

The inverse Fourier transform can be approximated by the discrete one. Approximating the integral by

$$f\left(x\right) \approx \frac{1}{2\pi}\int_{-a}^{a} \tilde{f}\left(k\right)\mathrm{e}^{ikx}dk, \tag{313}$$

and, introducing the following notations

$$k_n = -a + \frac{2a}{N}n,\ x_j = \frac{N\pi}{2a} - \frac{\pi}{a}j,\ \ C_j = \frac{a}{N\pi}\mathrm{e}^{-i\pi\frac{N}{2}}\left(-1\right)^j, \tag{314}$$

we obtain:

$$f\left(x_j\right) \approx C_j\sum_{n=0}^{N-1}\tilde{f}\left(k_n\right)\left(-1\right)^n\mathrm{e}^{-i\frac{2\pi nj}{N}} = C_j\mathrm{DFT}_j\left[\{\tilde{f}\left(k_n\right)\left(-1\right)^n\}_{0\le n\le N-1}\right]. \tag{315}$$

A.4 Multidimensional Inverse Fourier transform via DFT

Similar expressions can be written for the multidimensional Fourier transform. Approximating the integral by

$$f\left(\vec{x}\right) \approx \frac{1}{2\pi}\int_{\mathcal{C}} \tilde{f}\left(\vec{k}\right)\mathrm{e}^{i\vec{k}\cdot\vec{x}}d\vec{k}, \tag{316}$$

where $\mathcal{C} = \left[-a^{(1)}, a^{(1)}\right] \times \ldots \times \left[-a^{(d)}, a^{(d)}\right]$ and introducing the following notations

$$k^{(i)}_{n^{(i)},} = -a^{(i)} + \frac{2a^{(i)}}{N^{(i)}} n^{(i)}, \;\; x^{(i)}_{j^{(i)}} = \frac{N^{(i)}\pi}{2a^{(i)}} - \frac{\pi}{a^{(i)}} j^{(i)}, \tag{317}$$

$$C^{(i)}_{j^{(i)}} = \frac{a^{(i)}}{N^{(i)}\pi} \mathrm{e}^{-i\pi \frac{N^{(i)}}{2}} (-1)^{j^{(i)}}, \tag{318}$$

and we have

$$\begin{aligned} & f^{(d-1)}\left(k_{n^{(1)}}, \ldots, k_{n^{(d-1)}}, x^{(d)}_{j^{(d)}}\right) = \\ & = C_{j^{(d)}} \mathrm{DFT}_{j^{(d)}} \left[\{\tilde{f}\left(k_{n^{(1)}}, \ldots, k_{n^{(d)}}\right)(-1)^{n^{(d)}}\}_{0 \le n^{(d)} \le N^{(d)}-1}\right], \end{aligned} \tag{319}$$

and

$$\begin{aligned} & f^{(l-2)}\left(k_{n^{(1)}}, \ldots, k_{n^{(l)}}, x^{(l-1)}_{j^{(l-1)}}, \ldots, x^{(d)}_{j^{(d)}}\right) = \\ & = C_{j^{(l-1)}} \mathrm{DFT}_{j^{(l-1)}} \left[\{f^{(l-1)}\left(k_{n^{(1)}}, \ldots, k_{n^{(l-1)}}, x^{(l)}_{j^{(l)}}, \ldots, x^{(d)}_{j^{(d)}}\right) \times \right. \\ & \left. \times (-1)^{n^{(l-1)}}\}_{0 \le n^{(l-1)} \le N^{(l+2)}-1}\right], \end{aligned} \tag{320}$$

we apply this recurrently for $l = d, \ldots, 2$ and get

$$f\left(x^{(1)}_{j^{(1)}}, \ldots, x^{(d)}_{j^{(d)}}\right) = f^{(0)}\left(x^{(1)}_{j^{(1)}}, \ldots, x^{(d)}_{j^{(d)}}\right). \tag{321}$$

A.5 The inverse Laplace transform via the DFT

The inverse Laplace transform can be expressed via the Fourier transform:

$$\mathcal{L}^{-1}\tilde{f}(s) = \frac{\mathrm{e}^{\sigma t}}{2\pi} \int\limits_{-\infty}^{\infty} \tilde{f}(\sigma + ik)\, \mathrm{e}^{ikt} dk = \mathrm{e}^{\sigma t} \mathcal{F}_k^{-1} \tilde{f}(\sigma + ik), \tag{322}$$

where σ is the same as in (312) and subscript k stands for the fact that the transform is over k. Evaluating the inverse Fourier transform via (315), we obtain:

$$f(t_j) = \mathrm{e}^{\sigma t_j} C_j \mathrm{DFT}_j \left[\{\tilde{f}(\sigma + ik_n)(-1)^n\}_{0 \le n \le N-1}\right]. \tag{323}$$

Some other algorithms for computation of the inverse Laplace transform can be found in [36, 37].

A.6 The inverse Laplace-Fourier transform via the DFT

For the 1D problems, the inverse Laplace-Fourier transform can be computed via the DFT as follows:

$$\begin{aligned} f(x_i,t_j) =& C_i C_j \mathrm{e}^{\sigma t_j} \times \\ & \times \mathrm{DFT}_i\Big[\{\mathrm{DFT}_j\left[\{\tilde{f}\left(k_{n^{(1)}},\sigma+ik_{n^{(2)}}\right)(-1)^{n^{(2)}}\}_{0\le n^{(2)}\le N^{(2)}-1}\right]\times \\ & \times (-1)^{n^{(1)}}\}_{0\le n^{(1)}\le N^{(1)}-1}\Big], \end{aligned} \tag{324}$$

where superscript $^{(2)}$ corresponds to the Laplace transform, and $^{(1)}$ to the Fourier one.

A.7 Inverse (1,d)-D Laplace-Fourier transform via DFT

In the similar way we can write a formula fot the (1,d)-dimensional case. We just modify formulas (319) and (320): and we have

$$\begin{aligned} & f^{(d-1)}\left(k_{n^{(1)}},\,\ldots,k_{n^{(d-1)}},\,x^{(d)}_{j^{(d)}},t_{j^{(d+1)}}\right) = C_{j^{(d)}}C_{j^{(d+1)}}\mathrm{e}^{\sigma t_{j^{(d)}}}\times \\ & \times \mathrm{DFT}_{j^{(d)}}\Big[\{\mathrm{DFT}_{j^{(d+1)}}\left[\{\tilde{f}\left(k_{n^{(1)}},\,\ldots,\,k_{n^{(d+1)}}\right)(-1)^{n^{(d+1)}}\}_{0\le n^{(d+1)}\le N^{(d+1)}-1}\right]\times \\ & \times (-1)^{n^{(d)}}\}_{0\le n^{(d)}\le N^{(d)}-1}\Big], \end{aligned} \tag{325}$$

where superscript $^{(d+1)}$ corresponds to the Laplace transform and

$$\begin{aligned} & f^{(l-2)}\left(k_{n^{(1)}},\,\ldots,k_{n^{(l)}},\,x^{(l-1)}_{j^{(l-1)}},\,\ldots,x^{(d)}_{j^{(d)}},t_{j^{(d+1)}}\right) = \\ & = C_{j^{(l-1)}}\mathrm{DFT}_{j^{(l-1)}}\Big[\{f^{(l-1)}\left(k_{n^{(1)}},\,\ldots,k_{n^{(l-1)}},\,x^{(l)}_{j^{(l)}},\,\ldots,x^{(d)}_{j^{(d)}},t_{j^{(d+1)}}\right)\times \\ & \times\,(-1)^{n^{(l-1)}}\}_{0\le n^{(l-1)}\le N^{(l+2)}-1}\Big], \end{aligned} \tag{326}$$

then we apply this recursively for $l=d,\,\ldots,2$ and get

$$f\left(x^{(1)}_{j^{(1)}},\,\ldots,x^{(d)}_{j^{(d)}},t_{j^{(d+1)}}\right) = f^{(0)}\left(x^{(1)}_{j^{(1)}},\,\ldots,x^{(d)}_{j^{(d)}},t_{j^{(d+1)}}\right). \tag{327}$$

A.8 The fast Fourier transform algorithm

In this subsection, we describe a very important fast Fourier transform (FFT) algorithm [38]. The discrete Fourier transform (DFT) assigns to the set of

points $\{x_n\}_{0\le n\le N-1}$ the set of points $\{X_k\}_{0\le k\le N-1}$ via (328):

$$X_k = \sum_{n=0}^{N-1} x_n \mathrm{e}^{-2\pi i \frac{kn}{N}}. \tag{328}$$

Obviously, a naive algorithm computing X_k for each k from 0 to $N-1$ will have $O(N^2)$ complexity. It is possible to reduce complexity of this computation to $O(N \log N)$. For example, in our computations, we had $N = 2^{10} = 1024$; in this case $N^2 = 1048576$ and $N \log N = 10240$, which is much less; this will be even more important for the multidimensional Fourier transforms.

We will describe the Cooley-Tukey algorithm. It uses the "divide and conquer" idea, i.e., evaluation of the DFT of size N can be split into two DFT's of size $\frac{N}{2}$, and evaluation of initial DFT of size N using these two smaller DFT's has complexity $O(N)$. This leads to the following recurrence relation for the complexity $T(N)$:

$$T(N) = 2T\left(\frac{N}{2}\right) + O(N). \tag{329}$$

The binary tree corresponding to this relation has $\log N$ levels and N leaf nodes, this gives complexity:

$$T(N) = O(N \log N). \tag{330}$$

This splitting into two smaller Fourier transforms can be done via

$$X_k = \sum_{n=0}^{\frac{N}{2}-1} x_{2n} \mathrm{e}^{-2\pi i \frac{kn}{\frac{1}{2}N}} + \mathrm{e}^{-2\pi i \frac{k}{N}} \sum_{n=0}^{\frac{N}{2}-1} x_{2n+1} \mathrm{e}^{-2\pi i \frac{kn}{\frac{1}{2}N}} \equiv E_k + \mathrm{e}^{-2\pi i \frac{k}{N}} O_k, \tag{331}$$

where it is assumed that N is a power of 2, and E_k is a first sum and O_k is the second. Taking into account

$$E_k = E_{k+\frac{1}{2}N}, \tag{332}$$

$$O_k = O_{k+\frac{1}{2}N}, \tag{333}$$

we obtain

$$\begin{cases} X_k = E_k + \mathrm{e}^{-2\pi i \frac{k}{N}} O_k, & 0 \le k < \frac{1}{2}N, \\ X_k = E_{k-\frac{1}{2}N} + \mathrm{e}^{-2\pi i \frac{k}{N}} O_{k-\frac{1}{2}N}, & \frac{1}{2}N \le k < N. \end{cases} \tag{334}$$

Using $\mathrm{e}^{-2\pi i\frac{k+\frac{1}{2}N}{N}} = -\mathrm{e}^{-2\pi i\frac{k}{N}}$, we can further simplify:

$$\begin{cases} X_k = E_k + \mathrm{e}^{-2\pi i\frac{k}{N}} O_k, & 0 \le k < \frac{1}{2}N, \\ X_{k+\frac{1}{2}N} = E_k - \mathrm{e}^{-2\pi i\frac{k}{N}} O_k, & 0 \le k < \frac{1}{2}N. \end{cases} \tag{335}$$

This expresses the DFT of size N via two DFT's of size $\frac{N}{2}$. This splitting can be continued until the size of DFT's is 1, and DFT of that size is trivial, i.e., $X_0 = x_0$. This algorithm can be easily implemented recursively. This splitting scheme also allows to parallelize the computation increasing efficiency even further.

B Special Functions

In this appendix, we define some special functions that were used in section 2 and discuss their numerical evaluation.

B.1 The exponential integral functions

The exponential integral functions are defined by [27]:

$$\mathrm{Ei}\,(z) = -\int_{-z}^{\infty} \frac{\mathrm{e}^{-t}}{t} dt, \quad \mathrm{E}_1\,(z) = \int_{z}^{\infty} \frac{\mathrm{e}^{-t}}{t} dt, \tag{336}$$

these functions can be computed via the convergent series for a small argument:

$$\mathrm{E}_1\,(z) = -\gamma - \ln z + \sum_{k=1}^{\infty} \frac{(-1)^{k+1} z^k}{k k!}, \tag{337}$$

$$\mathrm{Ei}\,(z) = \gamma + \ln z + \sum_{k=1}^{\infty} \frac{z^k}{k k!}, \tag{338}$$

where $\gamma \approx 0.57721$ is the Euler-Mascheroni constant, and via the asymptotic series for a large one:

$$\mathrm{E}_1\,(z) = \frac{\mathrm{e}^{-z}}{z} \sum_{k=0}^{N-1} \frac{k!}{(-z)^n} + O\left(N! z^{-N}\right), \tag{339}$$

$$\mathrm{Ei}\,(z) = \frac{\mathrm{e}^z}{z}\sum_{k=0}^{N-1}\frac{k!}{z^n} + O\left(N!z^{-N}\right), \tag{340}$$

where it is assumed that $|\arg z| < \pi$.

B.2 The error function

The error function and the complementary error function are defined by [27]:

$$\mathrm{Erf}(z) = \frac{2}{\sqrt{\pi}}\int_0^x \mathrm{e}^{-t^2}dt, \quad \mathrm{Erfc}(z) = 1 - \mathrm{Erf}(z), \tag{341}$$

respectively, these functions can be computed via the convergent series for a small argument and via the asymptotic series for a large one:

$$\mathrm{Erf}(z) = \frac{2}{\sqrt{\pi}}\sum_{n=0}^{\infty}\frac{z}{2n+1}\prod_{k=1}^{n}\frac{-z^2}{k}, \tag{342}$$

$$\mathrm{Erf}(z) = 1 - \frac{\mathrm{e}^{-z^2}}{z\sqrt{\pi}}\sum_{n=0}^{N-1}(-1)^n\frac{(2n-1)!!}{(2z^2)^n} + O\left(z^{-2N+1}\mathrm{e}^{-z^2}\right). \tag{343}$$

To compute the density perturbation for the normal equilibrium distribution, we need to compute the following expression:

$$\mathsf{LF}_{\vec{\mathsf{kt}}}\left(\mathsf{tf}_0\left(\vec{\mathsf{v}}\right)\right) = \frac{2}{\mathsf{k}^2}\left[1 - \sqrt{\pi}\mathrm{e}^{\mathsf{z}^2}\mathsf{z}\mathrm{Erfc}(\mathsf{z})\right], \tag{344}$$

where $\mathsf{z} = \frac{\mathsf{s}}{|\mathsf{k}|}$. For certain values of z, $\mathrm{Erfc}(z)$ diverges, while $\mathrm{e}^{z^2}z\mathrm{Erfc}(z)$ is finite, thus we use the series expansions for the whole expression:

$$\mathrm{e}^{z^2}z\mathrm{Erfc}(z) = \mathrm{e}^{z^2}z\left(1 - \frac{2}{\sqrt{\pi}}\sum_{n=0}^{\infty}\frac{z}{2n+1}\prod_{k=1}^{n}\frac{-z^2}{k}\right), \tag{345}$$

$$\mathrm{e}^{z^2}z\mathrm{Erfc}(z) = \frac{1}{\sqrt{\pi}}\sum_{n=0}^{N-1}(-1)^n\frac{(2n-1)!!}{(2z^2)^n} + O\left(z^{-2N+2}\right). \tag{346}$$

To perform the FFT, one needs to compute the expression (344) exactly at $\mathsf{k} = 0$, for this case, we write the following series:

$$\mathsf{LF}_{\vec{\mathsf{kt}}}\left(\mathsf{tf}_0\left(\vec{\mathsf{v}}\right)\right) = \frac{1}{\mathsf{s}^2} - \frac{1}{\mathsf{s}^2}\sum_{n=2}^{N-1}(-1)^n \frac{(2n-1)!!}{\left(2\mathsf{z}^2\right)^{n-1}} + O\left(\mathsf{z}^{-2N+4}\right), \tag{347}$$

thus

$$\mathsf{LF}_{\vec{\mathsf{kt}}}\left(\mathsf{tf}_0\left(\vec{\mathsf{v}}\right)\right)\big|_{\mathsf{k}=0} = \frac{1}{\mathsf{s}^2}. \tag{348}$$

C Derivation of the formula for the 1D Cauchy distribution

In this appendix, we present derivation of the formula (72). We consider the 1D Cauchy distribution (69):

$$\mathsf{f}_0(\vec{\mathsf{v}}) = \frac{1}{\pi\left(1+\mathsf{v}^2\right)}, \tag{349}$$

and the expression for the perturbation's density is given by (71):

$$\mathsf{n}_1\left(\vec{\mathsf{x}},\mathsf{t}\right) = \mathsf{L}^{-1}\mathsf{F}^{-1}\left[\frac{\mathrm{e}^{-i\vec{\mathsf{k}}\cdot\vec{\mathsf{x}}_0}}{\left(1+(\mathsf{s}+|\mathsf{k}|)^2\right)\left(\mathsf{s}+i\vec{\mathsf{k}}\cdot\vec{\mathsf{v}}_0\right)}\right]. \tag{350}$$

This expression can be computed analytically using *Mathematica* [39], the actual expression given by the program is very bulky, but can be simplified

to the form:

$$
\begin{aligned}
\mathsf{n}_1\left(\vec{\mathsf{x}},\mathsf{t}\right) =& \frac{-1}{4\pi}\mathrm{e}^{-\frac{i}{1+\mathsf{v}_0^2}\left(\mathsf{t}(2-3i\mathsf{v}_0+\mathsf{v}_0^2)+2\mathsf{v}_0(\mathsf{x}+\mathsf{x}_0)\right)}\times \\
&\times\left[\mathrm{e}^{\frac{1}{1+\mathsf{v}_0^2}\left(2\mathsf{t}(i+\mathsf{v}_0+i\mathsf{v}_0^2)+\mathsf{x}+i\mathsf{v}_0\mathsf{x}+(-1+3i\mathsf{v}_0)\mathsf{x}_0\right)}\frac{1}{\mathsf{v}_0-i}\mathrm{Ei}\left[\frac{\mathsf{x}_0-\mathsf{x}+i\mathsf{t}}{1+i\mathsf{v}_0}\right]+\right. \\
&+\mathrm{e}^{-\frac{1}{1+\mathsf{v}_0^2}(-2\mathsf{t}(i+\mathsf{v}_0)+\mathsf{x}+\mathsf{x}_0)}\left(\mathrm{e}^{\frac{1}{1+\mathsf{v}_0^2}(2\mathsf{x}+i\mathsf{v}_0(3\mathsf{x}+\mathsf{x}_0))}\frac{1}{\mathsf{v}_0+i}\mathrm{Ei}\left[\frac{\mathsf{x}_0-\mathsf{x}-i\mathsf{t}}{1-i\mathsf{v}_0}\right]-\right. \\
&-\mathrm{e}^{\frac{i\mathsf{v}_0(\mathsf{x}+\mathsf{x}_0)}{1+\mathsf{v}_0^2}}\left(\frac{1}{\mathsf{v}_0-i}\left(\mathrm{e}^{\frac{2(i\mathsf{t}\mathsf{v}_0^2+\mathsf{x}+i\mathsf{v}_0\mathsf{x}_0)}{1+\mathsf{v}_0^2}}\mathrm{Ei}\left[\frac{\mathsf{t}\mathsf{v}_0-\mathsf{x}+\mathsf{x}_0}{1+i\mathsf{v}_0}\right]+\right.\right. \\
&\left.+\mathrm{e}^{\frac{2(\mathsf{t}\mathsf{v}_0+i\mathsf{v}_0\mathsf{x}+\mathsf{x}_0)}{1+\mathsf{v}_0^2}}\left(\Gamma\left(0,\frac{\mathsf{t}\mathsf{v}_0-\mathsf{x}+\mathsf{x}_0}{1+i\mathsf{v}_0}\right)-\Gamma\left(0,\frac{\mathsf{x}_0-\mathsf{x}+i\mathsf{t}}{1+i\mathsf{v}_0}\right)\right)\right)+ \\
&+\frac{1}{\mathsf{v}_0+i}\left(\mathrm{e}^{\frac{2i\mathsf{x}}{i+\mathsf{v}_0}}\mathrm{Ei}\left[\frac{\mathsf{t}\mathsf{v}_0-\mathsf{x}+\mathsf{x}_0}{1-i\mathsf{v}_0}\right]-\right. \\
&\left.\left.\left.\left.\left.-\mathrm{e}^{\frac{2i(\mathsf{t}\mathsf{v}_0+\mathsf{x}_0)}{1+i\mathsf{v}_0}}\left(\Gamma\left(0,\frac{\mathsf{x}_0-\mathsf{x}-i\mathsf{t}}{1-i\mathsf{v}_0}\right)-\Gamma\left(0,\frac{\mathsf{t}\mathsf{v}_0-\mathsf{x}+\mathsf{x}_0}{1-i\mathsf{v}_0}\right)\right)\right)\right)\right)\right],
\end{aligned}
\tag{351}
$$

where the exponential integral function $\mathrm{Ei}\left(z\right)$ and the incomplete gamma function $\Gamma\left(0,z\right)$ [27] are used, for definition and evaluation methods see appendix B.1. The formula (351) can be further simplified:

$$
\begin{aligned}
\mathsf{n}_1\left(\vec{\mathsf{x}},\mathsf{t}\right) =& \frac{1}{4\pi}\mathrm{e}^{\frac{\mathsf{t}\mathsf{v}_0+\mathsf{x}+\mathsf{x}_0}{-1+i\mathsf{v}_0}}\left[\mathrm{e}^{\frac{2(\mathsf{x}+i\mathsf{v}_0(\mathsf{t}\mathsf{v}_0+\mathsf{x}_0))}{1+\mathsf{v}_0^2}}\frac{1}{i-\mathsf{v}_0}\mathrm{Ei}\left[\frac{\mathsf{x}_0-\mathsf{x}+i\mathsf{t}}{1+i\mathsf{v}_0}\right]-\right. \\
&-\mathrm{e}^{\frac{2\mathsf{x}}{1-i\mathsf{v}_0}}\frac{1}{i+\mathsf{v}_0}\mathrm{Ei}\left[\frac{\mathsf{x}_0-\mathsf{x}-i\mathsf{t}}{1-i\mathsf{v}_0}\right]+ \\
&+\frac{1}{\mathsf{v}_0-i}\left(\mathrm{e}^{\frac{2(i\mathsf{t}\mathsf{v}_0^2+\mathsf{x}+i\mathsf{v}_0\mathsf{x}_0)}{1+\mathsf{v}_0^2}}\mathrm{Ei}\left[\frac{\mathsf{t}\mathsf{v}_0-\mathsf{x}+\mathsf{x}_0}{1+i\mathsf{v}_0}\right]+\right. \\
&\left.+\mathrm{e}^{\frac{2(\mathsf{t}\mathsf{v}_0+i\mathsf{v}_0\mathsf{x}+\mathsf{x}_0)}{1+\mathsf{v}_0^2}}\left(\mathrm{E}_1\left[\frac{\mathsf{t}\mathsf{v}_0-\mathsf{x}+\mathsf{x}_0}{1+i\mathsf{v}_0}\right]-\mathrm{E}_1\left[\frac{\mathsf{x}_0-\mathsf{x}+i\mathsf{t}}{1+i\mathsf{v}_0}\right]\right)\right)+ \\
&+\frac{1}{\mathsf{v}_0+i}\left(\mathrm{e}^{\frac{2i\mathsf{x}}{i+\mathsf{v}_0}}\mathrm{Ei}\left[\frac{\mathsf{t}\mathsf{v}_0-\mathsf{x}+\mathsf{x}_0}{1-i\mathsf{v}_0}\right]-\right. \\
&\left.\left.-\mathrm{e}^{\frac{2i(\mathsf{t}\mathsf{v}_0+\mathsf{x}_0)}{1+i\mathsf{v}_0}}\left(\mathrm{E}_1\left[\frac{\mathsf{x}_0-\mathsf{x}-i\mathsf{t}}{1-i\mathsf{v}_0}\right]-\mathrm{E}_1\left[\frac{\mathsf{t}\mathsf{v}_0-\mathsf{x}+\mathsf{x}_0}{1-i\mathsf{v}_0}\right]\right)\right)\right],
\end{aligned}
\tag{352}
$$

and even further, giving formula (72):

$$\begin{aligned}\mathsf{n}_1\left(\vec{\mathsf{x}},\mathsf{t}\right) =& \frac{1}{4\pi}\frac{1}{\mathsf{v}_0 - i}\left(\mathrm{e}^{-\mathcal{A}_+}\left(\mathrm{Ei}(\mathcal{A}_+) - \mathrm{Ei}(\mathcal{B}_+)\right) + \mathrm{e}^{\mathcal{A}_+}\left(\mathrm{E}_1(\mathcal{A}_+) - \mathrm{E}_1(\mathcal{B}_+)\right)\right) + \\ &+ \frac{1}{4\pi}\frac{1}{\mathsf{v}_0 + i}\left(\mathrm{e}^{-\mathcal{A}_-}\left(\mathrm{Ei}(\mathcal{A}_-) - \mathrm{Ei}(\mathcal{B}_-)\right) + \mathrm{e}^{\mathcal{A}_-}\left(\mathrm{E}_1(\mathcal{A}_-) - \mathrm{E}_1(\mathcal{B}_-)\right)\right),\end{aligned} \tag{353}$$

where

$$\mathcal{A}_\pm = \frac{\mathsf{t}\mathsf{v}_0 - \mathsf{x} + \mathsf{x}_0}{1 \pm i\mathsf{v}_0}, \quad \mathcal{B}_\pm = \frac{\mathsf{x}_0 - \mathsf{x} \pm i\mathsf{t}}{1 \pm i\mathsf{v}_0}. \tag{354}$$

We compared values that can be obtained via the expression (353) and via the initial expression given by *Mathematica* [39], they are exactly the same.

D FEL section

This section contains derivations of some formulas and equations from section 3.

D.1 From the modulator to the FEL amplifier

In the modulator, we have dimensionless density in the following form in a co-moving frame:

$$\mathsf{n}_1(\vec{\mathsf{x}}^{'}, \mathsf{t}^{'}), \tag{355}$$

in dimensional units:

$$\frac{1}{r_{\mathrm{D}}^d}\mathsf{n}_1\left(\frac{\vec{x}^{'}}{r_{\mathrm{D}}}, \frac{t^{'}}{t_{\mathrm{p}}}\right), \tag{356}$$

or in 1D we have:

$$\mathsf{n}_1\left(\mathsf{z}^{'}, \mathsf{t}^{'}\right), \text{ and } \frac{1}{r_{\mathrm{D}}}\mathsf{n}_1\left(\frac{z^{'}}{r_{\mathrm{D}}}, \frac{t^{'}}{t_{\mathrm{p}}}\right). \tag{357}$$

We have expressions for these quantities in a co-moving frame, to apply the FEL theory we need to transform them to the laboratory frame. If we have

two frames $K^{'}$ and K, such that $K^{'}$ moves with speed $\vec{v}$ in the positive z direction w.r.t K, and their origins are coincident at $t = t^{'} = 0$, the coordinates in $K^{'}$ are expressed as follows:

$$\begin{cases} t^{'}(z,t) = \frac{\gamma}{c}(ct - \beta z), \\ z^{'}(z,t) = \gamma(z - \beta ct), \end{cases} \tag{358}$$

we also know the transformation law for the phase-space density:

$$f(z,p) = f^{'}(z^{'}, p^{'}), \tag{359}$$

or

$$n(z)n_p(p) = n^{'}(z^{'})n_p^{'}(p^{'}), \tag{360}$$

where z and p are 4-vectors and should be expressed in terms of $z^{'}$ and $t^{'}$ via Lorentz transformations. If we assume cold beam in laboratory frame, we have:

$$n(z,t)\delta(v) = n^{'}(z^{'}, t^{'})\delta(\eta c) = n^{'}(z^{'}, t^{'})\frac{1}{c}\delta(\eta), \tag{361}$$

where we used

$$\eta \equiv \frac{\gamma - \gamma_r}{\gamma_r} = \frac{v}{c}, \tag{362}$$

which is valid for ultra-relativistic beams. If we integrate this expression over v, we obtain:

$$n(z,t) = n^{'}(z^{'}, t^{'}), \tag{363}$$

thus we can omit these momentum distributions. Thus we have for the density:

$$n_1^{(\mathrm{lab})}(z,t) \equiv \frac{1}{r_\mathrm{D}}\mathsf{n}_1\left(\frac{z^{'}(z,t)}{r_\mathrm{D}}, \frac{t^{'}(z,t)}{t_\mathrm{p}}\right), \tag{364}$$

where (z,t) are coordinates in the laboratory frame. In the modulator beam spends some "modulating time" $\mathsf{t}_i^{'}$, which is typically in the range $[0.25t_\mathrm{p}, 0.5t_\mathrm{p}]$ and, after modulation, we have density perturbation $\mathsf{n}_1\left(\mathsf{z}^{'}\right) =$

$\mathsf{n}_1\left(\mathsf{z}^{'}, \mathsf{t}_i^{'}\right)$. In the laboratory frame, the interaction time t_i equals $\frac{t_i^{'}}{\gamma}$ and we have:

$$t_i = \frac{L_m}{v_0}, \tag{365}$$

where v_0 is an hadron's velocity in the laboratory frame, which is related to the hadron's velocity in a co-moving frame $v_0{}'$, which we considered in the modulator, via

$$\vec{v}_0 = \frac{\vec{v_0^{'}} + v}{1 + \frac{\vec{v}\vec{v}_0{}'}{c^2}}, \tag{366}$$

where v is an electron beam velocity and all vectors here are one-dimensional, i.e., just signed scalars. We do space-time shift in the laboratory frame such that in new coordinates the hadron will have coordinates (0, 0) by the end of modulation:

$$\begin{cases} z^{(0)}(z,t) = z - L_m, \\ t^{(0)}(z,t) = t - t_i, \end{cases} \tag{367}$$

or

$$\begin{cases} z(z^{(0)}, t^{(0)}) = z^{(0)} + L_m, \\ t(z^{(0)}, t^{(0)}) = t^{(0)} + t_i. \end{cases} \tag{368}$$

Using these coordinates, we have for the density:

$$n_1^{(\mathrm{lab})(0)}(z^{(0)}, t^{(0)}) \equiv n_1^{(\mathrm{lab})}(z(z^{(0)}, t^{(0)}), t(z^{(0)}, t^{(0)})) \equiv \tag{369}$$

$$\equiv \frac{1}{r_{\mathrm{D}}} \mathsf{n}_1 \left(\frac{z^{'}(z(z^{(0)}, t^{(0)}), t(z^{(0)}, t^{(0)}))}{r_{\mathrm{D}}}, \frac{t^{'}(z(z^{(0)}, t^{(0)}), t(z^{(0)}, t^{(0)}))}{t_{\mathrm{p}}} \right), \tag{370}$$

In order to apply the standard FEL theory, we do the following change of variables:

$$(z^{(0)}, t^{(0)}) \mapsto (\theta^{(f)}, z^{(f)}), \quad \begin{cases} \theta^{(f)}(z^{(0)}, t^{(0)}) = (k_1 + k_u) z^{(0)} + c k_1 t^{(0)}, \\ z^{(f)}(z^{(0)}, t^{(0)}) = z^{(0)}, \end{cases} \tag{371}$$

where θ is a position of individual electrons from the bunch center. The "reference electron" is the one that has $\theta = 0$, it has the same position as the hadron.

We introduce the dimensional density perturbation in variables (θ, z) via:

$$n_1^{(\mathrm{lab})(f)}\left(\theta^{(f)}, z^{(f)}\right) \equiv n_1^{(\mathrm{lab})(0)}(z^{(0)}\left(\theta^{(f)}, z^{(f)}\right), t^{(0)}\left(\theta^{(f)}, z^{(f)}\right)), \tag{372}$$

where

$$\begin{cases} z^{(0)}\left(\theta^{(f)}, z^{(f)}\right) = z^{(f)}, \\ t^{(0)}\left(\theta^{(f)}, z^{(f)}\right) = \frac{\theta^{(f)} - (k_1+k_u)z^{(f)}}{ck_1}. \end{cases} \tag{373}$$

The density in a laboratory frame in the FEL coordinates is related to the one came from the modulator via:

$$\begin{aligned} & n_1^{(\mathrm{lab})(f)}\left(\theta^{(f)}, z^{(f)}\right) \equiv \frac{1}{r_{\mathrm{D}}} \times \\ & \times \mathsf{n}_1 \left(\frac{1}{r_{\mathrm{D}}} z^{'}(z(z^{(0)}(\theta^{(f)}, z^{(f)}), t^{(0)}(\theta^{(f)}, z^{(f)})), t(z^{(0)}(\theta^{(f)}, z^{(f)}), t^{(0)}(\theta^{(f)}, z^{(f)}))), \right. \\ & \left. \frac{1}{t_{\mathrm{p}}} t^{'}(z(z^{(0)}(\theta^{(f)}, z^{(f)}), t^{(0)}(\theta^{(f)}, z^{(f)})), t(z^{(0)}(\theta^{(f)}, z^{(f)}), t^{(0)}(\theta^{(f)}, z^{(f)}))) \right), \end{aligned} \tag{374}$$

where

$$\begin{cases} z^{'}(\theta^{(f)}, z^{(f)}) = \\ = z^{'}(z(z^{(0)}(\theta^{(f)}, z^{(f)}), t^{(0)}(\theta^{(f)}, z^{(f)})), t(z^{(0)}(\theta^{(f)}, z^{(f)}), t^{(0)}(\theta^{(f)}, z^{(f)}))) = \\ = \gamma \left(z^{(f)} + L_m - \beta c \left(\frac{\theta^{(f)} - (k_1+k_u)z^{(f)}}{ck_1} + t_i \right) \right), \\ t^{'}(\theta^{(f)}, z^{(f)}) = \\ = t^{'}(z(z^{(0)}(\theta^{(f)}, z^{(f)}), t^{(0)}(\theta^{(f)}, z^{(f)})), t(z^{(0)}(\theta^{(f)}, z^{(f)}), t^{(0)}(\theta^{(f)}, z^{(f)}))) = \\ = \frac{\gamma}{c} \left(c \left(\frac{\theta^{(f)} - (k_1+k_u)z^{(f)}}{ck_1} + t_i \right) - \beta(z^{(f)} + L_m) \right), \end{cases}$$

and finally

$$\begin{cases} \mathsf{z}^{'}(\theta^{(f)}, z^{(f)}) & = \frac{1}{r_{\mathrm{D}}} \gamma \left(z^{(f)} + L_m - \beta \left(\frac{\theta^{(f)} - (k_1+k_u)z^{(f)}}{k_1} + ct_i \right) \right), \\ \mathsf{t}^{'}(\theta^{(f)}, z^{(f)}) & = \frac{1}{t_{\mathrm{p}}} \frac{\gamma}{c} \left(\frac{\theta^{(f)} - (k_1+k_u)z^{(f)}}{k_1} + ct_i - \beta(z^{(f)} + L_m) \right), \end{cases} \tag{375}$$

for t_i we have:

$$t_i \equiv t_i(\vec{\mathsf{v}}_0^{'}) = \frac{L_m}{\vec{\mathsf{v}}_0} = L_m \frac{1 + \frac{\beta \vec{\mathsf{v}}_0{}'}{c}}{\vec{\mathsf{v}}_0^{'} + \beta c} = L_m \frac{1 + \frac{\beta \vec{\mathsf{v}}_0^{'} v_{\mathrm{rms}}}{c}}{\vec{\mathsf{v}}_0^{'} v_{\mathrm{rms}} + \beta c}, \tag{376}$$

where β_e is the scaled velocity of the electron beam in the laboratory frame, i.e., $\beta = v/c$, and $v_0^{'}$ is hadron's velocity in beam frame. We also can write these transformations in units of $t_{\rm p}$ for time and $r_{\rm D}$ for the length:

$$\begin{cases} \mathsf{z}^{'}(\theta^{(f)}, \mathsf{z}^{(f)}) & = \gamma \left(\mathsf{z}^{(f)} + \mathsf{L}_m - \beta \left(\frac{\theta^{(f)} - (\mathsf{k}_1 + \mathsf{k}_u)\mathsf{z}^{(f)}}{\mathsf{k}_1} + \mathsf{ct}_i \right) \right), \\ \mathsf{t}^{'}(\theta^{(f)}, \mathsf{z}^{(f)}) & = \frac{\gamma}{\mathsf{c}} \left(\frac{\theta^{(f)} - (\mathsf{k}_1 + \mathsf{k}_u)\mathsf{z}^{(f)}}{\mathsf{k}_1} + \mathsf{ct}_i - \beta(\mathsf{z}^{(f)} + \mathsf{L}_m) \right), \end{cases} \tag{377}$$

for t_i we have:

$$\mathsf{t}_i \equiv \mathsf{t}_i(\vec{\mathsf{v}}_0^{'}) = \mathsf{L}_m \frac{\mathsf{c} + \beta \vec{\mathsf{v}}_0{}'}{\vec{\mathsf{v}}_0^{'}\mathsf{c} + \beta \mathsf{c}^2}, \tag{378}$$

we distinguish between transformations (375) and (377) only by the arguments supplied.

D.2 The density perturbation from the modulator

Using the transformation derived, we can write an expression for the density from the modulator in terms of the FEL coordinates:

$$n_1^{(\mathrm{lab})(f)} \left(\theta^{(f)}, z^{(f)} \right) \equiv \frac{1}{r_{\rm D}} \mathsf{n}_1 \left(\mathsf{z}^{'}(\theta^{(f)}, z^{(f)}), \mathsf{t}^{'}(\theta^{(f)}, z^{(f)}) \right), \tag{379}$$

or in dimensionless form:

$$\mathsf{n}_1^{(\mathrm{lab})(f)} \left(\theta^{(f)}, \mathsf{z}^{(f)} \right) \equiv \mathsf{n}_1 \left(\mathsf{z}^{'}(\theta^{(f)}, \mathsf{z}^{(f)}), \mathsf{t}^{'}(\theta^{(f)}, \mathsf{z}^{(f)}) \right), \tag{380}$$

The relevant constants for the CeC PoP experiment are:

$$r_{\rm D} = 4.66 \cdot 10^{-5}\, m, \qquad v_{\rm rms} = 3 \cdot 10^5 m/s, \tag{381}$$

$$\omega_{\rm p} = 6.436 \cdot 10^9\, s^{-1}, \qquad t_{\rm p} = 0.155 \cdot 10^{-9}\, s, \tag{382}$$

$$\gamma = 42.937, \tag{383}$$

$$\beta = 0.999729, \tag{384}$$

$$L_m = 3.0\, m, \tag{385}$$

$$L_u = 7.5\, m, \tag{386}$$

$$k_1 = 4.99 \cdot 10^5\, m^{-1}, \qquad \lambda_1 = 1.26 \cdot 10^{-5}\, m, \tag{387}$$

$$k_u = 1.57 \cdot 10^2,\, m^{-1}, \qquad \lambda_u = 4.00 \cdot 10^{-2}\, m, \tag{388}$$

$$c = 2.997 \cdot 10^8\, m/s, \tag{389}$$

Omitting the superscript $^{(f)}$, we have the following initial value for the FEL section:

$$\delta n(\theta,0) = r_{\rm D} n_1^{({\rm lab})(f)}(\theta,0)\,. \tag{390}$$

Let us write an explicit expression for it. We start with the solution for the modulator for the hadron moving with velocity $\vec{\mathsf{v}}_0'$ from the initial position $\vec{\mathsf{x}}_0'$ (60):

$$\mathsf{n}_1(\vec{\mathsf{x}},\mathsf{t}) = \mathsf{L}^{-1}\mathsf{F}^{-1}\left[\frac{\mathrm{e}^{-i\vec{\mathsf{k}}\cdot\vec{\mathsf{x}}_0'}}{\left(\frac{f_d^{-1}v_{\rm rms}^{-d}}{\mathsf{LF}_{\vec{\mathsf{kt}}}(\mathsf{tf}_0(\vec{\mathsf{v}}))}+1\right)\left(\mathsf{s}+i\vec{\mathsf{k}}\cdot\vec{\mathsf{v}}_0'\right)}\right], \tag{391}$$

the expression in square brackets depends only on $\vec{\mathsf{k}}$ and s and we will denote it by $\mathsf{M}(\vec{\mathsf{k}},\mathsf{s})$:

$$\mathsf{n}_1(\vec{\mathsf{x}},\mathsf{t}) = \frac{1}{2\pi i}\frac{1}{2\pi}\int\limits_{\sigma-i\infty}^{\sigma+i\infty}\int \mathsf{M}(\vec{\mathsf{k}},\mathsf{s})\mathrm{e}^{\mathsf{st}+i\vec{\mathsf{k}}\vec{\mathsf{x}}}d\vec{\mathsf{k}}d\mathsf{s}, \tag{392}$$

and obtain:

$$n_1^{({\rm lab})(f)}(\theta,z) \equiv \frac{1}{r_{\rm D}}\mathsf{n}_1\left(\mathsf{z}'(\theta,z),\mathsf{t}'(\theta,z)\right) = \tag{393}$$

$$= \frac{1}{i(2\pi)^2}\frac{1}{r_{\rm D}}\int\limits_{\sigma-i\infty}^{\sigma+i\infty}\int \mathsf{M}(\vec{\mathsf{k}},\mathsf{s})\mathrm{e}^{\mathsf{st}'(\theta,z)+i\vec{\mathsf{k}}\mathsf{z}'(\theta,z)}d\vec{\mathsf{k}}d\mathsf{s}, \tag{394}$$

where the exponent is:

$$\mathrm{e}^{\mathsf{st}'(\theta,z)+i\vec{\mathsf{k}}\mathsf{z}'(\theta,z)} =$$
$$= \mathrm{e}^{\mathsf{s}\left(\frac{1}{t_{\rm p}}\frac{\gamma}{c}\left(\frac{\theta-(k_1+k_u)z}{k_1}+ct_i-\beta(z+L_m)\right)\right)+i\vec{\mathsf{k}}\left(\frac{1}{r_{\rm D}}\gamma\left(z+L_m-\beta\left(\frac{\theta-(k_1+k_u)z}{k_1}+ct_i\right)\right)\right)}, \tag{395}$$

or

$$\mathsf{n}_1^{({\rm lab})(f)}(\theta,\mathsf{z}) \equiv \mathsf{n}_1\left(\mathsf{z}'(\theta,\mathsf{z}),\mathsf{t}'(\theta,\mathsf{z})\right) = \tag{396}$$

$$= \frac{1}{i(2\pi)^2}\int\limits_{\sigma-i\infty}^{\sigma+i\infty}\int \mathsf{M}(\vec{\mathsf{k}},\mathsf{s})\mathrm{e}^{\mathsf{st}'(\theta,\mathsf{z})+i\vec{\mathsf{k}}\mathsf{z}'(\theta,\mathsf{z})}d\vec{\mathsf{k}}d\mathsf{s}. \tag{397}$$

The expressions for $\mathsf{M}(\vec{\mathsf{k}},\mathsf{s})$ for different distributions:

$$\text{KV: } \mathsf{M}(\vec{\mathsf{k}},\mathsf{s}) = \frac{\mathrm{e}^{-i\vec{\mathsf{k}}\cdot\vec{\mathsf{x}}_0'}}{\left(\frac{(\mathsf{s}^2+\mathsf{k}^2)^2}{\mathsf{s}^2-\mathsf{k}^2}+1\right)\left(\mathsf{s}+i\vec{\mathsf{k}}\cdot\vec{\mathsf{v}}_0'\right)}, \tag{398}$$

$$\text{WB: } \mathsf{M}(\vec{\mathsf{k}},\mathsf{s}) = \frac{\mathrm{e}^{-i\vec{\mathsf{k}}\cdot\vec{\mathsf{x}}_0'}}{\left((\mathsf{k}^2+\mathsf{s}^2)\sqrt{3}+1\right)\left(\mathsf{s}+i\vec{\mathsf{k}}\cdot\vec{\mathsf{v}}_0'\right)}, \tag{399}$$

$$\text{Cauchy: } \mathsf{M}(\vec{\mathsf{k}},\mathsf{s}) = \frac{\mathrm{e}^{-i\vec{\mathsf{k}}\cdot\vec{\mathsf{x}}_0'}}{\left((\mathsf{s}+\mathsf{k})^2+1\right)\left(\mathsf{s}+i\vec{\mathsf{k}}\cdot\vec{\mathsf{v}}_0'\right)}, \tag{400}$$

$$\text{Normal: } \mathsf{M}(\vec{\mathsf{k}},\mathsf{s}) = \frac{\mathrm{e}^{-i\vec{\mathsf{k}}\cdot\vec{\mathsf{x}}_0'}}{\left(\frac{\mathsf{k}^2}{\sqrt{2}}\left[1-\sqrt{\pi}\mathrm{e}^{\frac{\mathsf{s}^2}{\mathsf{k}^2}}\frac{s}{|\mathsf{k}|}\mathrm{Erfc}\frac{s}{|\mathsf{k}|}\right]^{-1}+1\right)\left(\mathsf{s}+i\vec{\mathsf{k}}\cdot\vec{\mathsf{v}}_0'\right)}. \tag{401}$$

D.3 The Maxwell-Vlasov system in the 1D FEL theory

In this subsection, we derive the Maxwell-Vlasov system for the 1D FEL theory. We will follow unpublished lecture notes [19], the related material can be found in [20, 21, 22]. We consider the Klimontovich distribution function:

$$F^{(K_1)}(\theta,\eta,z) = \frac{k_1}{\frac{I}{ec}}\sum_{j=1}^{N_e}\delta\big(\theta-\theta_j(z)\big)\delta\big(\eta-\eta_j(z)\big), \tag{402}$$

$$F^{(K_2)}(\theta,\eta,z) = \frac{k_1}{\frac{I}{ec}}F_0(\eta)\sum_{j=1}^{N_e}\delta\big(\theta-\theta_j(z)\big), \tag{403}$$

where η is the normalized dimensionless energy deviation from the energy γ_r, resonant with the electromagnetic field energy with the wavelength λ_1,

$\eta = \frac{\gamma-\gamma_r}{\gamma_r}$. In the frequency representation, we have:

$$F_\nu^{(K_1)}(\eta, z) = \frac{1}{2\pi}\int d\theta \mathrm{e}^{-i\nu\theta} F^{(K_1)}(\theta, \eta, z) = \frac{1}{N_\lambda}\sum_{j=1}^{N_e} \mathrm{e}^{-i\nu\theta_j(z)}\delta\big(\eta - \eta_j(z)\big), \tag{404}$$

$$F_\nu^{(K_2)}(\eta, z) = \frac{1}{2\pi}\int d\theta \mathrm{e}^{-i\nu\theta} F^{(K_2)}(\theta, \eta, z) = \frac{1}{N_\lambda}F_0(\eta)\sum_{j=1}^{N_e} \mathrm{e}^{-i\nu\theta_j(z)}, \tag{405}$$

where $N_\lambda = \lceil \lambda_1 \frac{I}{ec} \rceil$ is the number of electrons in one radiation wavelength λ_1. The Klimontovich distribution function contains the smooth θ, z-independent background $F_0(\eta)$ and the FEL interaction density perturbation:

$$F(\theta, \eta, z) = F_0(\eta) + \delta F(\theta, \eta, z). \tag{406}$$

In addition to undulator field, we consider the spontaneous radiation field, which we represent as a co-propagating with the electron beam electromagnetic wave:

$$E_x(z,t) = \tilde{E}(z,t)\cos(k_1 z - \omega_1 t + \phi),\ \omega_1 = ck_1 = \frac{2\pi c}{\lambda_1}, \tag{407}$$

this is a slowly-varying phase and amplitude (SVPA) approximation. For $E_x(z,t)$, we have the Maxwell equation in (z,t)-domain:

$$\left[\frac{1}{c^2}\frac{\partial^2}{\partial t^2} - \frac{\partial^2}{\partial z^2}\right] E_x(z,t) = -\frac{1}{\epsilon_0 c^2}\frac{\partial J_x}{\partial t}. \tag{408}$$

We then introduce the complex amplitude function:

$$E(z,t) = \frac{1}{2}\tilde{E}(z,t)\mathrm{e}^{i\phi(z,t)}, \tag{409}$$

for it, under certain assumptions, the time-domain Maxwell equation can be written as follows:

$$\left(\frac{\partial}{\partial z} + \frac{1}{c}\frac{\partial}{\partial t}\right) E(z,t) = -\chi_2 n_e \left\langle \mathrm{e}^{-i\theta_j}\right\rangle_\Delta, \tag{410}$$

where

$$\chi_2 = \frac{eK[JJ]}{4\epsilon_0\gamma_r}, \tag{411}$$

$$n_e = \frac{I}{ec(2\pi\sigma_x^2)}. \tag{412}$$

Then we introduce the SVPA approximation frequency domain amplitude $\tilde{E}_\nu$ via:

$$E_x(z,t) = \mathrm{e}^{ik_1(z-ct)} \int d\nu \tilde{E}_\nu(z) \mathrm{e}^{i\Delta\nu k_1(z-ct)} + c.c., \tag{413}$$

and then redefine the amplitude via:

$$\tilde{E}_\nu(z) = E_\nu(z) \mathrm{e}^{i\Delta\nu k_u z}. \tag{414}$$

For this redefined amplitude $E_\nu(z)$, the 1D Maxwell equation in the frequency domain looks as follows:

$$\left(\frac{\partial}{\partial z} + i\Delta\nu k_u\right) E_\nu(z) = -\chi_2 n_e \int d\eta \delta F_\nu(\eta, z), \tag{415}$$

where

$$\Delta\nu = \nu - 1. \tag{416}$$

The electric field is driven by the components of $F(\theta, \eta, z)$, for which $\nu = 1$, thus $F_0(\eta)$ doesn't contribute.
We have the continuity equation:

$$\frac{\partial F}{\partial z} + \frac{d\theta}{dz}\frac{\partial F}{\partial \theta} + \frac{d\eta}{dz}\frac{\partial F}{\partial \eta} = 0, \tag{417}$$

and

$$\frac{d\theta}{dz} = 2k_u\eta, \tag{418}$$

$$\frac{d\eta}{dz} = \chi_1 \int d\nu \mathrm{e}^{i\nu\theta} E_\nu(z) + \chi_1 \int d\nu \mathrm{e}^{-i\nu\theta} E_\nu^*(z), \tag{419}$$

where

$$\chi_1 = \frac{eK[JJ]}{2\gamma_r^2 mc^2}, \tag{420}$$

then we obtain the linearized continuity equation:

$$\left(\frac{\partial}{\partial z}+2i\nu k_u\eta\right)\delta F_\nu(\eta,z)=-\chi_1 E_\nu(z)\frac{d}{d\eta}F_0(\eta), \tag{421}$$

or

$$\left(\frac{\partial}{\partial z}+2k_u\eta\frac{\partial}{\partial\theta}\right)\delta F(\theta,\eta,z)=-\chi_1\int E_\nu(z)\mathrm{e}^{i\theta\nu}d\nu\frac{d}{d\eta}F_0(\eta). \tag{422}$$

This completes the derivation of 1D Maxwell-Vlasov equations:

$$\begin{cases}\left(\frac{\partial}{\partial z}+i\Delta\nu k_u\right)E_\nu(z)=-\chi_2 n_e\int d\eta\delta F_\nu(\eta,z),\\ \left(\frac{\partial}{\partial z}+2k_u\eta\frac{\partial}{\partial\theta}\right)\delta F(\theta,\eta,z)=-\chi_1\int E_\nu(z)\mathrm{e}^{i\theta\nu}d\nu\frac{d}{d\eta}F_0(\eta).\end{cases} \tag{423}$$

E Numerical integration

The most critical component of the piecewise polynomial collocation method is a numerical integrator. It must provide fast and accurate values for the integrals. We developed our own efficient integrators to do that. For the 1D integrals, we implemented a well-known adaptive Gauss-Kronrod method. For the multidimensional integrals, we developed a recursive integrator, which uses the 1D Gauss-Kronrod integrator. The code for all self-written integrators that we discuss here are available at [34].

E.1 Gauss-Kronrod method

The n-point Gaussian quadrature formula looks as follows:

$$\int_{-1}^{1} f(x)dx\approx\sum_{i=1}^{n}w_i f(x_i), \tag{424}$$

where w_i and x_i are Gaussian weights and nodes, they are can be computed for any odd n. For example, the 7-point Gaussian nodes and weights are

Nodes	Weights
±0.949107912342759	0.129484966168870
±0.741531185599394	0.279705391489277
±0.405845151377397	0.381830050505119
0.000000000000000	0.417959183673469.

For an integral with arbitrary limits

$$\int_a^b f(x)dx \approx \sum_{i=1}^{n} v_i f(y_i) \equiv G_n, \tag{425}$$

the weights and nodes can be computed via

$$\begin{cases} y_i = a + (x_i + 1)\frac{b-a}{2}, & i = 1 \dots n, \\ v_i = w_i \frac{b-a}{2}, & i = 1 \dots n. \end{cases} \tag{426}$$

It is possible to add $n + 1$ more points to the Gaussian rule and obtain the quadrature of the order $2n + 1$:

$$\int_a^b f(x)dx \approx \sum_{i=1}^{2n+1} u_i f(z_i) \equiv K_{2n+1}, \tag{427}$$

This quadrature is called the $2n + 1$-point Kronrod rule. For example, the 15-point Kronrod nodes and weights are

Nodes	Weights
±0.991455371120813	0.022935322010529
±0.949107912342759	0.063092092629979
±0.864864423359769	0.104790010322250
±0.741531185599394	0.140653259715525
±0.586087235467691	0.169004726639267
±0.405845151377397	0.190350578064785
±0.207784955007898	0.204432940075298
0.000000000000000	0.209482141084728.

n of the $2n + 1$-point Kronrod nodes are the same as the n-point Gaussian nodes, so only $n + 1$ extra function evaluations are required. In the Gauss-Kronrod rule, K_{2n+1} is taken as a value of the integral and error can be approximated by

$$\left(200|G_n - K_{2n+1}|\right)^{\frac{3}{2}}. \tag{428}$$

This error estimate is quite conservative. The error estimation of the Gauss-Kronrod rule is a non-trivial question and we refer interested readers to [40]. For details on computation of the nodes and weights, we refer to [41].

For difficult integrands, for example, oscillatory or singular functions, the Gauss-Kronrod method with $n \sim 10$ is not able to compute integral with good accuracy estimated via (428). For such integrands, we can do adaptive integration. The idea is the following. We compute integral via the Gauss-Kronrod integrator, compute error via (428), and if error is too big, we split the interval into two and compute integral and error for each interval via the Gauss-Kronrod integrator, then if error is good enough we stop, and if error is too big we continue splitting. Recursive implementation of this algorithm is trivial.

E.2 Multidimensional integration

For the multidimensional integrals, we developed a recursive integrator that can compute integrals of any dimension using one-dimensional integrator. At each step of recursion, it uses as an integrand the initial integral corresponding to this step, but with lowered by one number of integration variables. We also store the values of this step's integration variables and pass them to further steps. When dimension of the integral is one, the recursive integrator takes function as an integrand and evaluates it at the values of the integration variables, which were stored in previous steps of the recursion. To perform one-dimensional integration, we implemented the adaptive Gauss-Kronrod algorithm. Schematically, this recursion can be represented as follows:

$$\int \boxed{\int \boxed{\int \dots \boxed{\int \boxed{f(x_1, \dots x_n)}\, dx_1} \dots dx_{n-2}}\, dx_{n-1}}\, dx_n, \tag{429}$$

where boxes represent integrands at each recursion step.

We tested our integrator and did timing studies with integral

$$\int_{-1}^{1}\int_{-1}^{1}\int_{-1}^{1} \frac{1}{\sqrt{(x-0.3)^2+(y-0.4)^2+(z-0.5)^2}} dxdydz, \tag{430}$$

we requested absolute and relative errors 10^{-7}, 10^{-7}, respectively. This integral is similar to those, which we compute for the test charge problem. We used a laptop with a 1.8 GHz Intel Core i5 processor.

Method	Time, sec.	Result	Abs. Error	fun. eval.
GSL Monte Carlo	0.0062	8.5478	$2.068 \cdot 10^{-2}$	-
Rec. with GSL 1D	0.7803	8.5072	$8.220 \cdot 10^{-7}$	21178965
Rec. with adaptive GK	0.0929	8.5068	$3.133 \cdot 10^{-3}$	2674395
Rec. with non-adap. GK	0.0003	8.4863	$3.904 \cdot 10^{1}$	3375
Mathematica [39]	11.122	8.507	-	-

Table 1: Timing studies of different integrators. Columns are: method, time, result, absolute error, number of function evaluations.

The results are presented in Table 1. We tested Monte-Carlo integrator of the GSL library [42] and our recursive integrator with three different 1D integrators: GSL 1D integrator, our adaptive Gauss-Kronrod integrator and non-adaptive Gauss-Kronrod integrator. Absolute error is computed via (428). We see that recursive integrator with non-adaptive Gauss-Kronrod integrator is 24 times faster than GSL Monte-Carlo integrator, 350 times faster than recursive integrator with adaptive Gauss-Kronrod integrator, 3000 faster than recursive integrator with GSL 1D integrator, and 41,000 times faster than *Mathematica*'s [39] integrator.

We observe that error estimation (428) is too conservative for such integrals, for the recursive integrator with non-adaptive Gauss-Kronrod integrator, it gives absolute error 39.04, while the value differs from the exact just by 0.02. As it is seen from the table, this integrator requires much less number of function evaluations, thus works much faster, as it is clear from the table, while giving reasonable accuracy.

E.3 Improper integrals

Although, in most cases, it is possible to cut the infinite domain of an integral and use quadrature formula for the finite domain, the correct way to proceed is to do change of variables and transform the infinite interval into the finite one. For the integral

$$\int_0^{+\infty} f(x)dx, \tag{431}$$

we do the following change of variables:

$$x(t) = \frac{1-t}{t}, \tag{432}$$

and obtain:

$$\int_0^{+\infty} f(x)dx = \int_0^1 f\left(\frac{1-t}{t}\right)\frac{dt}{t^2}. \tag{433}$$

This fomula can be generalized:

$$\int_a^{+\infty} f(x)dx = \int_0^1 f\left(a + \frac{1-t}{t}\right)\frac{dt}{t^2}, \tag{434}$$

$$\int_{-\infty}^b f(x)dx = \int_0^1 f\left(b - \frac{1-t}{t}\right)\frac{dt}{t^2}. \tag{435}$$

And for the double-infinite interval, we have

$$\int_{-\infty}^{+\infty} f(x)dx = \int_0^1 f\left(\frac{1-t}{t}\right)\frac{dt}{t^2} + \int_0^1 f\left(\frac{t-1}{t}\right)\frac{dt}{t^2}. \tag{436}$$

This formula is too bulky and it is possible to use another change of variables:

$$x(t) = \tan t. \tag{437}$$

With this change of variables, we obtain

$$\int_{-\infty}^{+\infty} f(x)dx = \int_{-\frac{\pi}{2}}^{\frac{\pi}{2}} f\left(\tan t\right)\frac{dt}{\cos^2 t}. \tag{438}$$

Then the integrals can be computed using quadrature formulas for the finite segment, for example, the Gauss-Kronrod rule.

All these changes of variables are extensively used in section 4.

F Systems of linear equations

In this appendix we consider system of linear equations:

$$\mathbf{A}\vec{x} = \vec{b}, \tag{439}$$

where $\mathbf{A}$ is a known square matrix, $\vec{b}$ is a known vector, and $\vec{x}$ is an unknown vector.

F.1 Solution via LU decomposition

The system can be solved using LU decomposition of matrix $\mathbf{A}$:

$$\mathbf{A} = \mathbf{LU}, \tag{440}$$

where $\mathbf{L}$ is a lower triangular matrix and $\mathbf{U}$ is an upper triangular matrix. The system with either lower or upper triangular matrix can be easily solved line by line and the initial system can be reduced to two such systems, i.e., we first solve

$$\mathbf{L}\vec{y} = \vec{b}, \tag{441}$$

for $\vec{y}$, then we solve

$$\mathbf{U}\vec{x} = \vec{y}, \tag{442}$$

for $\vec{x}$.

F.2 Algorithm for LU decomposition

In this subsection, we describe a well-known algorithm for the LU decomposition [38, 43], its implementation is available in GSL Library [42].

Suppose, we are computing LU decomposition of matrix $\mathbf{A}$. We build a sequence of matrices $\mathbf{A}_i$, $i = 0, \ldots, N$, via

$$\mathbf{A}_0 = \mathbf{A}, \tag{443}$$

$$\mathbf{A}_i = \mathbf{L}_i\mathbf{A}_{i-1}, \;\; i = 1, \ldots, N \tag{444}$$

where

$$\mathbf{L}_i = \begin{pmatrix} 1 & 0 & \dots & \dots & 0 & 0 \\ 0 & \ddots & 0 & & & 0 \\ \vdots & & 1 & & & \vdots \\ 0 & \dots & l_{i+1,i} & \ddots & & 0 \\ \vdots & & \vdots & & \ddots & \vdots \\ 0 & \dots & l_{N,i} & \dots & \dots & 1 \end{pmatrix}, \tag{445}$$

and $l_{j,i},\ j = i+1, \dots, N$ are given by

$$l_{j,i} = -\frac{a_{ji}^{(i-1)}}{a_{ii}^{(i-1)}}, \tag{446}$$

where $a_{ii}^{(i-1)}$ is a matrix element of matrix $\mathbf{A}_{i-1}$. By multiplying $\mathbf{A} \equiv \mathbf{A}_0$ by $\mathbf{L}_1$ we nullify element below main diagonal in the first column of $\mathbf{A}$. Then, when we multiply $\mathbf{L}_1\mathbf{A}$ by $\mathbf{L}_2$ we nullify elements below main diagonal in the second column etc. We can write:

$$\mathbf{A} = \mathbf{L}_1^{-1}\mathbf{L}_1\mathbf{A}_0 = \mathbf{L}_1^{-1}\mathbf{A}_1 = \dots = \mathbf{L}_1^{-1} \dots \mathbf{L}_{N-1}^{-1}\mathbf{A}_{N-1}. \tag{447}$$

By construction, $\mathbf{A}_{N-1}$ is an upper triangular matrix, and, since inverse of lower triangular matrix is lower triangular matrix, and product of lower triangular matrices is a lower triangular matrix, $\mathbf{L}_1^{-1} \dots \mathbf{L}_{N-1}^{-1}$ is a lower triangular matrix. Thus, equation represents the LU decomposition

$$\mathbf{A} = \mathbf{L}\mathbf{U}, \tag{448}$$

where

$$\mathbf{L} = \mathbf{L}_1^{-1} \dots \mathbf{L}_{N-1}^{-1}, \tag{449}$$

$$\mathbf{U} = \mathbf{A}_{N-1}. \tag{450}$$

F.3 Parallel algorithm for LU decomposition

In this subsection, we describe a parallel algorithm for the LU decomposition, its implementation (in C++, with MPI) can be found at [34].

Let us take a closer look at the LU decomposition algorithm.

To build matrix $\mathbf{L}_i$, we need elements of i-th column (from the main diagonal to the end) of the matrix $\mathbf{A}$, and when we compute $\mathbf{L}_i\mathbf{A}_{i-1}$, we will need only i-th row (from the main diagonal to the end) of the matrix $\mathbf{A}$ and only i-th column (from the main diagonal to the end) of the matrix $\mathbf{A}$ will be affected. This means that computation of $\mathbf{A}_{N-1}$ can be easily parallelized. Moreover, the whole matrix A is not required on each process, thus from root process we can distribute one row and one column to other processes and then collect the results from them, this is important, when the matrix $\mathbf{A}$ is large and there is no enough memory to send the whole matrix to all processes.

Computation of $\mathbf{L}$ is even simpler and also can be parallelized in a similar way. Inverse of $\mathbf{L}_i$ is just

$$\mathbf{L}_i^{-1} = \begin{pmatrix} 1 & 0 & \dots & \dots & 0 & 0 \\ 0 & \ddots & 0 & & & 0 \\ \vdots & & 1 & & & \vdots \\ 0 & \dots & -l_{i+1,i} & \ddots & & 0 \\ \vdots & & \vdots & & \ddots & \vdots \\ 0 & \dots & -l_{N,i} & \dots & \dots & 1 \end{pmatrix}, \tag{451}$$

and

$$\mathbf{L}_1^{-1} \dots \mathbf{L}_{N-1}^{-1} = \begin{pmatrix} 1 & 0 & \dots & \dots & 0 & 0 \\ -l_{2,1} & \ddots & 0 & & & 0 \\ \vdots & & 1 & & & \vdots \\ -l_{i+1,1} & \dots & -l_{i+1,i} & \ddots & & 0 \\ \vdots & & \vdots & & \ddots & \vdots \\ -l_{N,1} & \dots & -l_{N,i} & \dots & -l_{N,N-1} & 1 \end{pmatrix}. \tag{452}$$

Computation of this matrix can be done simultaneously with computation of $\mathbf{A}_{N-1}$ with the same parallelization scheme.

References

[1] I. M. Kapchinskiy, "Theory of Resonance Linear Accelerators", Harwood Academic Publishers, New York, (1985).

[2] S. Y. Lee, "Accelerator Physics", World Scientific, (2011).

[3] V. N. Litvinenko, S. Belomestnykh, I. Ben-Zvi, M. M. Blaskiewicz, K. A. Brown, J. C. Brutus, A. Elizarov *et al.*, ICFA Beam Dyn. Newslett. **58**, pp. 52-71, (2012).

[4] V. N. Litvinenko, Y. S. Derbenev, Phys. Rev. Lett. **102**, 114801 (2009).

[5] I. Pinyaev *et al.*, in *Proceeding of the International Particle Accelerator Conference 2012*, (New Orleans, USA, 2012), p. 400, moppd016, `http://accelconf.web.cern.ch/accelconf/IPAC2012/papers/moppd016.pdf`; in *Proceeding of the International Particle Accelerator Conference 2013*, (Shanghai, China, 2013), p. 1535, tupfi081, `http://accelconf.web.cern.ch/AccelConf/IPAC2013/papers/tupfi081.pdf`.

[6] S. Webb, G. Wang, and V. Litvinenko, Phys. Rev. ST Accel. Beams **14**, 051003 (2011).

[7] A. Elizarov and V. Litvinenko, in *Proceeding of the Free Electron Laser Conference 2012*, (Nara, Japan, 2012), p. 77, mopd17, `http://accelconf.web.cern.ch/AccelConf/FEL2012/papers/mopd17.pdf`.

[8] A. Elizarov and V. Litvinenko, in *Proceedings of the Free Electron Laser Conference 2013*, (New York, USA, 2013), mopso17, `http://accelconf.web.cern.ch/AccelConf/FEL2013/papers/mopso17.pdf`.

[9] G. Wang, M. Blaskiewicz, Phys. Rev. E **78**, 026413 (2008).

[10] A. Elizarov and V. Litvinenko, Phys. Rev. ST Accel. Beams **16**, 124001 (2013).

[11] A. J. Turski, Ann. Phys. (N.Y.) **35**, 240, (1965); Ann. Phys. **22**, 180 (1969).

[12] R. L. Gluckstern, in *Proceedings of the Linac Conference, 1970* (Fermilab, Batavia, IL, 1970), p. 811.

[13] M. Venturini and R. L. Gluckstern, Phys. Rev. ST Accel. Beams **3**, 034203 (2000).

[14] R. Tegeback, A. S. Usenko, I. P. Yakimenko, and A. G. Zagorodny, Journal of Plasma Physics, **18**, pp. 113-125 (1977).

[15] G. Bell *et al.*, in *Proceeding of the 2011 Particle Accelerator Conference*, (New York, USA, 2011), p. 235, mop067, `http://accelconf.web.cern.ch/accelconf/PAC2011/papers/mop067.pdf`; in *Proceeding of the International Particle Accelerator Conference 2012*, (New Orleans, USA, 2012), p. 3231, theppb002, `http://accelconf.web.cern.ch/accelconf/IPAC2012/papers/theppb002.pdf`.

[16] G. Wang, M. Blaskiewicz, and V.N. Litvinenko, Phys. Rev. ST Accel. Beams **17**, 101004 (2014).

[17] `http://en.wikipedia.org/wiki/Free-electron_laser`

[18] E. Saldin, E.V. Schneidmiller, M.V. Yurkov, "The Physics of Free Electron Lasers", Springer, (2000).

[19] K.-J. Kim, Z. Huang, and R. Lindberg, "Synchrotron Radiation and Free Electron Lasers for Bright X-Rays", 2013 USPAS lecture notes, unpublished.

[20] K.-J. Kim, Nucl. Instr. and Methods in Physics Research A, **250**, 396-403 (1986).

[21] Z. Huang and K.-J. Kim, Phys. Rev. E **62**, 7295 (2000).

[22] Z. Huang, K.-J. Kim, Phys. Rev. ST Accel. Beams **10**, 034801 (2007).

[23] G. Wang, M. Blaskiewicz, V. N. Litvinenko, *IPAC'10 Proceedings*, mopd077 (2010).

[24] A. Elizarov, V. Litvinenko, in *Proceeding of the International Particle Accelerator Conference 2012*, (Shanghai, China, 2012), p. 1082, mopwo088 `https://accelconf.web.cern.ch/accelconf/IPAC2013/papers/mopwo088.pdf`.

[25] A. A. Vlasov, Sov. Phys. Usp. **10**, 721 (1968).

[26] I. Kapchinskij and V. Vladimirskij, in *Proc. of the Int. Conf. on High Energy Accel. and Instr.*, CERN, Geneva, (1959).

[27] M. Abramowitz and I. Stegun, Handbook on Mathematical Functions (Dover Publications, Inc., New York, 1965).

[28] Landau, L. D. and Lifshitz, E. M., "Electrodynamics of continuous media", Pergamon Press (1984).

[29] V. N. Litvinenko, Report No. C-A/AP/480, tech-note, BNL, 2013, `http://public.bnl.gov/docs/cad/Documents/On%20the%20FEL%20Gain%20Limit.pdf`.

[30] V. N. Litvinenko, Y. S. Derbenev, Phys. Rev. Lett. **110**, 269504 (2013).

[31] A. Elizarov, V. Litvinenko, G. Wang, in *Proceeding of the International Particle Accelerator Conference 2012*, (New Orleans, USA, 2012), p. 3171, weppr099, URL: http://accelconf.web.cern.ch/accelconf/IPAC2012/papers/weppr099.pdf.

[32] A. Elizarov and V. Litvinenko, Phys. Rev. ST Accel. Beams **18**, 044001 (2015).

[33] D. R. Nicholson, "Introduction to Plasma Theory", Wiley, (1983).

[34] `http://muline.sourceforge.net/`.

[35] G. Vainikko, "Multidimensional Weakly Singular Integral Equations", Springer, (1993).

[36] A. Cohen, "Numerical Methods for Laplace Transform Inversion", Springer, (2007).

[37] G. Honig, U. Hirdes, J. Comput. Appl. Math., **10**, 113 (1984).

[38] T. H. Cormen, C. E. Leiserson, R. L. Rivest, C. Stein, "Introduction to Algorithms", 3rd Edition, The MIT Press, (2009).

[39] Wolfram Research, Inc., Mathematica, Version 8.0, Champaign, IL (2010).

[40] P. Gonnet, ACM Computing Surveys (CSUR), **44**, issue 4, article No. 22 (2012).

[41] D. P. Laurie, Mathematics of Computation, **66**, No. 219, pp. 11331145 (1997).

[42] `http://www.gnu.org/software/gsl/`.

[43] `http://en.wikipedia.org/wiki/LU_decomposition`